May 2021

Innovative Thermal Management Systems for Autonomous Vehicles — Design, Model, and Test

Shervin Shoai Naini
Clemson University, sshoain@g.clemson.edu

Innovative Thermal Management Systems for Autonomous Vehicles - Design, Model, and Test

---

A Dissertation
Presented to
the Graduate School of
Clemson University

In Partial Fulfillment
of the Requirements for the Degree
Doctor of Philosophy
Mechanical Engineering

---

by
Shervin Shoai Naini
March 2021

Accepted by:
Dr. John Wagner, Committee Co-Chair
Dr. Richard Miller, Committee Co-Chair
Dr. Denise Rizzo
Dr. Xiangchun Xuan

Abstract

Emphasis on reducing fossil fuel consumption and greenhouse gas emissions, besides the demand for autonomy in vehicles, made governments and automotive industries move towards electrification. The integration of an electric motor with battery packs and on-board electronics has created new thermal challenges due to the heat loads' operating conditions, design configurations, and heat generation rates. This paradigm shift necessitates an innovative thermal management system that can accommodate low, moderate, and high heat dissipations with minimal electrical or mechanical power requirements.

This dissertation proposes an advanced hybrid cooling system featuring passive and active cooling solutions in a thermal bus configuration. The main purpose is to maintain the heat loads' operating temperatures with zero to minimum power requirements and improved packaging, durability, and reliability. In many operating instances, a passive approach may be adequate to remove heat from the thermal source (e.g., electric motor) while a heavy load would demand both the passive and active cooling systems operate together for reduced electric power consumption. Further, in the event of a failure (e.g., coolant hose leak, radiator tube leak) in the conventional system, the passive system offers a redundant operating mode for continued operation at reduced loads. Besides, the minimization of required convective heat transfer (e.g., ram air effect) about the components for supplemental cooling enables creative vehicle

component placement options and optimizations.

Throughout this research, several cooling system architectures are introduced for electric vehicle thermal management. Each design is followed by a mathematical model that evaluates the steady-state and transient thermal responses of the integrated heat load(s) and the developed cooling system. The designs and the mathematical models are then validated through a series of thermal tests for a variety of driving cycles. Then, the cooling system design configuration is optimized using the validated mathematical model for a particular application. The nonlinear optimization study demonstrates that a 50% mass reduction could be achieved for a continuous 12kW heat-dissipating demand while the electric motor operating temperature has remained below 65°C. Next, several real-time controllers are designed to engage the active cooling system for precise, stable, and predictable temperature regulation of the electric motor and reduced power consumption. A complete experimental setup compares the controllers in the laboratory's environment. The experimental results indicate that the nonlinear model predictive control reduces the fan power consumption by 73% for a 5% increase in the pump power usage compared to classical control for a specific 60-minute driving cycle.

In conclusion, the conducted experimental and numerical studies demonstrate that the proposed hybrid cooling strategy is an effective solution for the next generation of electrified civilian and combat ground vehicles. It significantly reduces the reliance on fossil fuels and increases vehicle range and safety while offering a silent mode of operation. Future work is to implement the developed hybrid cooling system on an actual electric vehicle, validate the design, and identify challenges on the road.

Dedication

I would like to dedicate my doctoral dissertation to my beloved parents, Hamid Reza Shoai-Naini, and Homeira Afshary-Kord, and my lovely sister, Sheida Shoai-Naini. Thank you for your unconditional love and for staying by my side all the time.

Acknowledgements

I would like to express my deepest gratitude to my Ph.D. advisors, Dr. John Wagner and Dr. Richard Miller, for their excellent guidance, supports, and encouragement during the doctorate program at Clemson University. I'm thankful to Dr. Denise Rizzo, who generously supported my Ph.D. research and for reviewing my research articles throughout these years. My gratitude also goes to Dr. Xiangchun Xuan for his assistance and review of my doctoral dissertation.

I would like to express my sincere appreciation to Dr. Ehsan Mousavi for providing me with financial assistance and for supporting my Ph.D. studies for two years. Working with him was a great learning experience, and I appreciate the friendship we made over these years. Thanks to my dearest friends who made my stay in Clemson memorable. I would also like to warmly thank my best friends in my home country who proved that a true friendship is neither a function of space nor time. And above all, I would like to thank to my parents, Hamid Reza Shoai-Naini, and Homeira Afshary-Kord; and my sister, Sheida Shoai-Naini. Nothing I have ever accomplished in my life would have been even possible without their unconditional love and support. I am fortunate to have them as my family.

Publications

- Shervin Shoai-Naini, Richard Miller, John R Wagner, and Denise Rizzo, "Multi-Objective Design Optimization of an Electric Motor Thermal Management System for Autonomous Vehicles", SAE paper no. 2021-01-0257, Detroit, MI., April 2021

- Shervin Shoai-Naini, Richard Miller, John R Wagner, Denise Rizzo, and Katherine Sebeck, "An Electric Motor Thermal Bus Cooling System for Vehicle Propulsion – Design and Test", International Journal of Advances and Current Practices in Mobility, vol. 2, no. 4, pp. 2011-2018, DOI: https://doi.org/10.4271/2020-01-0745.

- Huang, Junkui, Shervin Shoai-Naini, Richard Miller, Denise Rizzo, Katie Sebeck and John Wagner, " Development of a Heat Pipe Based Battery Thermal Management System for Hybrid Electric Vehicles", Part D: Journal of Automobile Engineering, vol. 234, no.6, pp. 1532-1543, DOI: JAUTO-19-0279.R1.

- Huang, Junkui, Shervin Shoai-Naini, Richard Miller, Denise Rizzo, Katie Sebeck and John Wagner, " Unmanned Autonomous Ground Hybrid Vehicle Thermal Management System - Design and Control", International Journal of Vehicle Performance, vol. 6, no.3, pp. 356-379, DOI: IJVP-273553.

- Shervin Shoai-Naini, Junkui Allen Huang, Richard Miller, John R Wagner, Denise Rizzo, Katherine Sebeck, and Scott Shurin, "An Innovative Electric Motor Cooling System for Hybrid Vehicles - Model and Test", SAE paper no. 2019-01-1076, Detroit, MI., April 2019.

- Huang, Junkui, Shervin Shoai-Naini, Richard Miller, Denise Rizzo, Katie Sebeck, Scott Shurin, and John Wagner, "A Hybrid Electric Vehicle Motor Cooling System - Design, Model, and Control", IEEE Transactions on Vehicular Technology, DOI: 101109/TVT.2019.2902135.

- Shervin Shoai-Naini, Junkui Allen Huang, Richard Miller, John R Wagner, Denise Rizzo, Katherine Sebeck, and Scott Shurin, "A Hybrid Thermal Bus for Ground Vehicles Featuring Parallel Heat Transfer Pathways", SAE International Journal of Commercial Vehicles vol. 11, no. 2018-01-1111, April 2018.

- Junkui Allen Huang, Shervin Shoai-Naini, John R Wagner, Denise Rizzo, Katherine Sebeck, Scott Shurin, et al., "An Integrated Cooling System for Hybrid Electric Vehicle Motors – Design and Simulation", SAE International Journal of Commercial Vehicles, vol. 11, no. 5, 2018.
- Shervin Shoai-Naini, Junkui Allen Huang, Richard Miller, John R Wagner, Denise Rizzo, Scott Shurin, and Katherine Sebeck, "A Thermal Bus for Vehicle Cooling Applications - Design and Analysis", SAE International Journal of Commercial Vehicles, vol. 10, no. 2017-01-0266, pp.122–131.

Table of Contents

List of Tables

List of Figures

Nomenclature

A	Heat pipe cross section area, m^2
A_F	Convective heat transfer surface area, m^2
A_e	Thermosyphon evaporator surface area , m^2
A_f	Fin surface area, m^2
A_r	Radiator heat transfer surface area, m^2
A_s	Shell heat transfer surface area, m^2
A_{AL}	Endcap heat transfer surface area, m
A_A	Heat exchanger surface area, m^2
A_{CF}	Carbon fiber surface area in thermal bus, m^2
A_{HTC}	High thermal conductivity material surface area in thermal bus, m^2
A_{LQ}	Coolant tube surface area, m^2
A_{cap}	Thermosyphon evaporator surface area, m^2
A_{cr}	Cradle surface area, m^2
A_{eff}	Effective fin surface area, m^2
A_e	Coil thermal contact surface area, m^2
A_{hs}	Heat sink surface area, m^2
A_{hx}	Heat sink heat transfer surface area, m^2
A_t	Total fin area, m^2
C	Integration constant
$C_{LQ,E}$	Liquid cooling evaporator heat capacity, J/K

$C_{LQ,R}$	Radiator heat capacity, J/K
$C_{TS,E}$	Thermosyphon's evaporator heat capacity, J/K
$C_{TS,E}$	Thermosyphon's evaporator heat capacity, J/K
$C_{TS,R}$	Heat exchanger heat capacity, J/K
C_W	Cradle wall heat capacity, J/K
C_{cap}	Endcap heat capacity, J/K
C_{em}	Electric motor heat capacity, J/K
C_{hx}	Heat exchanger heat capacity, J/K
C_{int}	Cylindrical cradle heat capacity, J/K
C_{wall}	Cradle wall heat capacity, J/K
C_{wall}	Cradle wall heat capacity,J/K
D_R	Reservoir diameter, m
D_l	Liquid line diameter, m
D_v	Vapor line diameter, m
$D_{C,i}$	Condenser tube diameter at inlet, m
$D_{C,o}$	Condenser tube diameter at outlet, m
$D_{E,i}$	Evaporator inner diameter, m
$D_{E,o}$	Evaporator outer diameter, m
D_{hp}	Heat pipe diameter, m
$D_{w,i}$	Wick structure inner diameter, m
$D_{w,o}$	Wick structure outer diameter, m
H_r	Radiator thickness, m
H_{hx}	Heat exchanger thickness, m
L	Fin length, m
L_E	Length of evaporator, m

L_W	Length of wick structure, m
L_c	Cold section length, m
L_e	Evaporator length, m
L_f	Fin length, m
L_h	Hot section length, m
L_l	Length of liquid line, m
L_p	Liquid slug length, Wick length, m
L_r	Radiator Length, m
L_w	Pipe length, m
$L_{2\phi}$	Pipe length which includes two-phase mixture, m
L_{AL}	Endcap effective length, m
L_{CF}	Length of carbon fiber pathway, m
L_{CR}	Cradle length, m
L_{HTC}	Length of high thermal conductivity pathway, m
L_{coil}	Length of the coil, m
L_{cr}	Cradle length, m
L_{eff}	Heat pipe effective length, m
L_{hx}	Heat exchanger's horizontal length, m
L_h	Heat pipe evaporator length, m
L_{pa}	Thermosyphon's evaporator effective length, m
L_s	Length of heat sink, m
M_{tb}	Thermal bus mass, kg
N	Number of capillary heat pipes/fins, -
Nu	Nusselt number, -
Nu_D	Averaged Nusselt number, -

Nu_b	Nusselt number for forced convection, -
Nu_s	Nusselt number for free convection, -
P	Preselected prediction horizon, sec
PM	Permeability, m^2
P_l	Liquid pressure, Pa
P_v	Vapor pressure, Pa
P_c	Capillary pressure, Pa
P_{v0}	Initial pressure of vapors, Pa
P_{v1}	Vapor 1 pressure, Pa
P_{v2}	Vapor 2 pressure, Pa
P_{vc}	Vapor pressure in condenser, Pa
P_{ve}	Vapor pressure in evaporator, Pa
Pr	Prandtl number, -
Q_R	Heat transferred through liquid-vapor interface, W
Q_{load}	Heat load heat generation rate, W
Q_{rej}	Heat exchanger heat rejection, W
Q_{rem}	Thermal bus heat removal, W
$Q_{sen_{in}}$	Sensible heat transferred in liquid, W
$Q_{sen_{out}}$	Sensible heat transferred out of liquid, W
Q_{total}	Total heat transferred by thermal bus, W
Q_{v1}	Latent heat from vapor 1, W
Q_{v2}	Latent heat from vapor 2, W
$Q_{v_{in}}$	Total latent heat input, W
$Q_{v_{out}}$	Total latent heat output, W
Q_{wall}	Heat transferred through the evaporator wall, W

R	Gas constant, $J/kg.K$
R_A	Thermal resistance of air, $W/m.K$
R_E	Thermal conductivity resistance of evaporator, K/W
R_r	Radiator convective thermal resistance, K/W
R_s	Heat pipe shell thermal resistance, K/W
R_w	Thermal conductivity resistance of the wick structure, K/W
R_{AL}	Axial thermal resistance towards the endcap, K/W
R_{CR}	Cradle thermal resistance, K/W
R_{E-R}	Thermal resistance between reservoir and evaporator, K
R_{HP}	Capillary heat pipe thermal resistance, K/W
R_{HTC}	High thermal conductivity thermal resistance, K/W
R_{LQ}	Liquid cooling system thermal resistance, K/W
R_{R-s}	Thermal resistance between reservoir and heat sink, K
R_{TS}	Thermosyphon thermal resistance, K/W
R_{TTL}	LHP thermal resistance, K/W
R_{cap}	Endcap thermal resistance, K/W
R_{ci}	Evaporator interface thermal resistance, K/W
R_{coil}	Coil thermal resistance, K/W
R_{cr}	Thermal resistance of cradle, K/W
R_e	Evaporator thermal resistance, K/W
R_{fg}	Heat pipe phase change thermal resistance, K/W
R_f	Conductive thermal resistance of fins, K/W
R_{hp}	Heat pipe thermal resistance, K/W
R_{hs}	Heat sink thermal resistance, K/W
R_{hx}	Thermal resistance of heat exchanger, K/W

R_{pa}	Thermal resistance of wick in adiabatic section, K/W
R_{pc}	Wick thermal resistance in condenser, K/W
R_{pe}	Wick thermal resistance in evaporator, K/W
R_{si}	Condenser interface thermal resistance, K/W
R_{va}	Vapor thermal resistance in adiabatic, K/W
R_{vc}	Vapor thermal resistance in condenser, K/W
R_{ve}	Vapor thermal resistance in evaporator, K/W
R_{wall}	Wall thermal resistance, K/W
R_{wa}	Wall thermal resistance in adiabatic, K/W
R_{we}	Wick structure thermal resistance at evaporato, K/W
R_w	Wall thermal resistance, K/W
Ra_s	Rayleigh number, -
Re_D	Reynolds number, -
Re_L	Reynolds number, -
S_{op}	Optimum vertical plate spacing, m
T_F	Local coolant temperature, K
T_L	Temperature of liquid, K
T_∞	Ambient temperature, °C
T_s	Source temperature, K
T_w	Wall temperature, K
T_{Ai}	Air inlet temperature, K
T_{Ao}	Air outlet temperature, K
T_{BI}	Evaporator temperature, K
T_{BO}	Condenser temperature, K
T_E	Evaporator temperature, K

$T_{R,i}$	Working fluid temperature at the reservoir inlet, K
T_R	Reservoir temperature, K
$T_{c,o}$	Working fluid temperature at the condenser outlet, K
T_{cap}	Cradle cap temperature, °C
T_{ci}	Coolant inlet temperature, K
T_{co}	Coolant outlet temperature, K
T_{cr}	Cradle temperature, K
T_c	Working fluid temperature within the condenser, K
T_{em}	Electric motor temperature, °C
$T_{fl,E}$	Coolant temperature in water-jacket, °C
$T_{fl,R}$	Coolant temperature in radiator, °C
T_{fl}	Coolant temperature, K
T_{hp}	Heat pipe operating temperature, K
$T_{int,e}$	Initial evaporator temperature, K
T_{int}	Initial temperature, K
T_{load}	Thermal load temperature, K
$T_{ref,max}$	Maximum prescribed operating temperature, K
$T_{ref,min}$	Minimum prescribed operating temperature, K
T_{set}	Reference temperature, °C
T_{su}	Cradle surface temperature, °C
T_s	Heat sink temperature, K
T_{v0}	Initial temperature of vapors, K
T_{v1}	Temperature of vapor 1, K
T_{v2}	Temperature of vapor 2, K
T_v	Vapor temperature, K

T_{wall}	Wall temperature, K
T_{wc}	Thermal resistance of condenser wall, K/W
T_{we}	Wall thermal resistance of evaporator wall, K/W
$T_{wf,E}$	Working fluid temperature in evaporator, °C
$T_{wf,R}$	Working fluid temperature in radiator, °C
T_w	Cradle wall temperature, °C
$U_{K,OPT}$	Optimum control inputs , -
U_{mac}	Maximum allowed input , -
U_{min}	Minimum allowed input , -
V_{LQ}	Coolant velocity, m/s
V_{ram}	Ram air velocity, m/s
V_r	Air velocity at radiator, m/s
W	Fin thickness, m
W_r	Radiator width, m
W_{hx}	Heat exchanger's width, m
W_{wc}	Wick structure thermal resistance at condenser, K/W
X	Displacement of liquid, m
X_{cr}	Thickness of cradle, m
Z_{opt}	Optimized fin spacing, m
$\bar{h}$	Convective heat transfer coefficient, $W/m^2.K$
ΔP_b	Pressure loss at bends, Pa
$\dot{Q}_F$	Heat removal due to the fluid circulation, W
$\dot{Q}_{HTC}$	Heat removal through high thermal conductivity material, W
$\dot{Q}_{em}$	Electric motor heat generation rate, W
$\dot{Q}_{fr}$	Heat loss due to friction, W

$\dot{Q}_{ind}$	Heat loss due to induction, W
$\dot{Q}_o$	Heat from outside world, W
$\dot{m}_a$	Air mass flow rate, Kg/s
$\dot{m}_r$	Air mass flow rate at radiator, kg/s
$\dot{m}_w$	Working fluid mass flow rate , kg/s
$\dot{m}_{LQ}$	Coolant flow rate, kg/s
$\dot{m}_a$	Air mass flow rate, kg/s
$\dot{m}_c$	Coolant mass flow rate, kg/s
$\dot{m}_{hx}$	Air mass flow rate at heat exchanger, kg/s
$\dot{q}$	Heat flow, W
μ	Working fluid dynamic viscosity , $N.s/m^2$
τ	Sample time, s
c_f	Coolant specific heat capacity, $J/kg.K$
c_p	Vapor heat capacity at constant pressure, $J/kg.K$
c_r	Radiator heat capacity, $J/kg.K$
c_v	Vapor heat capacity at constant volume, $J/kg.K$
c_{cr}	Specific heat capacity of cradle, $J/kg.K$
$c_{p,CF}$	Specific heat of carbon fiber, $J/kg.K$
$c_{p,a}$	Air heat capacity, $J/kg.K$
$c_{p,a}$	Air specific heat capacity, $J/kg.K$
$c_{p,c}$	Coolant heat capacity, $J/kg.K$
$c_{p,l}$	Liquid heat capacity, $J/kg.K$
$c_{p,w}$	Working fluid specific heat, $J/kg.K$
c_{su}	Cradle surface heat capacity, $J/kg.K$
$c_{v,w}$	Acetone specific heat, $J/Kg.K$

c_v	Specific heat of the acetone vapor, $J/kg.K$
d_e	Coil diameter, m
d_o	Outer diameter, m
d_{in}	Inner diameter, m
d_{pi}	Wick inner diameter, m
d_{po}	Wick outer diameter, m
d_{wi}	Pipe inner diameter, m
d_{wo}	Pipe outer diameter, m
e	Tracking error, K
g	Gravity factor, m/s^2
h	Convective heat transfer coefficient, $W/m^2.K$
h_c	Heat transfer coefficient at condenser, $W/m^2.K$
h_e	Heat transfer coefficient, $W/m^2.K$
h_f	Convection coefficient, $W/m^2.K$
h_r	Convective heat transfer coefficient, $W/m.K$
h_{fg}	Latent heat, J/kg
h_{fin}	Convection coefficient at fin structures, W/m^2
h_{fo}	Forced convection coefficient, $W/m^2.K$
h_{fr}	Free convection coefficient, $W/m^2.K$
h_{hx}	Convective heat transfer coefficient, $W/m.K$
h_{lse}	Heat transfer coefficient in liquid, W/m^2
k	Initial time step, sec
k_A	Air thermal conductivity, $W/m.K$
k_C	Thermal conductivity of condenser, W/m^2
k_E	Latent heat, J/kg

k_e	Coil thermal conductivity, $W/m.K$
k_f	Fin thermal conductivity, $W/m.K$
k_p	Wick thermal conductivity, $W/m.K$
k_s	Heat pipe shell thermal conductivity, $W/m.K$
k_w	Working fluid thermal conductivity, $W/m.K$
k_x	Directional thermal conductivity, $W/m.K$
k_{AL}	Aluminium thermal conductivity, $W/m.K$
k_{CF}	Carbon fiber thermal conductivity, $W/m.K$
k_{CR}	Cradle thermal conductivity, $W/m.K$
k_{HTC}	Thermal conductivity of high thermal conductivity material, $W/m.K$
k_{cu}	Copper thermal conductivity, $W/m.K$
k_{eff}	Effective thermal conductivity for a porous sintered material, $W/m.K$
k_{porous}	Thermal conductivity of porous material, $W/m.K$
k_{sub}	Overall heat transfer coefficient, $W/m.K$
k_w	Thermal conductivity of wick structure, $W/m.K$
l_v	Specific heat of vaporization, J/K
m_e	Mass of evaporator, kg
m_{v1}	Vapor 1 mass, kg
m_{v2}	Vapor 2 mass, kg
q_A	Heat dissipation induced by fan, J
q_c	Radiator heat rejection, J
q_f	Heat rejected due to fan operation, W
q_o	Heat output, J
q_{hp}	Heat pipe heat transfer, J
q_{ram}	Heat rejected due to air ram effect, W

r	Radius, m
r_1	Inner cylinder radius, m
r_2	Outer cylinder radius,m
r_{em}	Electric motor radius, m
r_{ev}	Evaporator distance from centerline, m
r_{inn}	Radial distance from the coil to the center, m
r_{int}	Radial distance from heat pipes to the center, m
r_{int}	Radial distance from heat pipes to the center, m
r_{pa}	Radius of thermosyphon's reservoir, m
r_{pore}	Pore size radius, m
r_{po}	Cylindrical cradle outer radius, m
r_{su}	Cradle outer radius, m
s	Minimum physical spacing between heat pipes, m
t_{TS}	Thermosyphon evaporator wall thickness, m
t_{cap}	Evaporator thickness, °C
v_a	Air velocity, m/s
v_e	Liquid viscosity, m^2/s
v_{air}	Wind velocity, m/s
$v_{c,LQ}$	Pump control signal, v
$v_{c,a}$	Fan control signal, v
v_{veh}	Vehicle speed, m/s
ΔH	Height difference, m
ΔP_g	Static pressure drop, Pa
ΔP_l	Pressure drop due to the friction loss over the liquid line, Pa
ΔP_v	Pressure drop due to the friction loss over the vapor line, Pa

$\Delta P_{PC,c}$	Transmission pressure drop in condenser, Pa
$\Delta P_{PC,e}$	Transmission pressure drop in evaporator, Pa
ΔT	Temperature difference, K
α	Thermal diffusivity, m^2/s
α_i	Coefficient , -
β	Thermal expansion coefficient, $1/K$
β_i	Coefficient , -
ϵ	Pressure loss coefficient, -
η_r	Radiator efficiency, -
η_{TS}	Heat exchanger's efficiency, -
γ	Air flow, CFM, and Ratio of c_p/c_v
λ	Thermal conductivity, $W/m.$
λ_i	Lagrange multipliers, -
μ	Viscosity, $kg/m.s$
ρ_E	Density of evaporator structure, kg/m^3
ρ_a	Air density, kg/m^3
ρ_{CF}	Density of carbon fiber, kg/m^3
ρ_{HTC}	Density of high thermal conductivity material, kg/m^3
ρ_{LQ}	Coolant density, kg/m^3
ρ_{cr}	Density of cradle structure, kg/m^3
ρ_l	Working liquid density, kg/m^3
τ_1	Shear stress, N/m^2

Chapter 1

Introduction

The global energy demand has significantly increased in the last decades, primarily due to dramatic industrial and economic growth in developing countries. Due to the increased demand, United States is required to import a portion of the consuming oil and gas from unstable regions, which creates concerns over the energy security [1]. In terms of energy, gasoline is the dominant transportation fuel, followed by distillates, jet fuel, biofuel, and natural gas. According to the U.S. Energy Information Agency, the U.S. transportation sector consumed 28% of the total U.S. energy which makes it the second-largest energy-consuming sector in the U.S. In 2019, fossil fuels accounted for about 90% of the total U.S transportation sector energy consumption while electric power accounted 1% in this sector. Using more energy-efficient vehicles like hybrid and plug-in electric vehicles will directly impact this large amount of fuel consumption. The mobility shift to electrified vehicles supports the U.S. economy, helps diversify the U.S. transportation fleet and reduces the impact of international supply disruptions. All of these advantages add to our nation's energy security.

In terms of environment, electric and hybrid vehicles can reduce greenhouse

gas emissions [2]. Environmental and economic issues associated with the traditional vehicle design configuration provide compelling motivation to develop an efficient vehicle with minimum reliance on fossil fuel consumption [3]. This impetus has increased the demand for hybrid and electric vehicles to enhance the United States' national security and reduce vehicle exhaust gas emissions. A hybrid electric vehicle (HEV) relies on the electric drive for many instances and consumes less fossil fuel during the operation. This strategy minimizes the demand for importing oil from foreign countries. Likewise, an all-electric vehicle (EV) is solely powered by electric power, which simply can be produced in the U.S. from natural gas, domestic coal, nuclear energy, and renewable resources. In addition, the electric propulsion enables autonomy for the next generation of combat and civilian vehicles.

This paradigm shift to electric propulsion systems creates new thermal challenges for mobility due to the heat loads' design configurations, unique operating conditions, and reduced heat generation rates. Therefore, there is an increasing demand for an advanced thermal management system that can maintain the integrated heat loads (e.g., electric motors, battery packs, on-board electronics, etc.) with optimum power consumption [4, 5].

1.1 Motivation

The prevalence of hybrid vehicles is continuously increasing in urban transportation. However, there are still mobility challenges that must be addressed. The challenges include, but are not limited to, restricted vehicle range, access to charging stations, and practicality in battlefields. Extensive research has been conducted on various types of hybrid vehicles to comply with the demands for improved vehicle performance, mobility, reliability, durability, and survivability for on-road and off-road

driving conditions. A suitable solution must address the constraints mentioned above while offering improved energy efficiency.

The advantages of vehicle electrification are illustrated by comparing hybrid vehicles with traditional vehicles in terms of efficiency, performance, weight, noise, mobility, and safety. Hybrid vehicles feature a rechargeable battery pack in addition to a fuel tank, which enhances the vehicle range on a single fill-up. They offer immediate, fast, and smooth acceleration due to continuous torque with high power to weight ratio delivered by electric motors. Additionally, hybrid vehicles are typically reduced in weight; the hybrid configuration allows the integration of a compact size internal combustion engine instead of using a single giant traditional engine. The new configuration impacts the power requirements due to the lower torque applied to the wheels. Vehicle electrification also offers a silent operating mode and reduces heat-sensing infrared scope detections on the electric mode. This electrification then enables a design that supplies a sufficient amount of electricity for powering non-vehicular applications. These distinct advantages have made hybrid and electric vehicles a sustainable alternative for the next generation of civilian and combat vehicles.

One of the critical design considerations for vehicle electrification is thermal management. For electric motors, the rated and peak torques are limited due to heat accumulated within the housing. The electric current flowing within the stator windings generates a significant amount of heat that must be properly carried out of the housing structure with low energy consumption. Otherwise, it raises the motor's temperature and restricts the operation. Similarly, a battery pack is generating heat while charging or discharging. The excess heat should be removed properly so that the battery pack's temperature is maintained around the target temperature. The temperature regulation secures the battery pack's operation and enhances its

durability over time.

Current cooling practices include conventional liquid cooling systems containing a mechanical belt-driven water pump, fan, radiator, wax-based thermostat, and hoses. The pump generally takes the engine's rotational energy to circulate the coolant fluid between the engine block and the radiator. The coolant can flow between the cylinder heads through built-in fluid passages that typically designed in an engine block. The heated coolant then flows towards the radiator structure, where the heat is dissipated to the ambient surroundings via free or forced convection. Although this approach is effective for internal combustion engines, it may pose unique challenges, including high power consumption, noise generation, and maintenance cost.

In recent developments, the cooling system's mechanical components are replaced with electromechanical actuators such as variable speed electric coolant pump, compressor, radiator fans, and variable position electric coolant valve. These electromechanical components enable the application of model-based controllers to predict heat rejection needs and regulate the actuator's operation to achieve them. Physics-based nonlinear controllers offer significant improvements in both cooling power conservation and component temperature tracking.

This dissertation aims to design and develop an advanced thermal management strategy that addresses the cooling challenges and minimizes the power requirements for hybrid and electric vehicles. The proposed strategy emphasizes passive cooling solutions besides a supplementary smart liquid cooling system. Some of the applications for the proposed thermal management strategy include (i) electric propulsion motors and associated battery banks, (ii) auxiliary power units (APUs) which are often characterized by high power stationary operation, (iii) silent field operation with extensive battery and power electronic usage with passive heat rejection, (iv) retrofit of existing cooling systems to avoid component peak heat loads for improved system

durability, and (v) cooling challenges due to electronic control units placed within engine compartments which result in a severe operating environment.

1.2 Hybrid Thermal Management

An enhancement in designing improved efficiency combustion engines and creating high-efficiency electric motors accelerate the mobility shift to low-cost, environmentally friendly vehicles. The integration of electric motors with battery packs significantly reduces the amount of heat generated during the operations. The heat reduction creates a demand for an advanced thermal management system that accommodates low, medium, and relatively high heat generations with zero to minimum power consumption. An innovative cooling system features a passive heat rejection pathway parallel with a supplementary intelligent liquid cooling system. In many operating scenarios, a passive approach may be adequate to remove heat from the thermal source (e.g., internal combustion engine, electric motor) while a heavy load cycle would demand that both the active and passive systems operate together (i.e., a hybrid mode).

The proposed hybrid cooling system schematic is displayed in Fig. 1.1. The heat source, or thermal load, will be interfaced to the thermal bus by designing an optimized heat transfer surface area to promote increased convective heat transfer performance. The thermal bus material selection will take into consideration the structure flexibility, system weight, packaging issues, and most importantly, thermal properties. The heat sink can be a conventional air-liquid heat exchanger or an air-cooling heat exchanger with micro-channels or finned surface inside. Ambient air circulates through the heat exchanger and discharges the heat to the surroundings. Both natural ram air cooling (passive method) and forced convection cooling (with

an electric fan array) will be investigated. The proposed cooling structure is expected to offer a more compact structure, fewer cooling actuators, improved overall system safety, and higher heat removal efficiency.

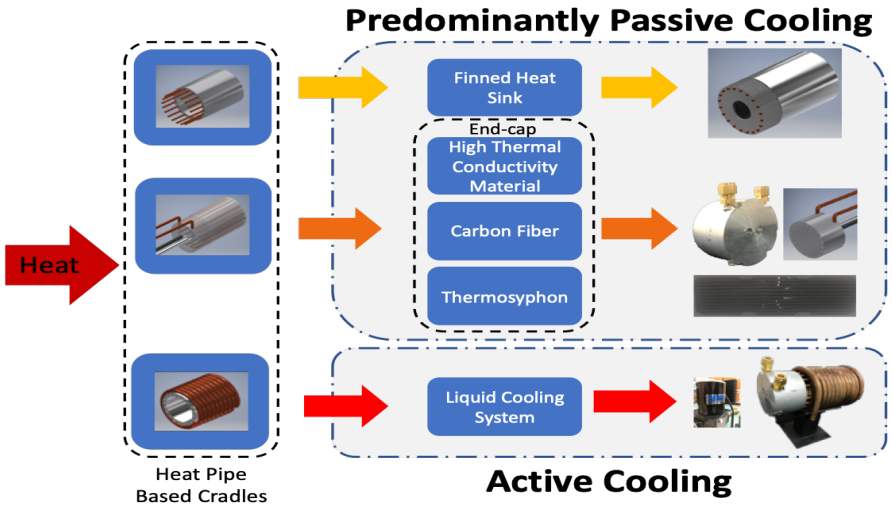

Figure 1.1: Hybrid cooling system architecture with multiple heat transfer pathways.

In the passive approach, an advanced material designed cradle, a two-phase system thermal bus, and a high-efficiency heat exchanger will be optimized to remove heat from the source and reject it to the ambient surroundings. For the active solution, a conventional liquid cooling with radiator and pump will be designed for large heat rejection needs. A real-time control system will engage the active cooling system for optimal heat rejection under heavy loads. As shown in Fig. 1.2, the heat source can be cooled by the conventional and/or passive system. In the latter, the cradle surrounds the component to remove heat, interface with the thermal bus, and then discharge to the ambient through an advanced heat exchanger.

Three immediate strengths are apparent in this proposed cooling system approach. First, an active switching strategy between passive and passive/active based on thermal load will allow for the minimization of cooling system power consump-

tion. Second, in the event of a failure in the conventional system (e.g., coolant hose leak, radiator tube leak), the passive system offers a redundant operating mode for continued operation at reduced thermal loads. Third, the minimization of required convective heat transfer (e.g., ram air flow) about the component, initially electric motors and power electronics, for supplemental cooling enables creative vehicle component placement options and optimizations.

The recognition that a passive cooling approach for large prolonged thermal loads, especially large electric motors and internal combustion engines, will be insufficient leads to a hybrid design that also features a conventional radiator-pump configuration. Accordingly, a control strategy will be incorporated to operate the three electro-mechanical actuators (e.g., radiator fans, coolant pump, and passive heat exchanger fans). In this manner, the fan and pump variable speeds (0-100%) can be regulated through the monitoring of system temperatures, requested power for vehicle propulsion and electrical equipment, and ambient conditions. A nonlinear control structure will be developed that adjusts the fan and pump speeds with sensor data to minimize power consumption while meeting the thermal demands for each component per various military operating scenarios, including convoy escort and urban assault. In the event of a conventional cooling system failure, a "limp home" mode will be identified that will allow continued operation at reduced performance levels to enable mission continuation.

1.3 Research Objective and Approach

A series of objectives are completed throughout this dissertation to develop mathematical models, analysis toolsets, and experiments to study and investigate the hybrid cooling system performance for electric vehicle applications. The research

objectives include:

- Propose a novel vehicle cooling system architecture that features a thermal bus structure created with advanced materials and devices.
- Design an innovative thermal interface cradle structure per given application to channel the emitted heat to the thermal bus structure for rejection to surroundings.
- Emphasize passive, active, and hybrid cooling strategies to minimize the thermal system power consumption.
- Develop mathematical models to evaluate the cooling system's performance. Validate the mathematical model through a series of experimental testing for steady-state and transient inputs.
- Minimize cooling system power usage with respect to the operating cycles and ambient conditions using supervisory control algorithms.
- Optimize the cooling system design configuration for a vehicle placement with respect to space limitations, heat-dissipating requirements, and operating conditions.

1.4 Dissertation Organization

The dissertation offers several cooling system architectures for electric vehicle thermal management. Each design is followed by a mathematical model that evaluates the steady-state and transient thermal responses of the integrated heat load(s) and the cooling system. The designs and the mathematical models are then validated

through a series of thermal tests for several driving cycles. Then, a nonlinear optimization approach optimized the cooling system configuration using the validated mathematical model for a particular application. Next, a complete numerical and experimental study designed and developed four real-time controllers to engage the active cooling system for precise, stable, and predictable temperature regulation of the electric motor and reduced power consumption.

Chapter two proposes a hybrid cooling system strategy for electric and hybrid vehicle. The integration of advanced materials in thermal bus structure is studied. A closed-loop pulsating heat pipe passively picks up the heat from a heat source (e.g., internal combustion engine, electric motor, battery pack, power electronic, etc.) and delivers the collected heat to a remote heat exchanger. A numerical modeled describes the cooling system's thermal behavior subject to a specific transient heat input. The simulation results indicated that the heat dissipation rate is significantly influenced by heat pipe length, diameter, and the temperature difference between the heat load and the bus.

Chapter three designs a hybrid cooling system featuring multiple heat rejection pathways for an in-hub electric motor used in electric vehicles. The cooling system contains a thermal bus created from a loop heat pipe, carbon fiber, high thermal conductivity material besides a conventional liquid cooling system to reject the excess heat to the ambient surroundings. A representative mathematical model studies the thermal stability, heat dissipation capabilities, and external power requirements for several driving cycles. The numerical results show that the heat transfer capabilities of high thermal conductivity and carbon fiber are limited for long-distance heat transfer applications, but the loop heat pipe could provide significant improvements for passive cooling.

Chapter three explains an experimental study conducted to evaluate the math-

ematical model developed for the hybrid system featuring multiple passive cooling channels with a traditional liquid cooling system. The laboratory experiment includes a thermal cradle, multiple heat rejection pathways, and heat exchangers to collect, transfer, and dissipate the generated heat to the ambient surroundings. The thermal bus design incorporates carbon fiber, high thermal conductivity material, and thermosyphon with a supplementary conventional active cooling system. A computer-controlled emulated electric motor is applied to the cooling system to investigate the thermal responses for two different operating scenarios. The experimental test results demonstrate that up to 93% energy consumption can be saved during a light load while the electric motor maintains a target core temperature of 70°C.

Chapter four investigates an innovative hybrid cooling system using heat pipes in a radial fashion embedded in thermal cradle structure for an electric motor. The cooling system's performance is explored through numerical modeling and benchtop experimental testing. The passive mode of heat transfer includes multiple capillary heat pipes embedded within the electric motor cradle structure. The heat pipes collect the generated heat from the electric motor housing structure for transferring to a local heat exchanger attached to the electric motor. A supplemental conventional cooling system, composed of a variable speed coolant pump and radiator fan, is then supplied to the electric motor through a copper pipe coiled around the thermal cradle. The hybrid cooling system is mathematically modeled using a lumped parameter approach, and the dynamic behavior of the system is examined. Then, an experimental setup was designed and fabricated in the laboratory to validate the numerical results. A good agreement between the numerical and experimental results are observed. The results compare the temperature, heat flux, and power consumptions for the hybrid cooling system subject to 250VA heat input. The results indicate that integrating the passive cooling system could save up to 33% of power usage while the electric motor

operating condition is secured.

Chapter five optimizes an electric motor cooling system design configuration for a light-duty electric vehicle. The design variables are the motor cradle volume, the number of heat pipes, the coolant reservoir dimensions, and the heat exchangers' sizes. The cost function represents the cooling system size, weight, and thermal performance. The constraints are imposed based on vehicle size and the maximum cooling capacity required per operating cycle. The numerical study demonstrate that a 50% mass reduction could be achieved for a continuous 12kW heat-dissipating demand while the electric motor operating temperature has remained below 65°C. The weight reduction could also significantly impact the amount of torque applied to the electric motor, which reduces the overall battery usage. The mathematical model establishes a design tool for system sizing for electric motor propelled vehicles.

Chapter six develops an intelligent liquid cooling system that offers on demand cooling in a hybrid configuration with a passive system. The conventional liquid cooling system is initially upgraded with a variable frequency drive, a variable speed AC fan and DC pump, and a real-time controller. Once it is incorporated with a passive cooling pathway, the advanced cooling system enables precise on-demand cooling with optimal coolant pump and radiator fan speeds to minimize the cooling system power consumption, operating time, and noise generation with an improved temperature tracking system. The study developed four real time controllers based on nonlinear model predictive controller, classical PI control, sliding mode control, and stateflow algorithms. The real-time controllers will engage the active cooling system for optimum operating under heavy load. An experimental setup is designed and established to compare the controllers' performance in terms of overall power consumption and temperature tracking. The experimental results indicate that the nonlinear model predictive control method is the most efficient method, which could

reduce the fan power consumption by 73% for a 5% increase in the pump power usage compared to classical control for a specific 60-minute driving cycle.

Overall, the presented research study aims to develop the basis for making a paradigm shift in electric vehicle thermal management systems. Electrified propulsion system with an electric motor, battery packs, and onboard electronics created new thermal challenges which need to be addressed for the next generation of ground vehicles. The dissertation introduces a hybrid cooling strategy that incorporates a passive cooling solution(s) besides an active cooling system in a thermal bus concept. When properly designed, the hybrid thermal management system relies on the passive mode for a low to moderate heat generation rate, while the coolant-based system offers supplemental cooling for immoderate heat-generating instances. The conducted numerical and experimental studies demonstrate the advantage of using a hybrid cooling strategy with the developed nonlinear controllers for military and civilian electric vehicle applications.

Chapter 2

A Thermal Bus for Vehicle Cooling Applications - Design and Analysis

2.1 Abstract

Designing an efficient cooling system with low power consumption is of high interest in the automotive engineering community. Heat generated due to the propulsion system and the on-board electronics in ground vehicles must be dissipated to avoid exceeding component temperature limits. In addition, proper thermal management will offer improved system durability and efficiency while providing a flexible, modular, and reduced weight structure. Traditional cooling systems are effective but they typically require high energy consumption which provides motivation for a paradigm shift. This study will examine the integration of passive heat rejection pathways in ground vehicle cooling systems using a "thermal bus". Potential solutions include heat pipes and composite fibers with high thermal properties and light weight properties to move heat from the source to ambient surroundings. An initial case study focuses on the integration of heat pipes in a thermal bus to transfer heat

from the thermal load (e.g., internal combustion engine, electric motor, battery pack, power electronic, etc.) to the heat exchanger. A mathematical U-shaped pulsating heat pipe model is used to numerically describe the thermal behavior of a heat pipe based thermal bus. This is combined with models for a "cradle" to move energy from the load to the bus and a model for a heat exchanger to ambient. Simulation results indicate that the heat dissipation rate is significantly influenced by heat pipe length, diameter and the temperature difference between the heat load and the bus. The integration of this heat pipe based thermal bus within an active / passive cooling system will be demonstrated in future work.

2.2 Introduction

Hybrid powertrains generate heat through the operation of the combustion engine, electric motors, generator, battery pack, and on-board electronics for propulsion. An important consideration is the cooling of these components to maintain the temperature within prescribed ranges. The emphasis on fuel consumption targets has necessitated a focus on power minimization including the cooling system in military vehicles [6–9] . A variety of thermal management strategies exist as shown in Fig. 2.1. The most common cooling system design features an ethylene glycol liquid cycle radiator with fan, thermostat valve, pump, hoses, and engine block water jackets. Air cooled engines and components may be optional for lower heat loads. A novel design integrates both passive and active features that can be selected based on the operating conditions.

The monitoring and control of vehicle propulsion system temperatures can help ensure mission viability. Friction losses of engine parts vary as a function of lubricant and coolant temperatures with 90°C to 100°C the suggested oil tempera-

ture range [10]. The battery pack performance will decrease if its temperature is not properly maintained. Likewise, electrical components must be operated within their rated temperature range. In previous studies, cooling system architectures and their energy consumptions have been investigated for different operation conditions. Park and Jung [11] examined the thermal behaviors of three different cooling system designs to identify power consumption factors. Bayraktar [12] integrated computational fluid dynamics to study cooling system thermal behaviors. Tao and Wagner [8,13,14] adopted nonlinear control theory to regulate the electro-mechanical actuators operation schedules in engines. Wang et al. [6, 15] established mathematical models to optimize convection-based heat transfer by regulating actuator (e.g., fans, pump, and smart valve) operation. The radiator fan(s) consumes the greatest power within the engine cooling system [7].

The integration of energy-efficient passive heat rejection pathways in parallel with an active cooling for ground vehicles has not been fully investigated. An opportunity exists to innovate on the conventional cooling system to realize a flexible design that can accommodate increasing thermal loads and offer a "silent sentry" operational mode. The inclusion of high conductive materials/devices (e.g., heat pipes, composite fibers, alloys, etc.) may offer a potential solution for passive heat rejection within a smart architecture to move heat from the heat load(s) to ambient surroundings. In this study, the term "passive heat rejection pathways" refers to heat transfer modes which do not require vehicle supplied power. A starting point for a hybrid passive-active cooling system design will be the introduction of heat pipes. Loop heat pipes have been recognized as two-phase passive devices with high effective thermal conductivity which are capable of transferring heat at any orientation with respect to gravity [16]. Heat pipes are utilized in various thermal management applications to increase thermal conductivity and temperature distribution uniformity. For ground

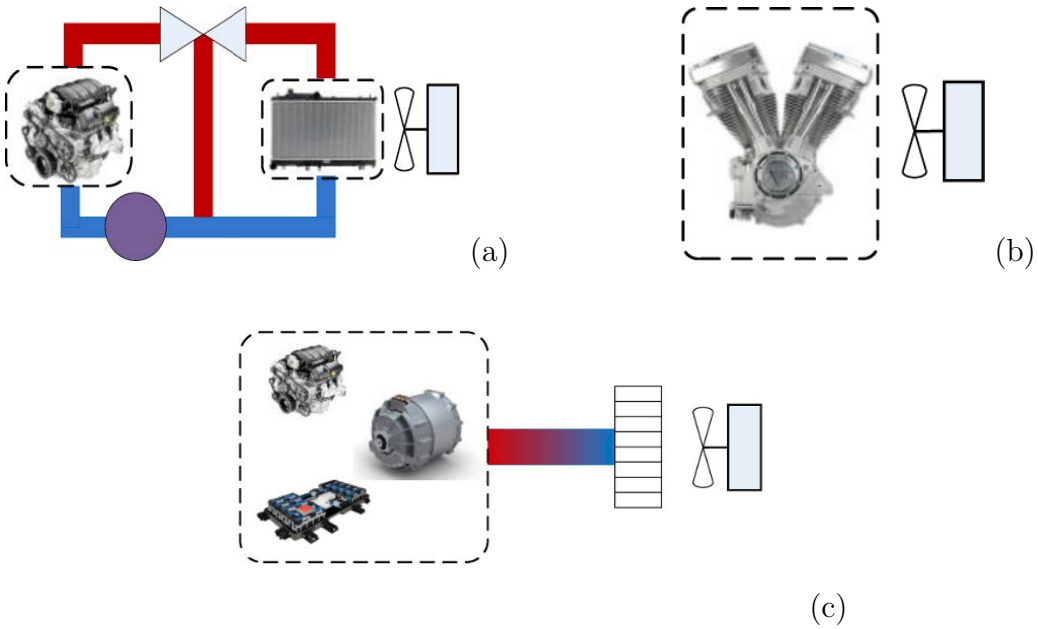

Figure 2.1: Overview of cooling strategies - (a) Traditional liquid system, (b) Forced convection system, and (c) Active/passive thermal bus

vehicles, heat pipes have been used to control component and compartment temperatures. Rao et al. [17] implemented an electric vehicle heat pipe based thermal management system to regulate the Li-ion battery temperature. El-Sharkawy [18] used heat pipes to control the catalytic converter temperature. Hendricks [19] introduced heat pipes to cool passenger cabins and reduce the A/C system operation schedule time. Lastly, Burban et al. [20] investigated the performance of pulsating heat pipes for vehicle cooling system applications in terms of number of turns and working fluids for various driving conditions.

The heat generated over the combustion process, propulsion and mechanical friction in ground vehicles must be managed effectively to ensure the system's durability and performance. An advanced automotive thermal management system is required to avoid exceeding the component's working temperature limits with minimum energy consumption in ground vehicles and enhance the engine performance. In

this paper, the integration of passive heat rejection pathways in ground vehicle cooling systems is examined using a heat pipe based thermal bus with an attached cradle and heat exchanger with electric fan. The remainder of the paper is organized as follows. Section 2.3 introduces the thermal bus concept with cradle and heat exchanger. The corresponding mathematical model is presented in Section 2.4 to describe the dynamic behavior. Representative numerical results are discussed in Section 2.5 for a convoy escort driving cycle. The conclusion and Nomenclature List are contained in Section 2.6, respectively.

2.3 Hybrid Cooling System Strategy

Hybrid ground vehicles are typically composed of an internal combustion engine with electrical motor, electro-mechanical components, and accompanying battery packs in either a parallel or series configuration. The powertrain components generate a significant amount of heat that must be dissipated through the cooling system. In some instances, the heat rejection may be modest which reflects either a sentry type operating mode or low speed high efficiency electrical motor propulsion. For this case, a passive thermal management system may be designed to handle the cooling needs. The proposed advanced cooling system structure features a passive cooling heat rejection pathway associated with a smart active cooling system structure which operates based on the heat rejection needs. The recognition that a passive cooling approach for large prolonged thermal loads, especially internal combustion engines, will be insufficient leads to a hybrid design that also features a conventional radiator-pump configuration.

The individual heat loads may be interfaced to a thermal bus through an optimized surface area called a “cradle”. The cradle must be designed based on each

individual heat load heat generation rate, operation conditions, and shape. Components with low convective heat transfer to surroundings may benefit by large cradle coverage. A cradle with high thermal conductivity and small thermal expansion provides the needed thermal connection between the heat sources and thermal bus. The external surface of the cradle will be encased in a low conductivity insulating material to route energy in the desired direction.

The thermal bus transports heat from the cradle to the radiator with attached fan(s). The thermal bus is defined as any devices, including passive or active heat transfer pathways, used to transfer heat from a given entity. For instance, devices using liquid based cooling to passive advanced materials with high thermal conductivity. The proposed thermal bus concept features a computer-controlled liquid cooling system which give the system capabilities to handle high heat removal needs if the temperatures of the heat load components become excessive. Figure 2.2 shows a concept of a hybrid cooling system which benefits from passive cooling system in parallel with active cooling strategy. High conductive materials such as composite fibers, alloys, phase change materials as well as high thermal conductive passive devices like heat pipes will be implemented into the passive cooling strategy. Heat will be transferred between two points with temperature gradient. Studying high thermal conductive materials provides the foundation of understanding their thermal performance. Similarly, heat pipe structures are highly efficient systems which can be integrated in a wide variety of cooling applications which essentially extends their functional possibilities in practical applications.

The integration of a high efficiency heat exchanger with an optional electrical fan(s) will increase the efficiency of the cooling system. A control strategy will be needed to operate the heat exchanger fan(s) through the monitoring of system temperatures and minimize power consumption while meeting the thermal demands

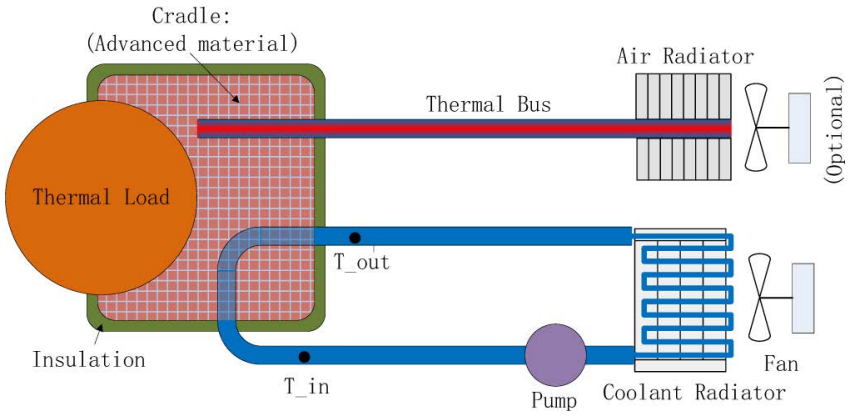

Figure 2.2: Advance hybrid cooling system design.

for each component per various operating scenarios. Overall, the proposed cooling system may benefit from a lower weight system structure, enhanced flexibility and reliability, silent mode operation, high effective thermal conductivity, and smaller external power consumption.

2.4 Mathematical Model

Several mathematical models have been developed for the thermal bus system from the heat load, to the cradle to the heat exchanger. These include several models for pulsating U-shaped heat pipes (PHP) to study the impacts of various design parameters such as initial conditions, diameter, charge ratio, temperature difference and working fluid on the oscillatory behavior and performance of heat pipes [21, 22]. Heat pipes can be included as both parts of the cradle and/or the thermal bus. Results have shown the heat pipe diameter and temperature difference are effective factors on heat pipe heat transfer rates. It's been proven that heat is mainly transferred due to the exchange of sensible heat compared with latent heat [21]. Ma et al. [23] studied the effect of nano-fluid on oscillating heat pipe heat transfer rate. They proved

that using nano-fluid as working fluid results in a significant temperature difference reduction between the evaporator and condenser sections in oscillating heat pipes. Yang et al. [24] have examined heat pipes in terms of light weight and performance and highlighted some limitations to the application of light weight material in heat pipes.

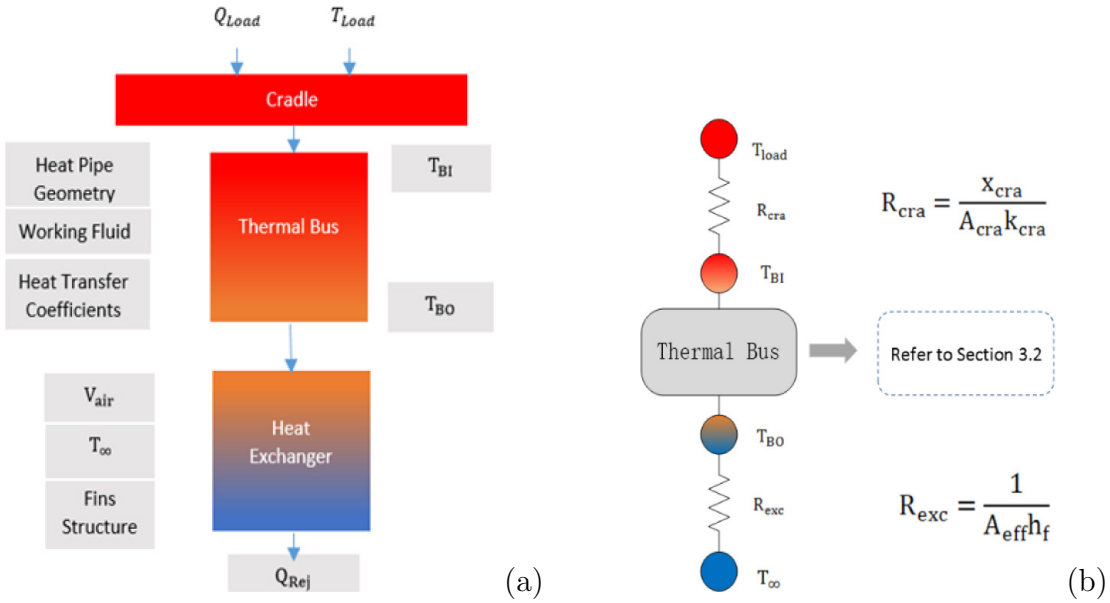

Figure 2.3: Integration of cradle, thermal bus, and heat exchanger in the (potentially hybrid) cooling system - (a) System architecture and (b) Temperature nodal network.

A reduced order passive cooling system containing a heat load, cradle, thermal bus, and a finned heat exchanger is numerically formulated and analyzed to describe the thermal behavior over the operation cycle. Figure 2.3(a) shows the flow of thermal energy and Fig. 2.3(b) displays the corresponding nodal network. The heat generation rate of the heat load will be set based on each heat load individually. The e-motor generates a significant amount of heat in comparison with the other heat loads in the ground vehicle. Therefore, a passive cooling system with the associated e-motor with respect to an actual driving cycle is investigated in this study.

2.4.1 Cradle Structure

The heat load cradle is used to efficiently transfer heat from the thermal load to the thermal bus (in this case the evaporation section of the pulsating heat pipe). High thermal conductivity metals are widely used as the media to transfer heat from the thermal load to the evaporation section of the heat pipe. Heat pipe embedded copper bases are widely used to transfer heat from microelectronics. A heat pipe-based cradle can operate to dissipate heat from the heat load to the thermal bus. The configuration of the cradle is dependent on the structure of the thermal load. The cradle is assumed to be ideal in the current simulation so that the cradle can be considered as a simple thermal resistance so that

$$R_{cr} = \frac{x_{cr}}{A_{cr} k_{cr}} \tag{2.1}$$

where R_{cr} is the thermal resistance of the cradle, x_{cr} is the thickness of the cradle, A_{cr} is the surface area vertical to the heat flow direction, and k_{cr} is the thermal conductivity of the cradle. The entire system temperature of the cradle selected as the output such that

$$T_{load} = \frac{Q_{load}}{R_{cr}} + T_{BI} \tag{2.2}$$

where T_{BI} is the thermal bus input temperature.

2.4.2 Thermal Bus

The thermal bus is composed of multiple U-shaped pulsating heat pipes which is in thermal contact with the heat load. The pulsating heat pipes are partially filled with working fluid. The working fluid is specified based upon the rated operation

temperate range of the intended heat load, in this case an e-motor. Once the heat load generates heat, the vapor pressure quickly increases within the evaporator section. The pressure difference between the vapor plug and liquid plug keeps the vapor in one end and moves the liquid toward the other end of the pipe. The liquid section condenser releases the latent heat toward the ambient or a heat exchanger. The vapor is always exposed to the liquid at the split line where vapor continuously condenses, or liquid vaporizes due to the temperature difference between the evaporator and condenser sections. The heat pipe condenser section is always exposed to ambient surrounding or attached to an external heat sink. In the developed numerical model, the heat pipe based thermal bus is attached to a heat exchanger. Figure 2.4 shows a schematic diagram of a pulsating heat pipe where L_h is the evaporator length and L_c is the condenser length. Since it is partially filled there are both liquid and vapor in the tube. The straight tube shown in Fig. 2.4b illustrates the condenser, evaporator, and total length of the pulsating heat pipe model.

For practical purposes, the pulsating heat pipe model [17] is applied hereinafter for each single heat pipe. A summary of the model is presented below and further details can be found in the citation. For present purposes a heat pipe based model for only the thermal bus is developed (while future work could incorporate heat pipes into the cradle and/or heat exchanger).

Establishing the mathematical model of the U-shaped pulsating heat pipe needs six fundamental assumptions to simplify the problem: A.1: Vapors follow the ideal gas law. A.2: Liquid is incompressible. A.3: Mass transfer between the liquid and vapor is small and does not affect the liquid's total mass. A.4: Evaporation and condensation heat transfer coefficients are constants. A.5: Evaporation only happens when liquid is in the evaporator section and condensation only happens when vapor is in the condenser section. A.6: The heat pipe is ideally insulated. Once the heat

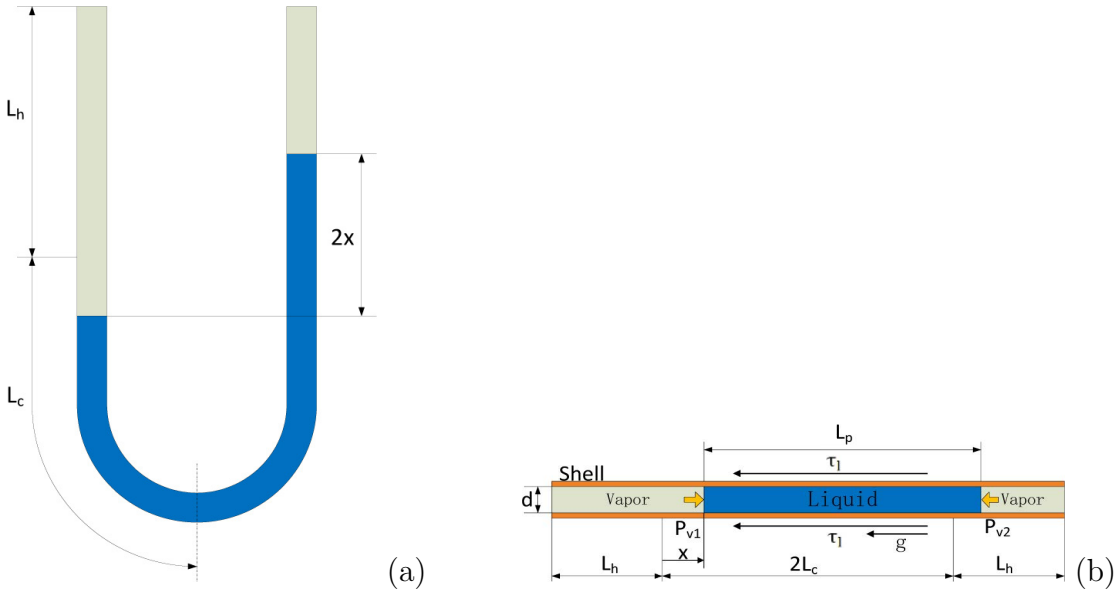

Figure 2.4: A diagram of a U-shaped pulsating heat pipe - (a) U-shaped pulsating heat pipe, and (b) Control volume of a liquid slug.

source generates heat, the working fluid is accumulated in the liquid condenser section and vapor occupies the volume to the evaporator section as shown in Fig. 2.4(a). The liquid slug can be assumed as a particle in tube since the liquid is in-compressible and the mass transfer between the liquid and vapor sections is assumed negligible. The vapor apply force toward the liquid section from both vapor sides (shown by yellow arrays in Fig. 2.4(b) due to the pressure difference created due to their temperature difference between the condenser and evaporator sections. Other forces that influence the fluid motion include shear stress that acts on the shell and gravity if the tube is oriented in a vertical direction. The momentum equation of the liquid is expressed based on Newton second law:

$$\rho_l L_p A \frac{d_{in}^2 x}{dt^2} = (p_{v1} - p_{v2} - \Delta P_b)A - 2\rho_l g A x - \pi d L_p \tau_1 \tag{2.3}$$

where ρ_l denotes the density of the liquid,L_p is the length of the liquid, and p_{v1} as

well s p_{v2} represent the pressure of the left hand and right-hand sides of the vapor, respectively. The term ΔP_b corresponds to the pressure loss at the bend. The cross section area of the heat pipe is denoted by A while d_{in} is the tube diameter. The shear stress and the pressure loss due to the bend in the pipe are expressed as follows:

$$\tau_1 = \frac{8\rho_l v_e}{d}\frac{dx}{dt} \tag{2.4}$$

$$\Delta P_b = \begin{cases} 1/2\zeta\rho_l(\frac{dx}{dt})^2, & \frac{dx}{dt} > 0 \\ -1/2\zeta\rho_l(\frac{dx}{dt})^2, & \frac{dx}{dt} < 0 \end{cases} \tag{2.5}$$

where ζ is the pressure loss coefficient and v_e denotes the liquid viscosity.

Eq. (2.3) can be rearranged as Eq. (2.6):

$$\frac{d^2x}{dt^2} + \frac{32v_e}{d^2}\frac{dx}{dt} + \frac{2g}{L_p x} = \frac{\Delta P}{\rho L_p} \tag{2.6}$$

Applying the first law of thermodynamics to the energy equations of the vapor plugs, the following equations are achieved:

$$\frac{d(m_{v1}c_v T_{v1})}{dt} = \frac{c_p T_{v1} dm_{v1}}{dt} - p_{v1}A\frac{dx}{dt} \tag{2.7}$$

$$\frac{d(m_{v2}c_v T_{v2})}{dt} = \frac{c_p T_{v2} dm_{v2}}{dt} + p_{v2}A\frac{dx}{dt} \tag{2.8}$$

Solving partial derivative of Eqs. (2.7) and (8) with respect to Eq. (2.9) and simplifying the results, Eqs. (2.7) and (2.8) can be rearranged as follows:

$$c_p - c_v = R \tag{2.9}$$

$$m_{v1}c_v\frac{d(T_{v1})}{dt} = RT_{v1}\frac{dm_{v1}}{dt} - p_{v1}A\frac{dx}{dt} \tag{2.10}$$

$$m_{v2}c_v\frac{d(T_{v2})}{dt} = RT_{v2}\frac{dm_{v2}}{dt} + p_{v2}A\frac{dx}{dt} \tag{2.11}$$

The equations of vapors are simplified with respect to ideal gas law as:

$$p_{v1}A(L_h + x) = m_{v1}RT_{v1} \tag{2.12}$$

$$p_{v2}A(L_h - x) = m_{v2}RT_{v2} \tag{2.13}$$

Differentiating Eqs. (12) and (13) leads to:

$$\frac{dp_{v1}}{dt}A(L_h + x) + \frac{dx}{dt}p_{v1}A = \frac{(dm_{v1})}{dt}RT_{v1} + \frac{dT_{v1}}{dT_{v1}}m_{v1}R \tag{2.14}$$

$$\frac{dp_{v2}}{dt}A(L_h - x) + \frac{dx}{dt}p_{v2}A = \frac{dm_{v2}}{dt}RT_{v2} + \frac{dT_{v2}}{dT_{v2}}m_{v2}R \tag{2.15}$$

Substituting Eq. (2.10) into Eq. (2.14), and Eq. (2.11) into Eq. (2.15):

$$RT_{v1}\frac{dm_{v1}}{dt} = A\frac{c_v}{c_p}(L_h + x)\frac{dp_{v1}}{dt} + p_{v1}A\frac{dx}{dt} \tag{2.16}$$

$$RT_{v2}\frac{dm_{v2}}{dt} = A\frac{c_v}{c_p}(L_h - x)\frac{dp_{v2}}{dt} + p_{v2}A\frac{dx}{dt} \tag{2.17}$$

Defining $\gamma = c_p/c_v$ and integrating Eqs. (2.16) and (2.17), the mass of vapors

can be expressed as:

$$m_{v1} = Cp_{v1}^{1/\gamma}(x + L_h) \tag{2.18}$$

$$m_{v2} = Cp_{v2}^{1/\gamma}(x - L_h) \tag{2.19}$$

where C is an integration constant. The integration constant is constant in the tube since the tube is assumed to be symmetric. The vapor temperatures are acquired by substituting Eq. (2.18) into Eq. (2.12), and Eq. (2.19) into Eq. (2.13):

$$T_{v1} = (A/CR)p_{v1}^{(\gamma-1)/\gamma} \tag{2.20}$$

$$T_{v2} = (A/CR)p_{v2}^{(\gamma-1)/\gamma} \tag{2.21}$$

The equations of mass change rate between the liquid and vapor slugs are expressed as follows:

$$dm_{v1}/dt = \begin{cases} -h_c\pi dx(T_{v1} - T_{BO})/h_{fg}, & x > 0 \\ h_e\pi d(L_h + x)(T_{BI} - T_{v1})/h_{fg}, & x < 0 \end{cases} \tag{2.22}$$

$$dm_{v2}/dt = \begin{cases} h_e\pi dx(T_{v2} - T_{BO})/h_{fg}, & x > 0 \\ h_e\pi d(L_h - x)(T_{BI} - T_{v1})/h_{fg}, & x < 0 \end{cases} \tag{2.23}$$

where h_{fg} is the latent heat coefficient. The final equations for the latent heat can be obtained by:

$$Q_{v1} = \frac{dm_{v1}}{dt}h_{fg} \tag{2.24}$$

$$Q_{v2} = \frac{dm_{v2}}{dt} h_{fg} \tag{2.25}$$

The total latent heat in and out of the heat pipe can be calculated by adding the latent heat in vapor 1 and vapor 2 together:

$$Q_{v_{in}} = Q_{v1} + Q_{v2}, \qquad When \;\; Q_{v1} > 0, Q_{v2} > 0 \tag{2.26}$$

$$Q_{v_{out}} = -Q_{v1} - Q_{v2}, \qquad When \;\; Q_{v1} < 0, Q_{v2} < 0 \tag{2.27}$$

It is essential to determine the temperature field of the liquid slug in the heat pipe to acquire the sensible heat. Since the liquid temperature varies with both time and location a small unit liquid slug was analyzed. It is assumed that the temperature of liquid equals the vapor temperature at their interface. Figure 2.5 shows the heat transferred considering a small unit length of the liquid slug.

The total heat in this unit element can be expressed as $\rho_l c_{p,l} \frac{dT_l}{dt}$, heat transferred from the left end to the right end can be expressed as $\lambda A \frac{dT_l}{dx}$, heat transferred between liquid and the outside surroundings which could be either the heat exchanger or the cradle can be expressed as $h_{lse} \pi d dx (T_l - T_w)$ where T_w is the wall temperature. It could be either the thermal bus input temperature $T_B I$ in the evaporator section or the heat exchanger temperature in condenser section. As a result, the temperature of the liquid can be written as:

$$\rho_l c_{p,l} \frac{dT_l}{dt} = \lambda \frac{d}{dx} (\frac{dT_l}{dx} - \frac{4 h_{lse}}{d(T_l - T_w)} \tag{2.28}$$

where ρ_l and $c_{p,l}$ are the liquid's density and heat capacity, respectively. And, λ represents the thermal conductivity.

The sensible heat transfer can be expressed by Eqs. (2.29) and (2.30) once the liquid temperature distribution is obtained:

$$Q_{sen_in} = \begin{cases} \int_{L_p}^{L_p-|x|} h_{lse}\pi d(T_{BI} - T_l)dx, & x > 0 \\ \int_0^{|x|} h_{lse}\pi d(T_{BI} - T_l)dx, & x < 0 \end{cases} \tag{2.29}$$

$$Q_{sen_{out}} = \begin{cases} \int_0^{|x|} h_{lse}\pi d(T_l - T_{BO})dx, & x > 0 \\ \int_{|x|}^{L_p} h_{lse}\pi d(T_l - T_{BO})dx, & x < 0 \end{cases} \tag{2.30}$$

After the sensible heat is acquired, the total heat transferred by this heat pipe based thermal bus can be calculated by adding the sensible heat and the latent heat together:

$$Q_{TTL} = Q_{v_{out}} + Q_{sen_{out}} \tag{2.31}$$

The heat removal by the thermal bus then can be expressed by multiplying by the number of heat pipes, n:

$$Q_{rem} = Q_{TTL}n \tag{2.32}$$

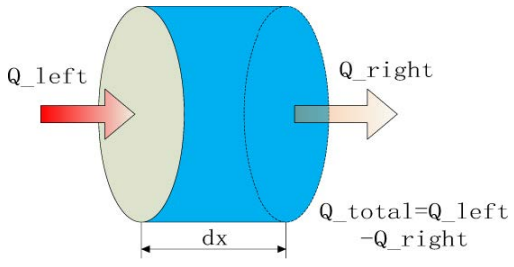

Figure 2.5: Diagram of heat transferred in a unit length of a liquid slug.

2.4.3 Heat Exchanger and Fan Assembly

Implementing a heat exchanger into the cooling structure will increase the system capabilities in dissipating heat to ambient surrounding. Shah [25] explored the recent improvements in heat exchanger and radiator designs. An ideal heat exchanger should be able to dissipate the heat through natural convection in normal conditions while an active cooling cycle is always available to start operating once temperatures become excessive. The advanced cooling system is essentially featured with a mechanism which operates the active mode in harsh conditions. In this manner, the passive heat exchanger always cools the system with low energy consumption while the active mode can handle high heat rejection needs once heat rejection requirements exceed passive heat rejection mode capacity. The proposed advanced heat exchanger benefits of fin structure which enhances heat rejection capacity. Fin structures can greatly promote the heat transfer by enlarging the heat transfer surface area. The governing equations for the heat exchanger are set up as follows once the air velocity due to the fan operation, angel of attack and the speed of the vehicle are determined:

$$q_f = \frac{dm_f}{dt} c_{p,a}(T_{BO} - T_\infty) \tag{2.33}$$

Here, q_f corresponds to the heat rejected due to the radiator fan operation, $m_f$denotes radiator fan air mass flow rate, $T_{BO}$and T_∞ are radiator and ambient temperatures, respectively, and $c_{p,a}$ corresponds to heat capacity of the air. The air ram effect is:

$$q_{ram} = f(v_{veh}, v_{air}, \alpha) \tag{2.34}$$

where q_{ram} denotes the heat rejected due to ram effect, v_{veh} represents the vehicle speed, v_{air} is the wind velocity, and α corresponds to the attack angel of the wind

with respect to the position of the radiator. The radiator temperature is calculated as:

$$\frac{dT_{BO}}{dt}c_r = Q_{rem} - q_f - q_{ram} \tag{2.35}$$

where $\frac{dm_c}{dt}$ is the coolant mass flow rate, and c_r and $c_{p,c}$denote the heat capacity of the radiator and the coolant, respectively, and T_{BO} represents the radiator temperature.

In the thermal bus output section an air heat exchanger with fin structures is applied to enhance heat rejection. And a fan can be used to blow air to increase heat transfer. Fin structures can greatly promote heat transfer by enlarging the heat transfer surface area. When the fin dimensions are determined the forced convection coefficient can be approximately expressed by:

$$h_f = 10.45 - v_{air} + 10(v_{air})^{1/2} \tag{2.36}$$

where v_{air} is the air velocity. Fin efficiency theory is adopted to calculate the fin effective area:

$$A_{eff} = A_t(1 - (NA_f/A_t)(1 - \eta_f)) \tag{2.37}$$

in which A_f is the area for one fin A_t is the total fin areaη_f is the fin efficiency [10]. The thermal resistance of the heat exchanger then can be acquired based on Eqs. (26) and (27):

$$R_{exc} = \frac{1}{A_{eff}h_f} \tag{2.38}$$

The heat rejection then can be calculated by:

$$Q_{rej} = \frac{T_{BO} - T_{\infty}}{R_{exc}} \tag{2.39}$$

The above set of governing equations thereby describe the overall system performance from heat load to energy transfer to ambient.

2.5 Case Study – Electric Motor with Passive Thermal Management System

A numerical simulation study was conducted to evaluate the thermal behavior of an electric motor with integrated passive cooling system. The complete cooling system has been modeled and simulated including the heat load, cradle, passive thermal bus, and a finned air-cooled heat exchanger with electric fan. This case study will examine the system performance for representative driving scenarios. The convoy escort, shown in Fig. 2.6, displays the vehicle speed and electric motor heat generation as functions of time. This simulated driving profile corresponded to a group of military vehicles traveling at moderate speed with some variations in power train demand. The heat generation of electric motors rate does not typically exceed 3 kW over normal driving conditions in hybrid vehicles for drive cycles analyzed in this study, but sudden accelerations may influence the heat generation rate significantly.

Figure 2.7 displays the structure of the simulated passive cooling model. The heat is initially channeled to the thermal bus through a designed aluminum cradle surrounding the electric motor. A wide variety of high thermal conductive materials and passive devices were considered. A heat pipe based thermal bus is the preferred initial solution for the thermal bus studies due to the high heat flux transport ca-

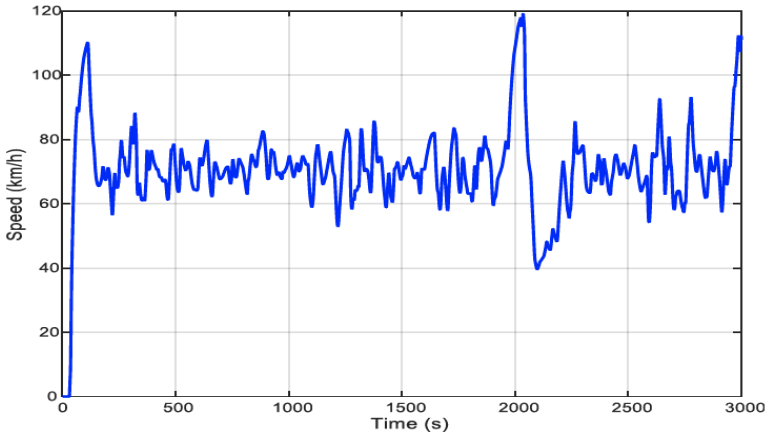

(a)

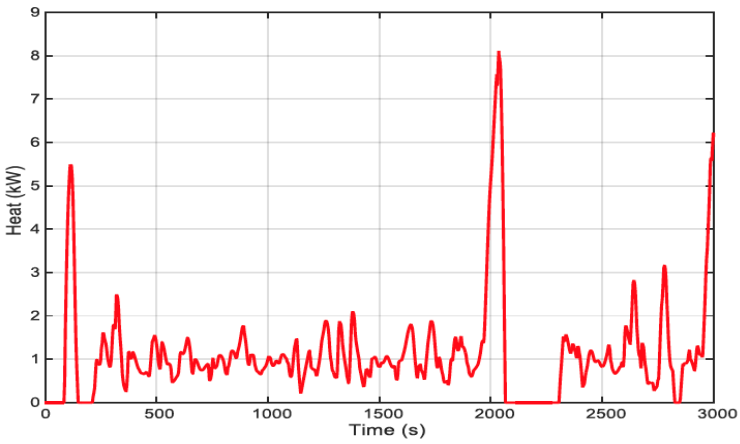

(b)

Figure 2.6: Convoy escort profile - (a) Vehicle speed, and (b) Electric motor heat generation rate as functions of time.

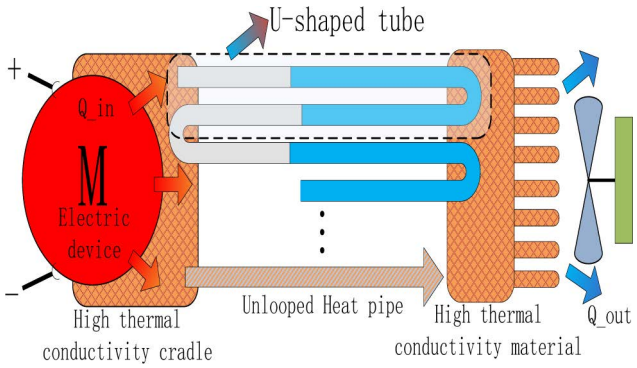

Figure 2.7: Passive cooling concept using U-shaped heat pipe based thermal bus with cradle and heat exchanger.

pability and structure flexibility. The heat pipe based thermal bus is driven by the temperature gradient. As long as the temperature difference exists across the thermal bus, the heat is continuously transferred from the heat load to the heat exchanger with attached electric fan. A reduced order passive cooling system has been numerically modeled per Section 3 to transfer motor generated heat from the cradle to the heat exchanger. The model parameters are summarized in Table 2.1.

The convoy escort driving cycle (refer to Fig. 2.6(b)) was supplied to simulate the temperature of the electric motor. The corresponded electric motor temperature is shown in Fig. 2.8. It is interesting to examine the event at t=2000 (s) which reflects the vehicle acceleration. It causes a sudden growth in the generated heat and consequently the temperature of the heat load rises. The cradle temperature, as expected, follows the electric motor temperature variation trend with small temperature difference. Then, the heat is moved to the thermal bus which transfers the heat to the heat exchanger. Finally, the heat exchanger discharges the heat to the ambient surrounding set on 25°C. Figure 2.8 contains the data of the heat exchanger temperature. The peak in heat exchanger temperature at t=2000 (s) occurs as the consequence of the vehicle acceleration. The operation temperature of the e-motor is

generally maintained lower than 90 over normal driving conditions. However, integration of an active cooling system in parallel with the passive cooling strategy will improve the capability of the cooling system in handling the higher heat rejection needs over aggressive driving conditions or sudden accelerations or decelerations.

Symbol	Value	Unit	Symbol	Value	Unit
A_{cr}	0.065	m^2	p_{v0}	31164	Pa
A_{eff}	0.3549	m^2	R	462	J/kg.K
c_p	1930	J/kg.K	ΔT	10-4	s
$c_{p,l}$	4182	J/kg.K	T_{v0}	303	K
c_v	1460	J/kg.K	T_∞	298	K
d	0.005	m	v_{air}	2	m/s
g	9.8	m/s^2	v_e	0.801e-6	m^2/s
h_c	200	$W/(m^2.K)$	x_{cr}	0.0254	m
h_e	200	$W/(m^2.K)$	x_0	0.05	m
h_{fg}	2257	J/kg	ρ_l	1000	kg/m^3
L_c	0.3	m	λ	0.61	$W/m.K$
L_h	0.3	m	ζ	0.31	-
L_p	0.6	m			

Table 2.1: Summary of model parameters.

The performance of the heat pipe based thermal bus is shown in Fig. 2.9. It shows how the liquid slug is fluctuating due to the heat transfer between the vapor and liquid slugs in the pulsating heat pipe. The heat transfer between the liquid and the vapor slugs is a continuous process as long as there is temperature gradient across the heat pipe based thermal bus. Figure 2.9 also shows vapor temperature variations, vapors pressure variations and the vapors mass variations as functions of time. The vapor mass variations over the evaporation and condensation process are infinitesimal which confirms the assumption made for constant liquid length.

The heat entering the cooling system and the heat exiting the heat exchanger with respect to convoy escort driving cycle as plotted in Fig. 2.10.

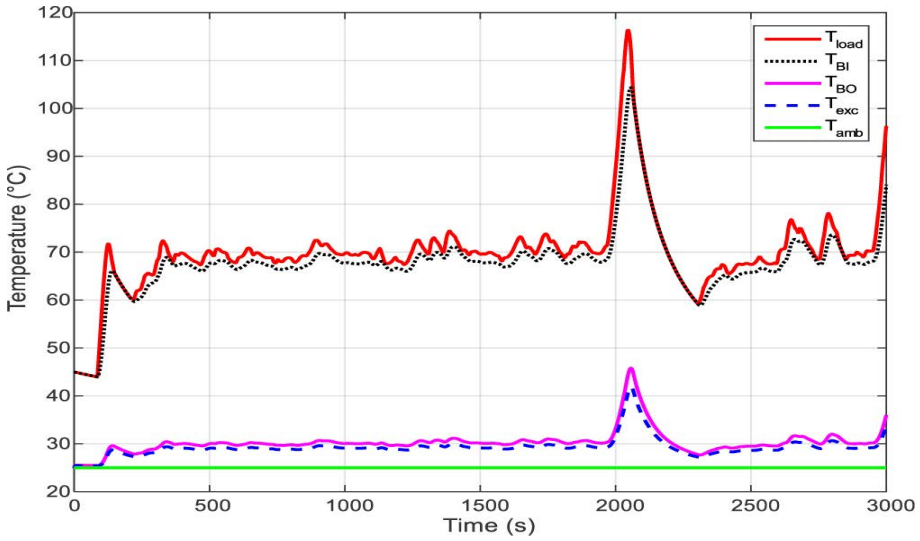

Figure 2.8: Electric motor, cradle, heat exchanger, and ambient temperature as a function of time for convoy escort driving cycle.

2.6 Conclusion

The cooling of the powertrain components and electronics in ground vehicle remains an open challenge. The integration of a passive cooling strategy with active features offers a potential solution to reduce the energy consumption in military ground vehicles. This study investigated the passive heat rejection using a heat pipe based thermal bus with attached cradle and heat changer with electric fan. Mathematical U-shaped pulsating heat pipe model was used to numerically describe the thermal behavior of heat pipe based thermal bus. The case study focused on the convoy escort driving cycle for hybrid vehicles to investigate the system performance based on e-motor loadings. The simulation results demonstrate that moderate thermal load can be transferred to the ambient for heat rejection. This approach avoids the operating of a fluid cooling system and radiator fan cycled off if ram air speed is sufficient across the heat exchangers. Simulation results indicate that the heat dissipation rate of the thermal bus is significantly influenced by heat pipe length,

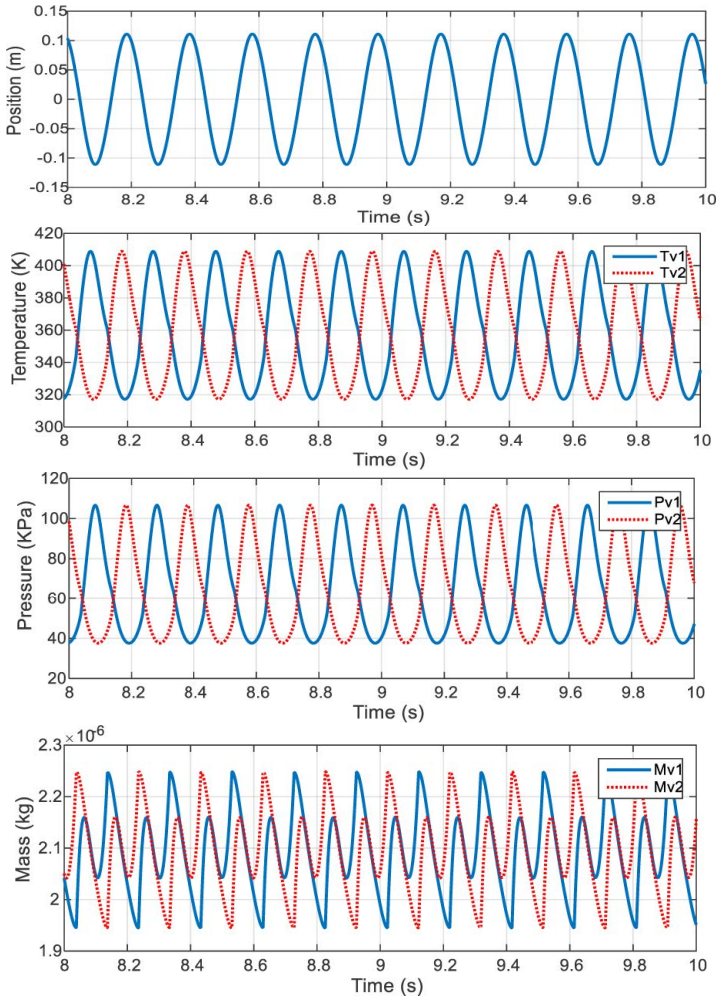

Figure 2.9: Diagram of (a) liquid slug displacement, (b) temperature of vapor plugs, (c) pressure of vapor plugs, and (d) mass of vapor plugs as functions of time.

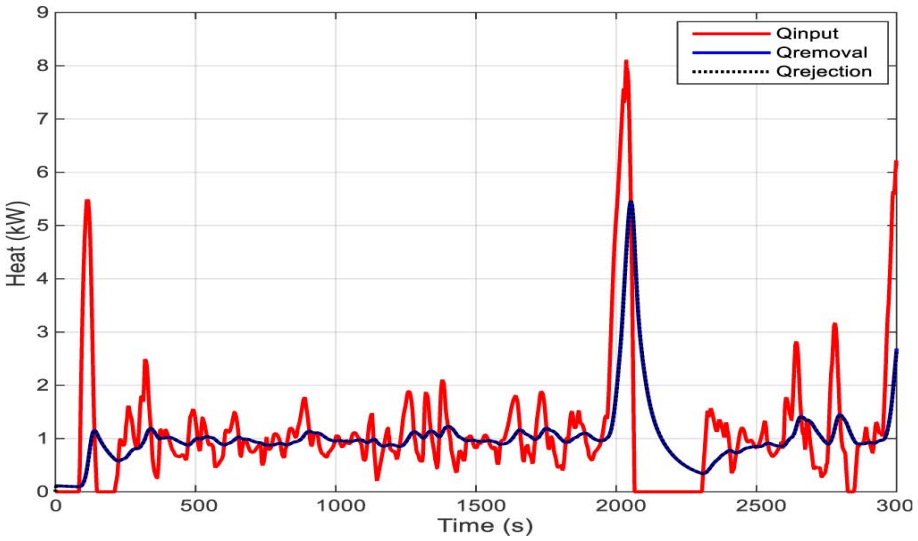

Figure 2.10: Convoy escort driving cycle and heat exchanger heat removal.

diameter and the temperature difference between the heat load and the ambient surrounding. The next step will be experimental validation of the numerical findings through laboratory tests.

Chapter 3

A Hybrid Thermal Bus for Ground Vehicles Featuring Parallel Heat Transfer Pathways

3.1 Abstract

Improved propulsion system cooling remains an important challenge in the transportation industry as heat generating components, embedded in ground vehicles, trend toward higher heat fluxes and power requirements. The further minimization of the thermal management system power consumption necessitates the integration of parallel heat rejection strategies to maintain prescribed temperature limits. When properly designed, the cooling solution will offer lower noise, weight, and total volume while improving system durability, reliability, and power efficiency. This study investigates the integration of high thermal conductivity materials, carbon fibers, and heat pipes with conventional liquid cooling to create a hybrid "thermal bus" to move the thermal energy from the heat source(s) to the ambient surroundings. The inno-

vative design can transfer heat between the separated heat source(s) and heat sink(s) without sensitivity to gravity. A case study examines the thermal stability, heat dissipation capabilities, power requirements, and system weights for several driving cycles. Representative numerical results show that the high thermal conductivity materials and carbon fibers offer moderate cooling while loop heat pipes provide significant improvements for passive cooling.

3.2 Introduction

The integration of heat generating components continues to grow in military vehicles due to alternative propulsion strategies and electronic payloads. The emitted heat due to the operation of electric motor battery packs, electronic devices, etc. needs to be dissipated to the ambient surroundings to promote system efficiency, durability, and performance. The thermal management challenge is to efficiently remove this heat and maintain temperatures within prescribed operating limits while minimizing noise, energy consumption, and maintenance costs. This challenge may be more demanding in military ground vehicles due to the unique vehicle configurations and extraordinary operating conditions. The restrictions may include the finite area for fluid flow and limited space for extended heat transfer surface area. In the current combat vehicles, the air-side heat runs through a restrictive grille which lowers the heat rejection capabilities. In addition, the emphasis on reducing fuel usage in ground vehicles necessitates a smart cooling system design which offers multiple heat rejection pathways, including active and passive strategies, to enhance the heat transfer capabilities with a compact structure and flexible design.

Passive heat rejection typically requires a large heat transfer surface area. However, enlarging the surface area is not always a feasible solution due to space and

weight limitations in vehicle cooling applications. The integration of high thermal conductivity materials, composite fibers, phase change materials, and high performance passive devices may be potential solutions for improved passive heat rejection in automotive cooling applications. The thermal properties of select materials may be enhanced through high thermal conductivity reinforcement. Composite materials, such as carbon fiber reinforced aluminum, offer improved thermal and mechanical properties, including high thermal conductivity, high stiffness, relatively low density, reduced thermal expansion, etc. [26–30]. Composite fiber has been widely used in cooling microelectronics, electric motors, and lithium batteries [31–33]. Greco et al. [34] applied computational analysis to study the influence of composites on battery pack temperature distributions. Mallik et al. [35] investigated different composites and thermal conductive materials for improved thermal management of vehicle electronic control units.

Aside from the composite materials, heat pipes are passive heat transfer devices with ultra-low effective thermal resistance which can transfer a relatively large amount of heat over a fairly long distance with no need for external pumping power [16]. Different heat pipe configurations, including capillary, loop, pulsating, etc. have been studied [36]. The inclusion of heat pipes in a variety of cooling applications for power electronics temperature regulation, including Lithium-Ion batteries have been explored [17,37,38]. Park et al. [39,40] studied the thermal performance of the hybrid two phase cooling loop technology within a thermal bus concept for military vehicle thermal management systems. The designed hybrid cooling system is composed of an active liquid pumping and a passive capillary liquid that run the working fluid through the cooling system. Tang et al. [41] explored the integration of a passive capillary driven cooling device, heat pipe loop (HPL), for improved electronic cooling in military vehicles.

Conventional fluid cooling systems, composed of a water pump, radiator, wax based thermostat, fan, hoses, etc., is well developed. Tao and Wagner [13,14] reduced the energy consumption of ground vehicle cooling systems using nonlinear control theory to optimize the electro-mechanical actuator operation time. Likewise, several hybrid cooling strategies have been introduced to regulate the operating temperature of Lithium ion batteries [42, 43]. The integration of hybrid cooling in ground vehicle applications is also investigated to efficiently move the heat from the thermal load(s) towards the heat exchanger using pulsating heat pipes in a thermal bus concept [44].

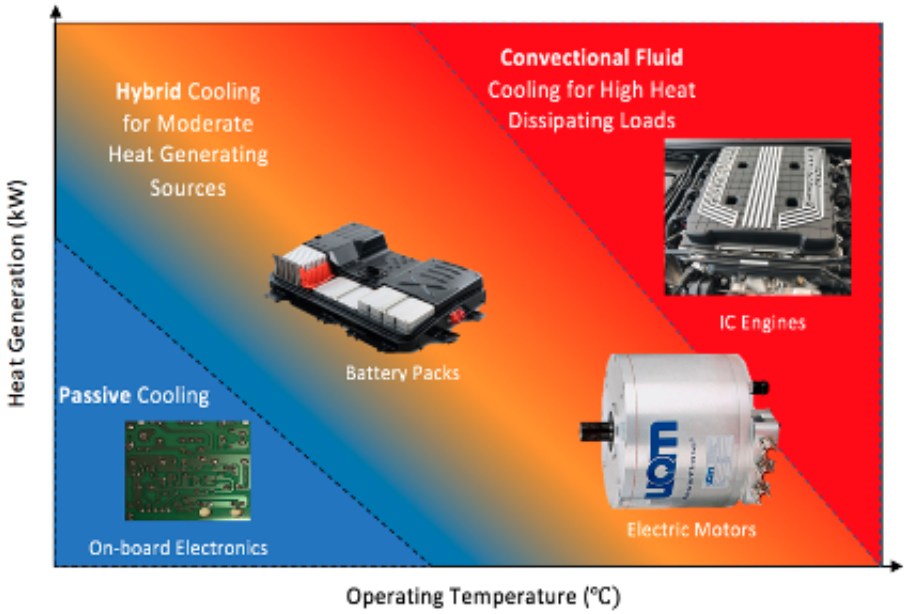

Figure 3.1: Relative heat generation and operating temperatures for various automotive components with possible thermal management strategies.

The design of high efficiency hybrid cooling systems featuring multiple passive heat rejection pathways in parallel with a regular conventional radiator-pump cooling system in ground vehicle cooling applications has not been widely studied. The increased heat generating loads in ground vehicles provide an opportunity to inno-

vate a novel thermal management system featuring an advanced computer controlled hybrid thermal bus. The hybrid thermal bus offers separate heat rejection pathways for different thermal generation ranges. Therefore, low and moderate heat loads may be dissipated through conduction and free convection heat transfer, which is referred to as passive hereinafter, with no external power supplied.

In this project, the integration of parallel heat rejection pathways including passive and active strategies will be examined. The proposed cooling system is composed of four different heat rejection routes - high thermal conductivity materials, composite fiber, a loop heat pipe structure, and conventional active fluid cooling. The primary heat rejection may begin with high thermal conductivity materials and composite fibers while a loop heat pipe structure with a cylindrical evaporator is integrated in the passive configuration. Beside the passive pathways, a complete conventional cooling system is provided to respond to high heat rejection demands that exceed purely passive strategies. The remainder of the paper is organized as follows. Section 3.3 is the introduction for an innovative cooling system featuring a cradle which transfers energy from the load to the hybrid thermal bus and then passes it to the heat exchanger(s). A cradle is any mechanism for transferring heat from the heat load to the thermal bus enroute to the ultimate heat exchanger to ambient which will typically be load geometry dependent. The corresponding mathematical model is presented in Section 3.4 which evaluates the thermal performance of the cooling system. Section 3.5 discusses representative numerical results with respect to a convoy escort driving cycle. Finally, Section 3.6 contains conclusion.

3.3 Cooling System Strategy

Ground vehicles are typically composed of different heat load components (e.g., electric motor, combustion engine, battery pack, propulsion system, on-board electronics, etc.) which generate a significant amount of heat that needs to be dissipated through an efficient cooling system. Variation of operation modes and ambient conditions may directly influence the heat source(s) heat generation rate(s) such that a passive heat rejection strategy may be sufficient for high efficiency operating modes such as a sentry type operating mode or low speed electrical motor propulsion. Passive systems may also be integrated in small autonomous vehicles to improve their durability. A hybrid thermal management system, composed of passive and active heat rejection pathways, may be designed to dissipate the emitted heat towards ambient surroundings and maintain the heat load components within their prescribed temperature limits with minimal to no energy consumption. The proposed advanced hybrid thermal management system offers a high efficiency passive heat rejection pathway for modest heat rejection needs associated with a conventional radiator-pump cooling system for large prolonged thermal loads and harsh conditions. Different passive heat rejection pathways will be identified and their advantages in terms of performance, weight, noise and heat rejection capability will be illustrated in this research.

All mechanical and/or electrical systems contain heat generating components which need to be addressed so that the device temperatures are maintained within prescribed operating limits. A thermal interface, or cradle, is needed to route the thermal energy from the heat load(s) to the thermal bus. The thermal properties of the cradle have a great influence on the thermal performance of the cooling system. Cradles inherently employ specific geometries which are optimized with respect to the heat load geometries, thermal characteristics, and operating conditions. A proper

cradle design with high thermal conduction, low thermal expansion, and high thermal diffusivity can promote enhance heat transfer within the system. An advanced cradle design may feature fluid pathways to enhance the heat transfer between the heat source(s) and thermal bus. The external surface area of the cradle is surrounded by low thermal conductive insulation materials in order to more efficiently route thermal energy to the bus.

The thermal bus generally transfers the thermal energy from the heat load to the heat exchanger and ultimately to the ambient environment. A hybrid thermal bus benefits from both passive heat rejection pathways and conventional liquid cooling and should satisfy low, moderate, and high heat rejection needs with minimal energy consumption. High thermal conductivity materials (e.g., alloys, copper, carbon fibers, etc.) and high performance passive devices (e.g., heat pipes) will be integrated to improve the passive thermal conductivity. The preferred operation mode is passive for low and moderate heat source(s) heat dissipation rate(s) while conventional fluid cooling is introduced if the temperature exceeds established limits.

The hybrid thermal bus structure needs to be flexible enough to support different ground vehicle designs and applications. The proposed bus construction offers a flexible design which can be bent or rerouted with little sensitivity to gravity while maintaining its thermal performance. Figure 3.2(a) displays a basic bus design with attached heat exchanger and optional fan. Figures 3.2(b) and 3.2(c) illustrate flexible and straight thermal bus structures attached to a thermal load and heat sink.

A cooling system needs a high efficiency heat exchanger that significantly increases the heat dissipation to the ambient surroundings. If the convective heat transfer coefficient, heat transfer surface area, and material thermal conductivity increase, the heat exchanger heat dissipation rate will rise. The integrated heat exchanger is designed to benefit from ram-air intake while an optional fan is attached to in-

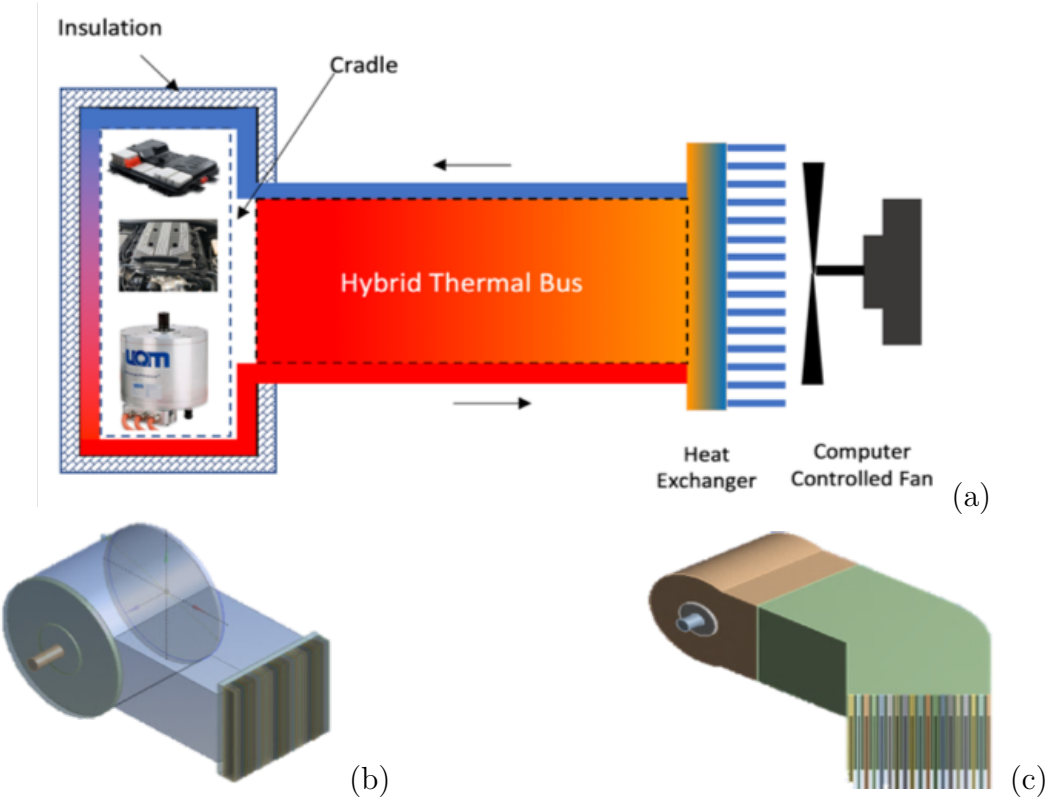

Figure 3.2: Hybrid cooling system strategy – (a) Advanced cooling system featuring hybrid thermal bus with four heat transfer paths in parallel for efficient heat dissipation; (b) Possible design for thermal bus attached to an e-motor; (c) Flexible thermal bus design.

crease the convective heat transfer when the ram-air is insufficient (e.g., a low speed driving mode or stationary conditions). The surface area of the heat exchanger(s) should be optimized for particular applications. The heat transfer surface area is usually extended by adding fins: plain, wavy, and louvered fins are common examples. Louvered fins enhance the heat transfer coefficient and surface area simultaneously. The thermal conductivity of the heat exchanger is more limited due to manufacturing costs, total weight, and operating conditions. Integration of high thermal conductivity materials (e.g., copper, aluminum, etc.) with embedded high thermal conductivity passive devices may improve the thermal conductivity of the heat exchanger at a specific operating temperature range. Lately, a control strategy has been designed which operates the heat exchanger fan(s) with respect to temperatures and lowers the external power consumption while in a "silent sentry" operating mode [13, 14].

3.4 Mathematical Modeling

The thermal behavior of an active/passive cooling system, composed of hybrid cradle and thermal bus structures, is numerically modeled to evaluate its performance over prescribed operating cycles. The heat source, applied to the cradle, will be transported through the thermal bus to the heat exchanger(s). Such thermal systems shall be modeled using nodal networks which feature thermal resistance in series and parallel configurations. The hybrid bus is modeled with four subassemblies: (i) high thermal conductivity material(s), (ii) carbon fibers, (iii) high performance heat pipe, and (iv) conventional cooling. The thermal load corresponds to an electric motor heat generation rate over a driving cycle. The dissipated heat may be removed using passive cooling strategies over low and moderate heat generating scenarios, and the fluid cooling system is utilized should the electric motor temperature exceed the

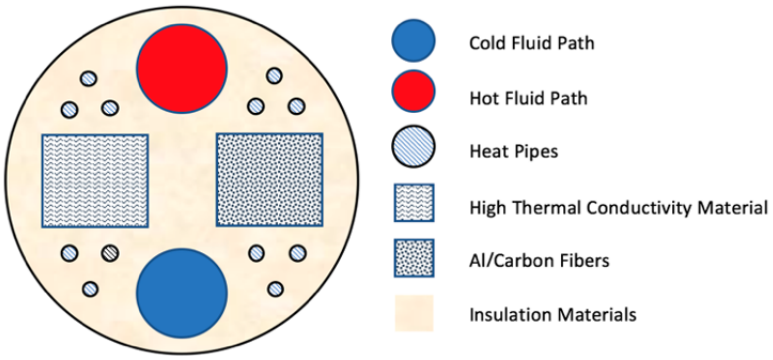

Figure 3.3: cross-section of a hybrid thermal bus concept composed of convectional cooling pipes, heat pipes paths, high thermal conductivity materials, and carbon fibers.

recommended temperature limit. This study will numerically investigate the thermal behavior of a hybrid cooling system containing the cradle, thermal bus, and heat exchanger(s) for an electric motor subject to a convoy escort driving cycle over a single ambient temperature.

3.4.1 Hybrid Cradle

Improvement of the thermal interface between the heat source and the thermal bus has been a challenge due to the load configurations, operation conditions, and space limitations. Generally, the thermal load(s) need to be interfaced with a high thermal conductivity surface area, the cradle, which enhances the heat transfer between the heat source(s) and the thermal bus. A proper material for a cradle may benefit from high thermal conductivity, high thermal diffusivity, low density, and low thermal expansion to transmit the generated heat towards the thermal bus while minimizing the temperature difference across the thermal interface. The heat transfer characteristics of the cradle can be evaluated using a thermal resistance, R_{Cr}, such

that

$$R_{cr} = \frac{L_{cr}}{A_{cr} k_{cr}} \tag{3.1}$$

where L_{cr} represents the cradle thickness, while A_{cr} and k_{cr} denote the conductive heat transfer surface area and conductive heat transfer coefficient, respectively. An advanced cradle features a built-in passage for coolant circulation. Therefore, once the heat generation rate exceeds the passive heat rejection thermal capacity, a controlled servo valve allows the coolant flowing through the passages to pick up the excess heat. The removed heat due to coolant fluid circulation, Q_f, is calculated based on the local convective heat transfer coefficient

$$Q_F = h_f A_f (T_{wall} - T_f) \tag{3.2}$$

where h_f is the local convective heat transfer coefficient and A_f denotes the total convective heat transfer surface area. The symbols T_{wall} and T_f represent the wall and local coolant temperatures.

3.4.2 Hybrid Thermal Bus

The proposed hybrid thermal bus is composed of multiple heat transfer paths including high thermal conductivity material (e.g., copper), carbon fibers, and high-performance loop heat pipe(s), in addition to a conventional cooling system with the associated components (e.g., pump, valves, and fluid jacket). Figure 3.3 presents a schematic for a hybrid thermal bus which efficiently moves the emitted heat towards the heat exchanger(s). At present, passive heat transfer pathways are assumed to contain no thermal capacitance and are treated as pure thermal resistances. A summary

of the mathematical models used for the subassemblies will be presented below.

3.4.2.1 High Thermal Conductivity Materials (HTC)

High thermal conductivity materials (HTC) are efficient medias for passive heat transfer purposes in thermal management. Metals and alloys with high thermal conductivity may be used to efficiently transfer heat from hot to cold with no power consumption. The structure of the HTC material path in the hybrid thermal bus needs to be optimized with respect to the specific heat source configuration and space limitation. Ideal HTC materials can be modeled using a thermal resistance, R_{HTC}, over a limited temperature range as

$$R_{HTC} = \frac{L_{HTC}}{A_{HTC}\, k_{HTC}} \tag{3.3}$$

where L_{HTC} is the length of the thermal bus, A_{HTC} is the effective surface area, and k_{HTC} represents the thermal conductivity of the integrated material.

The heat removed, Q_{HTC}, through the high thermal conductivity material pathway becomes

$$Q_{HTC} = \frac{\Delta T}{R_{HTC}} \tag{3.4}$$

where ΔT is the temperature difference between the HTC materials and the thermal bus ends.

3.4.2.2 Carbon Fibers (CF)

Unique thermal and mechanical properties of composites offer attractive solutions for thermal management improvements characterized by low weight and low flammability, as well as high efficiency, flexibility, and high heat rejection. Car-

bon fibers (referred as CF hereinafter), such as carbon nanotubes and vapor-grown carbon fibers, are advanced materials which may be used in thermal management applications due to their ultra-high thermal conductivity and relatively low thermal expansion. The thermal conductivity of carbon nanotubes has been experimentally measured up to 3,000 W/mK, while theoretically calculated as high as 6,600 W/mK at room temperature [45, 46]. The thermal conductivity of carbon fibers is direction dependent meaning that the thermal conductivity may be higher in a particular direction. This property may be exploited to more efficiently route energy down the axis of the thermal bus. Carbon fibers may be introduced to pure materials (e.g., aluminum, copper, etc.) to enhance their thermal conductivity. For instance, carbon fiber reinforced aluminum composites offer exceptional thermal and mechanical properties. The desired thermal characteristics of aluminum/carbon composites include high thermal conductivity, high stiffness, and low density in compression with aluminum alloys. The effective thermal conductivity of composites depends on the fillers, their corresponding properties, and physical structure. Aluminum composites have been well studied. The in-plane thermal conductivity of aluminum-carbon composites have been evaluated in several studies at approximately 695 W/mK, which is greater than that of pure copper [26,27,30]. The carbon fiber reinforced materials can be integrated as an effective thermal interface between the components to minimize the thermal resistance of the cooling system. The directional heat transfer rate, $\frac{dQ_x}{dt}$, may be expressed as

$$\frac{dQ_x}{dt} = -k_x A_{CF} \frac{dT}{dx} \tag{3.5}$$

where k_x denotes the CF thermal conductivity in the x direction and A_{CF} corresponds to the CF surface area pathway in the thermal bus. The temperature

differential with respect to x becomes $\frac{dT}{dx}$.

The carbon fiber heat transfer pathway is numerically modeled using a thermal resistance, R_{CF}, with thermal conductivity of carbon fibers or

$$R_{CF} = \frac{L_{FC}}{A_{CF} k_{CF}} \tag{3.6}$$

Similar to Section 3.4.2.1, L_{CF}, A_CF, and k_CF represent the CF length, surface area, and thermal conductivity, respectively.

3.4.2.3 Loop Heat Pipes (LHP)

Heat pipes are passive two-phase heat transfer devices with high efficiency thermal capabilities. They are recognized as popular thermal devices to integrate in thermal management systems due to their exceptional thermal conductivity, high flexibility, long lasting durability, simple structure, low temperature drop, and no external power requirements. Heat pipes have been designed in various shapes and lengths with different capabilities for a large variety of applications. Heat pipes typically consist of an evaporator(s) and a condenser(s) which are connected through a typically assumed adiabatic section. For practical purposes, loop heat pipes (referred to as "LHP" hereinafter) are integrated into the hybrid thermal bus due to their unique capabilities including the ability to transmit a large amount of heat over a long distance with small temperature drop and limited sensitivity to gravity.

Figure 3.4 shows a simple schematic of a loop heat pipe. Loop heat pipes are composed of evaporator and condenser components with a specific amount of working fluid driven by a capillary pressure created passively within a wick structure. The wick features a fine-pore material with an effective pore radius and porosity which provides the required capillary pressure for liquid return. The embedded wick struc-

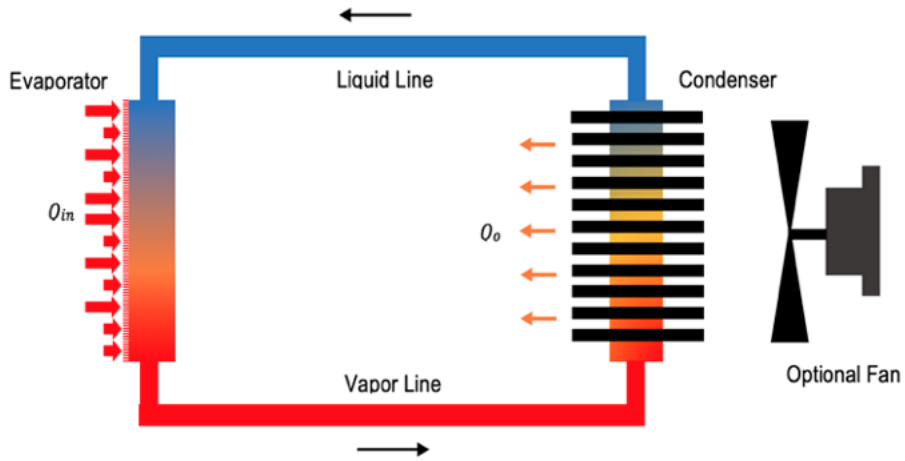

Figure 3.4: Loop heat pipe configuration with an attached optional fan.

ture and the reservoir are placed within the evaporator component. The wick pore size is generally specified based on the required heat removal capability, working fluid, and heat transfer distance. Two separated liquid and vapor lines transport the liquid and the vapor between the separated evaporator and condenser. The operation of loop heat pipes has been characterized with different mathematical and computational models to predict the loop heat pipe thermal characteristics over a variety of operating conditions based on momentum and energy conservation principles as well as thermodynamic relationships. A mathematical model [47] is applied to the hybrid thermal bus model to describe the thermal characteristics of the heat transported through the loop heat pipe. The following assumptions are imposed to establish the loop heat pipe mathematical model within the hybrid thermal bus concept:

A.1: All flows are considered incompressible.

A.2: Reservoir always contains liquid and vapor.

A.3: Vapor temperature variation within the evaporator and vapor line are negligible.

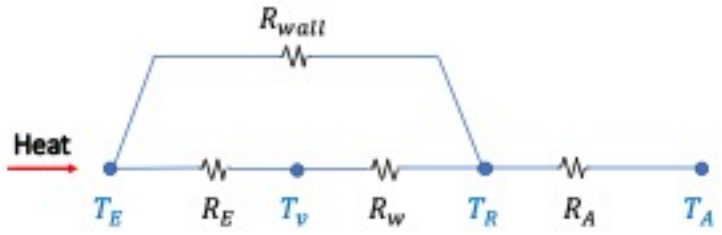

Figure 3.5: Schematic diagram for loop heat pipe evaporator thermal nodal network.

A.4: The phase change process in the condenser is isobaric.

A.5: Thermodynamic properties of the fluid vary with respect to the local temperature.

A.6: The heat input, "heat leak", is transferred to the reservoir through the evaporator wall and the wick structure.

A.6: Heat leakage between the hot and cold sides is negligible in comparison with the amount of the heat input.

Loop heat pipe thermal modeling is generally developed based on energy balance principles and thermodynamic relations. The loop heat pipe is modeled using a thermal nodal network to describe the heat transfer pathway behavior, shown in Fig. 3.5. The terms R_E, R_w, R_A, and R_{wall} represent the thermal conductivity resistances of the evaporator, wick structure, air, and the heat pipe wall, receptively. Once the heat is received by the evaporator, it will be absorbed by the evaporator wall and the liquid-vapor interface section at the wick structure as

$$Q_{in} = Q_{wall} + Q_R \tag{3.7}$$

which can be expressed as thermal resistances

$$Q_{in} = \frac{(T_E - T_R)}{R_{wall}} + \frac{(T_E - T_v)}{R_E} \tag{3.8}$$

In this expression, T_E, T_v and T_R are the temperatures of the evaporator, vapor of the working fluid, and reservoir structure, respectively. The symbol R_E is the thermal conductive resistance of the interface and R_{wall} is the resistance of the evaporator wall.

The heat received by the liquid-vapor interface is used to heat the working fluid and vaporization while some is transmitted to the primary wick structure as

$$\frac{(T_E - T_v)}{R_E} = mh_{fg} + mc_p(T_v - T_R) + \frac{(T_v - T_R)}{R_w} \tag{3.9}$$

where m is the mass flow rate of the working fluid and h_{fg} is the latent heat of vaporization. The term R_w corresponds to the conductive thermal resistance of the primary wick. The thermal resistance of the wick for a cylindrical-shaped evaporator may be expressed as

$$R_w = \frac{\frac{mc_{\rho,l}}{2\pi k_{eff} L_w} Ln(\frac{D_{w,o}}{D_{w,i}})}{mc_{\rho,l}} \tag{3.10}$$

where $D_(w, o)$ and $D_(w, i)$ represent the outer and inner diameters of the wick structure, $mc_{\rho,l}$ denotes the specific heat of the liquid, L_w is the length of wick structure, and k_eff is the effective thermal conductivity for a porous sintered material [48].

The heat transferred to the wick structure is relatively small compared to the heat flux received by the interface for vaporization. Therefore, Eq. 3.9 may be reduced to

$$mh_{fg} = \frac{T_E - T_v}{R_E} \tag{3.11}$$

The heat transfer from the wall and the wick structure is also balanced with the heat leaking to the ambient from the wick structure and the heat required to heat

up the liquid returning from the condenser section at the temperature $T_{C,o}$ so that

$$\frac{(T_E - T_R)}{R_{wall}} + \frac{(T_v - T_R)}{R_w} = mc_{\rho,l}(T_R - T_{C,o}) + \frac{(T_R - T_A)}{R_A} \tag{3.12}$$

The absorbed heat is transferred through the vapor line towards the condenser where it is released. The energy balance at the condenser becomes

$$Q_o = mh_{fg} + mc_{\rho,l}(T_C - T_{C,o}) \tag{3.13}$$

where T_C is the temperature of the liquid within the condenser, and $T_(C, o)$ is the working fluid temperature at the condenser outlet.

The governing thermodynamic equations between the components, including the evaporator, reservoir, and condenser, complete the analytical thermal model of the loop heat pipe. The vapor temperature leaving the evaporator grooves and the vapor temperature entering the condenser may be expressed as

$$T_v - T_C = (\frac{\delta T}{\delta P})\Delta P_v \tag{3.14}$$

where ΔP is the pressure drop due to the friction loss over the vapor line connecting the evaporator to the condenser.

The liquid temperatures of the condenser outlet and the evaporator inlet may be related by

$$T_C - T_R = (\frac{\delta T}{\delta P})(\Delta P - \rho_l g \Delta H) \tag{3.15}$$

where H is the elevation difference between the condenser and the evaporator. The term $\frac{\delta T}{\delta P}$ is the slope of the pressure-temperature saturation curve which can be calculated using the Clausius-Clapeyron relationship. The symbols ρ and g denote

the liquid density and gravity, respectively.

The temperature difference between the reservoir and heat sink can be separated as

$$T_R - T_s = (T_R - T_{R,i}) + (T_{R,i} - T_{C,o}) + (T_{C,o} - T_s) \tag{3.16}$$

The combination of Eqs. 3.10, 3.12, 3.14, 3.15 and 3.16 yields

$$T_R - T_{R,i} = \frac{R_E}{R_{wall}} \frac{h_{fg}}{c_{\rho,l}} + \frac{1}{Q_{in}} \left[\frac{T_R}{\rho_v c_{\rho,l}} \left(\frac{1}{R_w} + \frac{1}{R_{wall}} \right) (\Delta P_l + \Delta P_v - \rho_l g \Delta H) - \frac{h_{fg}}{c_{\rho,l} R_A} (T_R - T_A) \right] \tag{3.17}$$

The analysis goal is to characterize the total thermal nodal network of the loop heat pipe to describe its performance. The total nodal network includes the thermal resistance between the evaporator and vaporization interface (R_E), and the thermal resistance between the reservoir and heat sink (R_{R-s}).

$$R_{TTL} = R_E + R_{R-s} = R_E + \frac{T_R - T_s}{Q_{in}} \tag{3.18}$$

There are generally two main operating modes which reflect the thermal behavior of loop heat pipes. Each mode needs a specific set of assumptions to accurately predict the thermal behavior over the operating cycles and simplify the calculation. One operating scenario, Variable Conductance Mode (VCM), occurs when the temperature of the subcooled liquid at the condenser outlet reaches the temperature of the heat sink. In other words, the temperature difference between the heat sink and the working fluid at the condenser outlet is negligible ($T_s T_C o$). Therefore, Eq. 3.17 yields

$$T_{R,i} - T_{C,o} = (T_A - T_s) \left[1 - exp \left(- \frac{\pi D_L L_L k_L h_{fg}}{Q_{in} c_{\rho,l}} \right) \right] \tag{3.19}$$

where K_L is the heat transfer coefficient between the working fluid flowing in the liquid line and ambient. The symbols L_L and D_L denote the length and the diameter of the liquid line, respectively.

Finally, the combination of Eqs. 3.16, 3.17 and 3.19 leads to

$$T_{R,VCM} = \frac{T_s + \frac{h_{fg}}{c_{\rho,l}}\left[\frac{R_{E-R}}{R_{wall}} + \frac{T_A}{Q_{in}R_A}\right] + (T_A - T_s)\left[1 - exp\left(-\frac{\pi D_L L_L k_L h_{fg}}{Q_{in}c_{\rho,l}}\right)\right]}{\left[(\frac{1}{\rho_v c_{\rho,l}})(\frac{1}{R_w} + \frac{1}{R_{wall}})(\Delta P_l + \Delta P_v - \rho_l g \Delta H) - \frac{h_{fg}}{c_{\rho,l}R_A}\right]} \tag{3.20}$$

which models the operating temperature of the loop heat pipe over the VCM as a function of heat sink temperature and heat input.

The second loop heat pipe operating mode, Fixed Conductance Mode (FCM), represents the condition where the working fluid temperature variation is negligible in comparison with the temperature difference between the heat sink and the condensation temperatures. The following assumption is imposed to predict the LHP operating temperature over the FCM condition:

A.8: The following temperature difference relationships are all assumed. $T_v - T_C, T_v - T_R, T_R - T_C << T_C - T_s$

At the condenser component, the energy balance can be written as

$$mh_{fg} = \frac{\pi L_{2\phi}}{\frac{1}{h_C D_{C,i}} + \frac{1}{h_s D_{C,o}}}(T_C - T_S) \tag{3.21}$$

where h_C represents the condensation heat transfer coefficient. The term $L_{2\phi}$ indicates the pipe length which contains the liquid and vapor mixture. The symbols $D_{C,i}$ and $D_{C,o}$ are the diameters of the condenser tube at the inlet and outlet, respectively.

Then, Eq. 3.21 can be reduced with respect to the assumptions made for the

FCM operating mode so that

$$T_R - T_s \approx T_C - T_s = \frac{mh_{fg}}{\pi D_C L_{2\phi} K_C} \tag{3.22}$$

The energy balance within the condenser, assuming the working fluid temperature variation is negligible, can be expressed as

$$Q_{in} - mh_{fg} \approx \pi D_C (L_C - L_{2\phi}) K_{sub} (T_C - T_s) \tag{3.23}$$

where k_sub denotes the overall heat transfer coefficient between the working fluid and the heat sink.

The heat input, Q_in, may also be expressed as the heat of vaporization and the heat leakage to the evaporator wall such that

$$Q_{in} \approx (T_E - T_v)\left[\frac{1}{R_{wall}} + \frac{1}{R_E}\right] = mh_{fg}\big(1 + \frac{R_E}{R_{wall}}\big) \tag{3.24}$$

The length of the two-phase flow section within the condenser can be calculated from the combination of Eqs. 3.22 and 3.23 such that

$$L_{2\phi} = \frac{L_C}{\dfrac{R_E k_C}{R_{wall} K_{sub}} + 1} \tag{3.25}$$

The operating temperature of the loop heat pipe over the FCM can be expressed using Eqs. 3.22, 3.23 and 25 as

$$T_{R,FCM} = T_S + \frac{Q_{in}}{\pi D_C L_C k_C} \frac{1 + \dfrac{R_E K_C}{R_{wall} K_{sub}}}{1 + \dfrac{R_E}{R_{wall}}} \tag{3.26}$$

Finally, the operating temperature of loop heat pipes as a function of heat

input may be predicted using

$$T_{op} = max(T_{R,FCM}, T_{R,VCM}) \tag{3.27}$$

The loop heat pipe mathematical model has been validated with experimental measurements conducted using Ammonia as the working fluid. Figure 3.6 demonstrates the comparison of the LHP mathematical model predictions with experimental results [49]. It is generally reported in literature that the loop heat pipe thermal performance is typically estimated using two distinct operating modes: Variable Conductance (VCM), and Fixed Conductance (FCM). The decreasing part of this operating curve corresponds to the loop heat pipe VCM where the condenser offers sufficient heat transfer surface area for liquid condensation and subcooling process. Therefore, the liquid temperature reaches the heat sink temperature,T_sink, before it exits the condenser, $T_Co \approx T_sink$. A further decrease in the loop heat pipe operating temperature can be observed by increasing the heat input to the system during the VCM. Adding more heat to the system raises the working fluid mass flow rate within the loop heat pipe which leads to a lower temperature variation along the liquid line. The slope where the curve decreases is estimated with respect to the amount of heat transferred between the evaporator and reservoir compartments as well as the reservoir and the liquid line. The minimum operating temperature corresponds to the condition where the condenser is no longer able to cool down the working fluid to the heat sink temperature. At this point, any further increase in heat input will elevate the loop heat pipe operating temperature since the liquid at the condenser outlet is no longer subcooled.

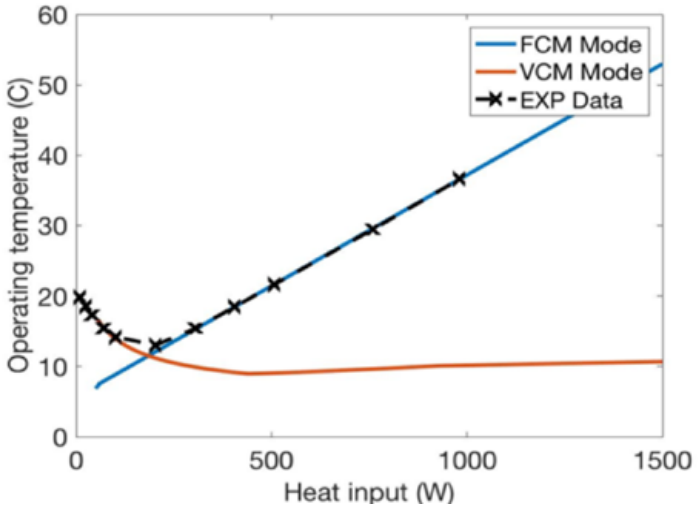

Figure 3.6: Loop heat pipe operating temperature as a function of heat input - validation of mathematical model.

3.4.2.4 Liquid Cooling (LC)

Ground vehicles typically utilize fluid cooling systems to dissipate heat to the ambient environment. The engine block, including but not limited to, internal combustion engines and electric motors is known as the main heat source in ground vehicles. Models for active cooling systems are typically composed of heat load-to-coolant and coolant-to-ambient surroundings heat rejection through a radiator with an attached fan. The heat emitted by the engine block is typically transferred to the coolant through a water jacket within the engine block. The cooling system is composed of a water pump and a thermostat. The water pump circulates the coolant through the heat source block and the radiator. The thermostat regulates the heat exchange between the heat source, radiator, coolant, and the ambient environment to maintain the heat load within a specified temperature range. A complete fluid cooling system, composed of a fluid jacket block, thermostat, expansion tank, radiator, water pump, and bypass hoses, is numerically modeled [13, 50]. A computer-controller can

open a smart thermostat valve and run a servo-motor coolant pump and/or radiator fan once the heat source temperature exceeds the prescribed operating temperature limits or the emitted heat exceeds the heat rejection capacity of the passive cooling strategy.

3.4.3 Heat Exchanger

A heat exchanger absorbs or dissipates heat in a variety of applications. The component performance can be improved by either extending the effective heat transfer surface area, increasing the thermal conductivity of the surface area, or enhancing the convective heat transfer coefficient. The heat transfer coefficient is typically improved by optimizing the fin length, thickness, width, spacing, and/or introducing forced convection to promote air flow through the fin arrays. There are a wide variety of fin designs including, but not limited to, plain fin surfaces, louvered fins, and wavy fins. Each of the fin designs may increase the heat transfer due to surface area extension, as well as improvement of the convective heat transfer coefficient.

A heat exchanger is numerically designed based on the space limitations and heat rejection requirements. A properly designed heat exchanger is a high thermal conductivity heat sink with plain fin surfaces which is optimized in fin spacing with respect to a space limitation [51]

$$Z_{opt} = 3.24 L_s Re_L^{-1/2} Pr^{-1/4} \tag{3.28}$$

where L_s is the length of the heat sink, Re_L represents the Reynolds number, and Pr denotes the Prandtl number. The profile length of the fins may be optimized as a

function of the fin thickness so that

$$Nu = \frac{h_{fin}L_s}{k_A} = 0.664Re_L^{1/2}Pr^{1/3}, \quad b = \beta\left(\frac{k_S W}{2h_{fin}}\right) \tag{3.29}$$

where h_fin is the convective heat transfer coefficient of the fin arrays, k_A and k_s represent the thermal conductivities of air and the heat sink, respectively, W denotes the fin thickness and β is an empirical constant.

An electric radiator or heat exchanger fan increases the heat dissipation rate to the ambient by creating dynamic air pressure. The fan is mathematically modeled using a lumped parameter approach

$$q_f = \gamma\rho_A c_\rho(T_s - T_A) \tag{3.30}$$

where γ and c_ρ represents the fan air flow rate and specific heat of the air intake, respectively, while ρair is the air density.

The ram-effect may also promote convection heat transfer while the vehicle is moving. The relative velocity between the intake air and the vehicle motion may be used to model the ram-effect and calculate the convection heat transfer coefficient for moving vehicle scenarios. In other words, the ram effect is a function of vehicle speed, the air intake speed, and the angle of the air hitting the heat sink so that

$$Q_{ram} = m_f c_\rho(T_s - T_A) \tag{3.31}$$

$$m_f = \int \rho V_f dA = \rho V_f A\cos\alpha \tag{3.32}$$

where Q_{ram} represents the heat removed due to the ram-effect, m_f denotes the air flow rate, V_f is the relative velocity between the vehicle speed and the air-intake, and

α is the angle of attack.

The overall cooling system thermal performance is described by applying the above governing equations from the heat source to the heat exchanger and the ambient surroundings.

Symbol	Value	Unit	Symbol	Value	Unit
A_{cr}	756	cm^2	L_{cr}	0.1	m
A_{CF}	57.75	cm^2	L_{CF}	462	J/kg.K
A_{HTC}	57.75	cm^2	L_E	0.3	m
$c_{\rho,CF}$	-	J/kg.K	L_{HTC}	1	m
$c_{\rho,HTC}$	900	J/kg.K	L_l	7.4e-1	m
$c_{\rho,cr}$	450	J/kg.K	L_v	3.66	m
$D_{C,i}$	4.6e-3	m	L_W	3e-1	m
$D_{E,i}$	2e-2	m	m_e	20	kg
$D_{E,o}$	2.4e-2	m	PM	2.e-14	m^2
D_l	5.3e-3	m	r_{pore}	1.6e-6	m
D_R	6.8e-2	m	R_A	5.85	K/W
D_v	5.3e-3	m	R_E	3e-3	K/W
$D_{w,i}$	9.5e-3	m	R_{wall}	11.25	K/W
$D_{w,o}$	1.9e-2	m	W	1.2e-3	m
g	9.81	m/s^2	T_A	18.15	°C
h_{fin}	47.11	W/m^2K	$T_{int,e}$	35	°C
k_E	2.9e-2	W/mK	T_{int}	18	°C
k_C	600	W/mK	$T_{ref,max}$	55	°C
k_{CF}	700	W/mK	$T_{ref,max}$	32	°C
k_{cr}	200	W/mK	V_A	20	°C
k_E	200	W/mK	ρ_A	1.2	kg/m^3
k_{eff}	90	W/mK	ρ_{CF}	-	kg/m^3
k_{HTC}	401	W/mK	ρ_{cr}	2700	kg/m^3
k_{porous}	220	W/mK	ρ_{HTC}	8960	kg/m^3
k_s	0.3	W/mK	ρ_E	2700	kg/m^3
k_{sub}	230	W/mK	ΔH	0	m
k_w	394	W/mK	α	0	-
L_s	1.4e-3	m	γ	210	CFM

Table 3.1: Summary of model parameters with values.

3.5 Numerical Results – Low, Moderate, and High Thermal Cooling Applications

A complete cooling system, including an e-motor heat load, a hybrid cradle, a hybrid thermal bus, and multiple heat exchangers is numerically modeled on MATLAB/Simulink platform. The hybrid thermal bus is composed of three separate passive heat rejection pathways which include copper, aluminum, composite fibers, and the loop heat pipe structure. The coolant fluid flows between the cradle and the radiator through integrated hoses contained within the thermal bus assembly. Once a thermal load is imposed, the cradle acquires the heat and routes it towards the thermal bus where it is shared between the passive pathways with respect to their thermal resistances. The thermal resistance for each pathway is modeled. The model parameters can be found in Table 3.1. The performance parameters of an electric motor "UQM Power-phase 145" are considered as the references in this case study [52].

For large heat dissipation requirements, a computer controlled conventional liquid cooling system exists. The cooling system performance is initially investigated for steady state heat inputs while the heat load is maintained below 55°C. Table 3.2 presents the heat dissipated to the ambient surrounding through each individual heat rejection pathway and their combinations. The heat load temperature should not exceed 55°C. Configurations 1-7 represent passive heat removal with the fan off while Configurations 8-14 illustrate the cooling system heat removal capabilities with the fan operating. Configuration 15 demonstrates the hybrid cooling system strategy with the conventional cooling added to the passive thermal bus.

Numerical simulations are conducted to predict the thermal performance of the developed hybrid cooling system for the convoy escort driving profile. Convoy escort drive cycles represent the speed of platooning ground vehicles as a function of

Configuration	Thermal Bus				Heat Transfer (W)	Fan
	HTC	CF	LHP	LC		
1	x				250	OFF
2		x			360	
3			x		566	
4	x	x			310	
5	x		x		816	
6		x	x		926	
7	x	x	x		860	
8	x				330	ON
9		x			580	
10			x		1,150	
11	x	x			450	
12	x		x		1,480	
13		x	x		1,730	
14	x	x	x		1,575	
15	x	x	x	x	10,000	

Table 3.2: Thermal response of cooling system methods for several operating conditions

time over moderate operating conditions. Figure 3.7 shows the vehicle speed and the corresponding heat generation of the electric motor versus time for this cycle. The heat generation is estimated based on the electric motor load. All components of the vehicle cooling system are numerically modeled as described in Section 3. As needed, other heat load components with known heat generation rates over a driving cycle can be integrated.

The performance of the proposed hybrid cooling system is also investigated for the convoy escort driving cycle. Three distinct cooling system configurations are employed to describe the thermal behavior of the passive and active cooling systems. The thermal bus structures corresponding to Configurations 4, 7, 14, and 15 are selected to interface with the electric motor. Note that in all aforementioned cases, the initial temperature of the electric motor is set to 35°C, and the initial temperature of the other components is initialized to 18.5°C which is the assumed ambient temperature.

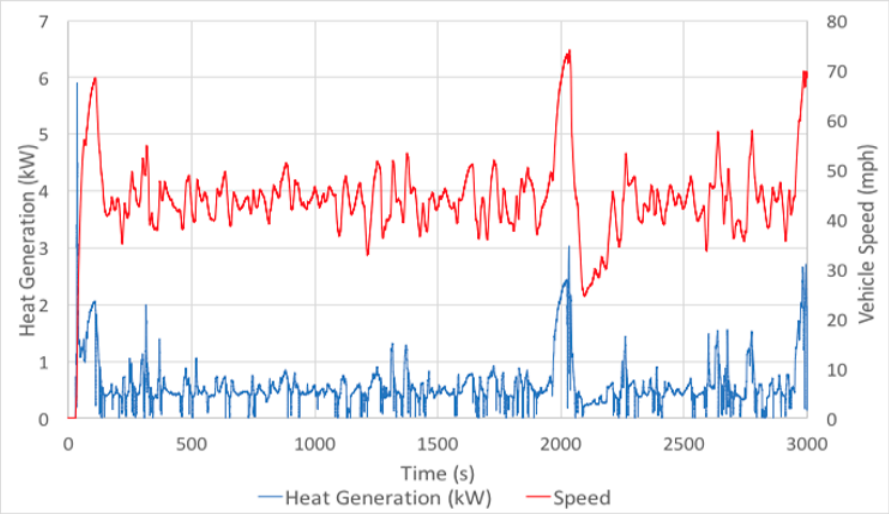

Figure 3.7: Convoy escort profile - Electric motor heat generation rate and vehicle speed as functions of time.

The additional space required for placing the complete thermal bus, including HTC, CF, and LHP pathways, in the vehicle is estimated to be 0.011 m^3. In terms of weight, a one-meter HTC thermal pathway will add up about 50 kg to the conventional cooling system while the additional weight associated with CF pathway for the same size thermal path is only 8.5 kg. The density of the CF can be found in the literature [1]. The LHP will not significantly enlarge the thermal bus as the vapor and liquid lines are only 5.3 mm in diameter.

Configuration 4: In this study, the convoy escort driving profile is supplied to a passive thermal bus composed of HTC and CF pathways between the e-motor and the heat exchanger. The electric motor, cradle, and heat sink temperatures are shown in Fig. 3.8(a). The e-motor temperature continuously rises as the heat enters the system. Figure 3.8(b) presents the heat transfer rate in the cooling system components. The heat transferred through CF is higher than HTC due to the lower thermal resistance. However, the passive cooling system with HTC and CF cooling

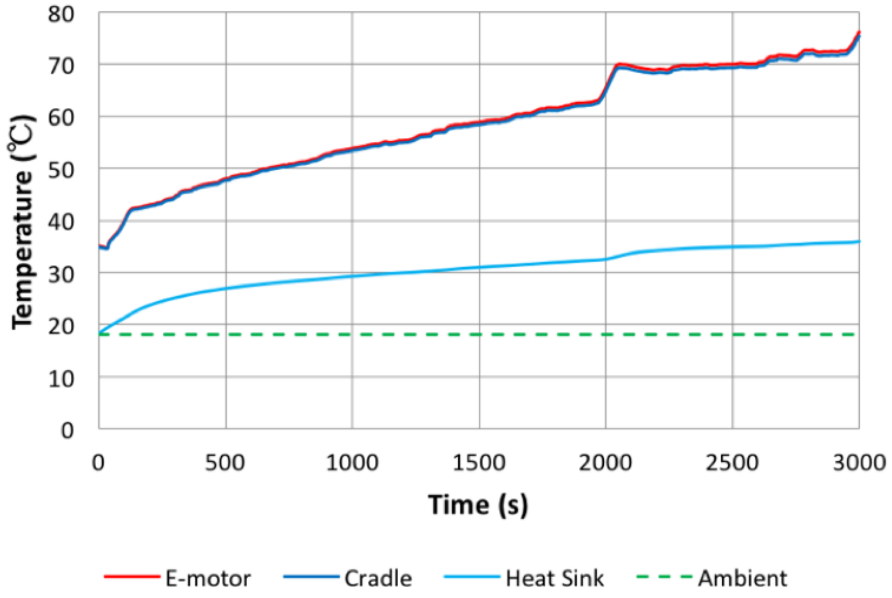

(a)

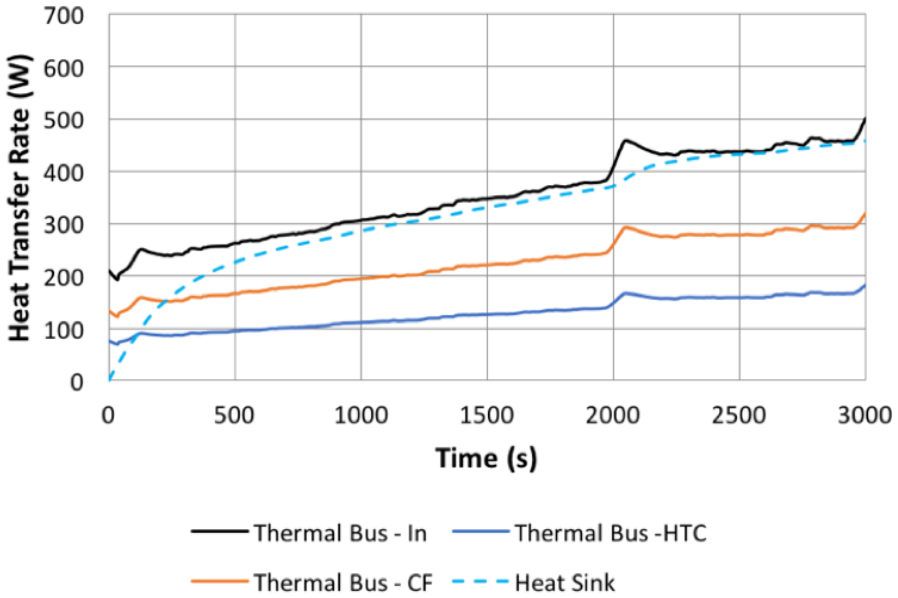

(b)

Figure 3.8: Configuration 4 - System response for (a) Electric motor, cradle, heat exchanger, and ambient temperatures for convoy escort driving cycle using CF and HTC heat rejection pathway; and (b) Cradle, thermal bus and heat exchanger heat removal over passive heat rejection strategy.

pathways is not able to maintain the e-motor temperature below the prescribed temperature which is set at 55°C. Therefore, an additional heat rejection pathway, with low thermal resistance and high thermal capabilities, is required to secure the electric motor operating temperature.

Configurations 7 and 14: This simulation configuration represents a passive thermal bus with HTC, CF, and LHP heat rejection pathways operating in a parallel configuration with the fan off (Configuration 7) and the fan operating at t=800 (s) (configuration 14). The transported heat is dissipated to the ambient through natural and forced convections. The corresponding thermal behaviors of the electric motor, cradle, thermal bus, and heat sink are shown in Fig. 3.9. The dotted lines represent passive cooling strategy (configuration 7) while the solid lines demonstrate the effect of the fan operation with on the same cooling system configuration (configuration 14). These results indicate that the designed passive thermal bus is able to handle moderate heat dissipation with the fan on/off and keep the electric motor's temperature below 50°C during the electric motor operating time. Figure 3.9(a) illustrates the electric motor, cradle, and heat sink temperatures as a function of time. Figure 3.9(b) displays the heat transferred through each individual pathway while the electric motor temperature is maintained within prescribed limits. This case study shows that passive cooling system can dissipate relatively significant amounts of heat while the heat sink fan operation may be necessary for high heat generation instances.

Configuration 15: The thermal performance of the system may be further investigated with integration of a computer controlled conventional fluid cooling system, with electro-mechanical actuators, to the passive cooling system which completes the hybrid cooling system design. The heat transfer primarily occurs through the passive thermal bus until the e-motor temperature exceeds the upper operating temperature limit which is set on 50°C for this simulation. Once the load's temperature

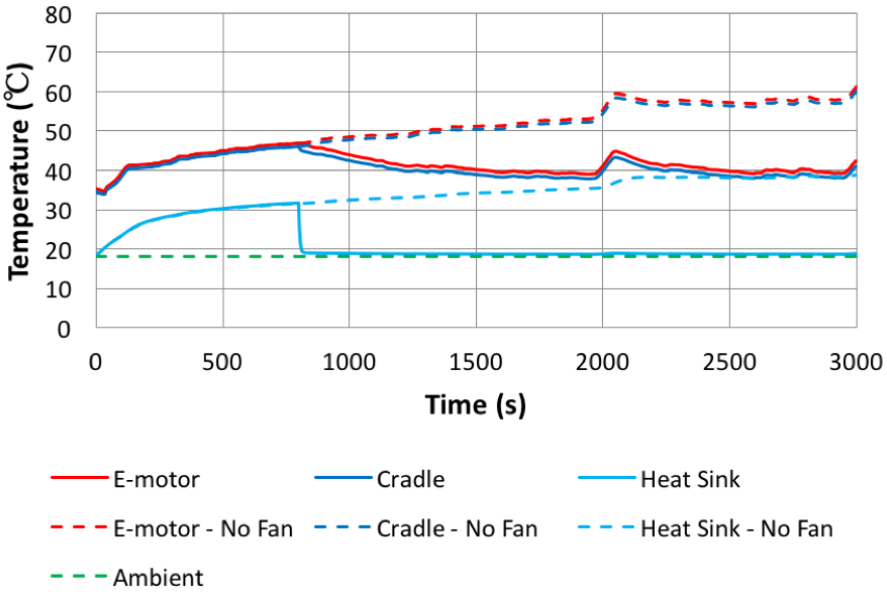

(a)

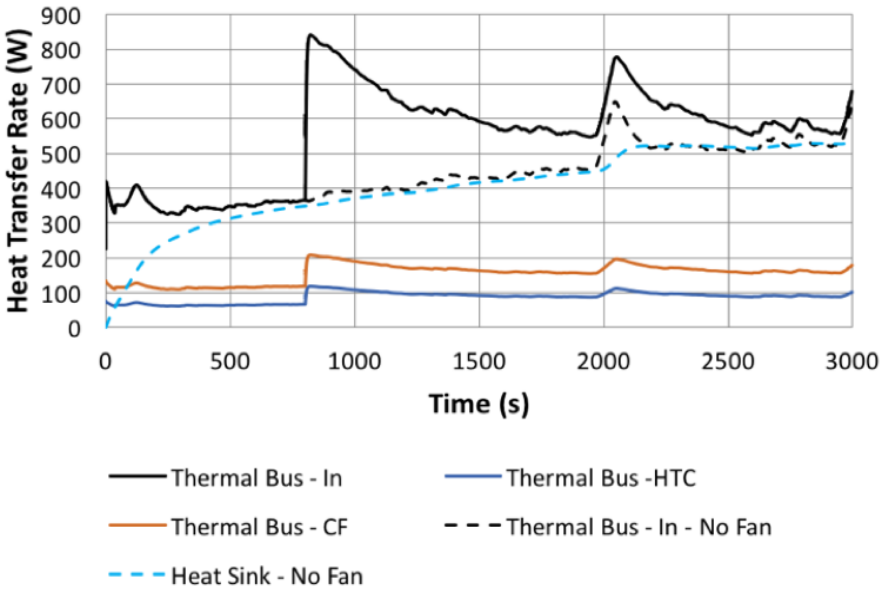

(b)

Figure 3.9: Configurations 7 (free convection), and 14 (forced convection at t=800 sec) - System response for (a) Electric motor, cradle, heat exchanger, and ambient temperatures as functions of time for convoy escort driving cycle using passive heat rejection pathways; (b) Cradle, thermal bus and heat exchanger heat removal over passive heat rejection strategy.

reaches its rated operating temperature, a controller operates the water pump and runs the coolant fluid through the system to cool it down to the minimum operating temperature and then turns the water pump off. This strategy secures the electric motor's temperature below 55°C for the presented convoy escort driving profile (refer to Fig. 3.10(a)) with optimized energy consumption needed for running the water pump, actuators, and radiator fan. The fluid cooling cycle operates at 0.06 (Hz) after 1,000 (s) to remove the emitted heat to the ambient through the radiator. The corresponding e-motor, cradle, and heat sink temperatures are shown in Fig. 10(a). The designed hybrid cooling system regulates the e-motor temperature within the operating temperature limit set on 32°C – 50°C. The heat transfer rates are shown in Fig. 3.10(b).

In this set of computational simulations, the effect of thermal capacitances has been neglected. The improved model may contain the associated thermal capacitances which should be calculated based on the specific heat and the mass for each pathway. In addition, an advanced controller may be employed to optimize the actuator operating time for further minimization of cooling system energy consumption.

3.6 Conclusions

A novel hybrid thermal management has been designed for improved heat rejection with minimal to no energy consumption. Improved thermal management in military ground vehicles still remains an open challenge due to the increased heat load from electro-mechanical components needed for enhanced performance and capabilities. The integration of multiple passive heat rejection pathways, composed of high thermal conductivity material, aluminum carbon fibers, and loop heat pipes, in parallel with an active cooling system configuration, offers an improved thermal

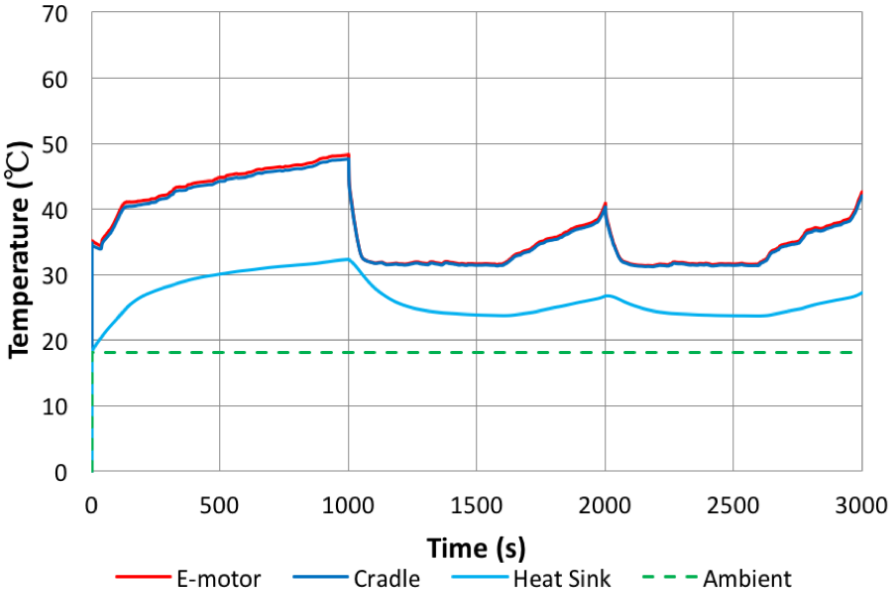

(a)

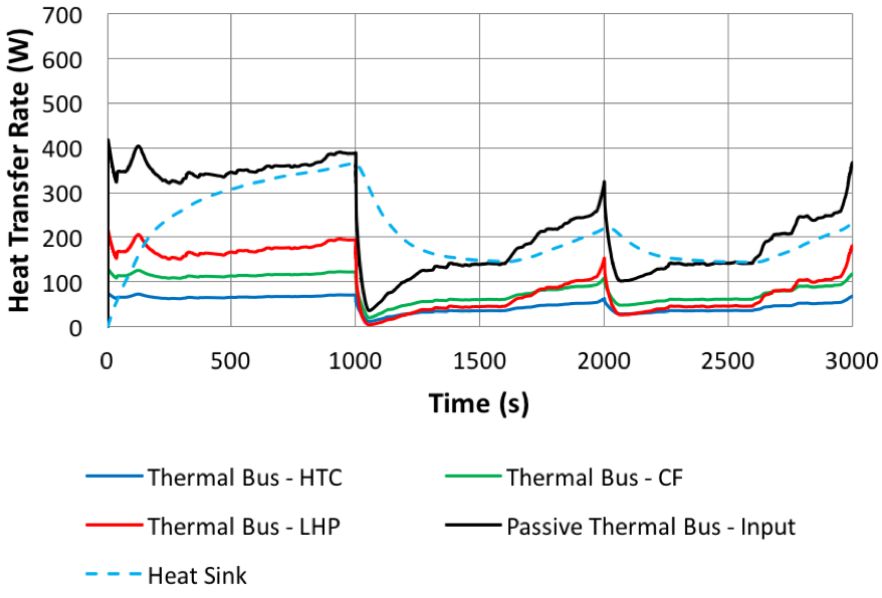

(b)

Figure 3.10: Configuration 15 - System response for (a) Electric motor, cradle, heat exchanger, and ambient temperatures as functions of time – A complete hybrid thermal management regulates the e-motor's temperature with optimized energy consumption; and (b)Thermal bus and heat exchanger heat transfer rates as a function of time.

management system to satisfy the demands for low, moderate, and high heat rejection to the ambient surroundings. A mathematical model for each individual heat rejection pathway has been developed and/or adopted from the literature to predict the thermal behavior of the proposed hybrid ground vehicle cooling system. The case studies, based on e-motor loadings with respect to a convoy escort driving cycle, indicate that the integration of parallel passive heat rejection pathways offers sufficient heat transport and dissipation for moderate heat rejections over a single ambient temperature. Further, the proposed strategy avoids a pump, mechanical actuators, and radiator fans when purely passive operation can achieve target temperature limits. The future work includes the optimization of the cradle, thermal bus, and heat exchanger(s) structures for targeted e-motor loads followed by the integration of the designed hybrid thermal management system into a variety of ground vehicle simulation applications using scalability techniques.

Chapter 4

An Electric Motor Thermal Bus Cooling System for Vehicle Propulsion – Design and Test

4.1 Abstract

Automotive and truck manufacturers are introducing electric propulsion systems into their ground vehicles to reduce fossil fuel consumption and harmful tailpipe emissions. The mobility shift to electric motors requires a compact thermal management system that can accommodate heat dissipation demands with minimum energy consumption in a confined space. An innovative cooling system design, emphasizing passive cooling methods coupled with a small liquid system, using a thermal bus architecture has been explored. The laboratory experiment features an emulated electric motor interfaced to a thermal cradle and multiple heat rejection pathways to evaluate the transfer of generated heat to the ambient surroundings. The thermal response of passive (e.g., carbon fiber, high thermal conductivity material, thermosyphon) and

active cooling systems are investigated for two operating scenarios. The test results demonstrate that up to 93% improvement can be achieved in cooling system energy consumption during a light load electric motor condition while maintaining a target core temperature of 70°C. The governing thermal system dynamics will be reviewed in discussion of the experimental observations.

4.2 Introduction

The integration of electric propulsion systems in the next generation of military ground vehicles will enable improved mobility, energy efficiency, and reliability while offering significant reduction in greenhouse gas emission, weight, and noise generation. Hybrid propulsion systems typically feature an electric motor with a battery pack in a series hybrid configuration with a diesel engine to propel the vehicle. A significant amount of heat may be generated through the operation of the integrated engine, electric motor, battery pack, and on-board electronics. The challenge is to design a compact thermal management system which can handle heat rejection demands for expected operating conditions. The innovative thermal management system may offer a high efficiency cooling solution which enables this paradigm shift towards long range electric vehicles.

The advent of advanced computers, sensors, and controllers enables on-demand cooling with replacement of mechanical components with electro-mechanical actuators in a conventional cooling system. The actuators' operating cycles have been optimized using advanced control algorithms to achieve further minimization in energy consumption [8, 13, 53]. In recent developments, military vehicles' functionalities and capabilities have become advanced with highly increasing use of electric motors in propulsion systems [54]. Figure 4.2 conceptually displays a six wheeled hybrid vehicle

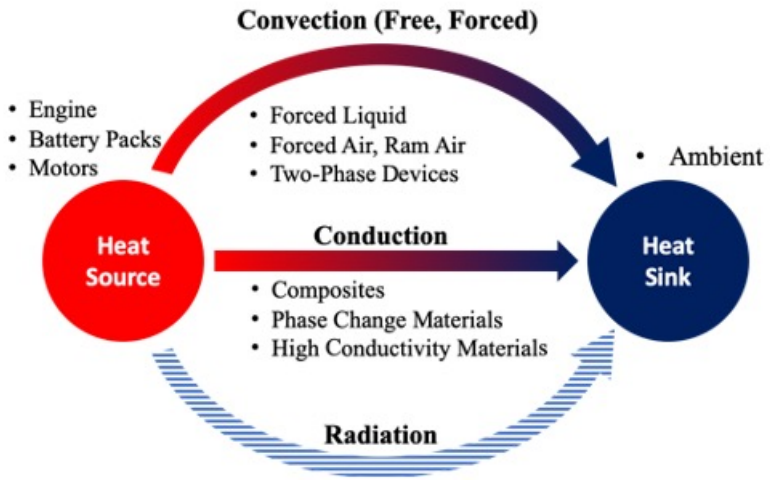

Figure 4.1: Heat transfer modes in automotive applications with limited temperature difference.

featuring in-hub electric propulsion system. The number of heat-generating components continues to grow in the next generation of military ground vehicles to meet the demanding functions and tasks in battle fields. The integration of more powered component in a confined space creates a thermal challenge called high heat density. This makes thermal management even more challenging as prolonged operating in these conditions will ultimately lead to failure in operation. Several experimental and numerical studies have been conducted to address thermal challenges associated with integration of electric motors, battery packs, and on-board electronics in automotive applications [55–57].

With recent developments in material sciences, a wide variety of advanced materials (e.g., composites, fibers, phase change materials, etc.) has been recognized as an attractive cooling solution due to their unique thermal and mechanical properties [58]. The thermal behavior of advanced materials has been widely explored experimentally and numerically. A thermal conductivity of 3,000W/mK has been experimentally measured for carbon nanotubes at room temperature [46]. Their car-

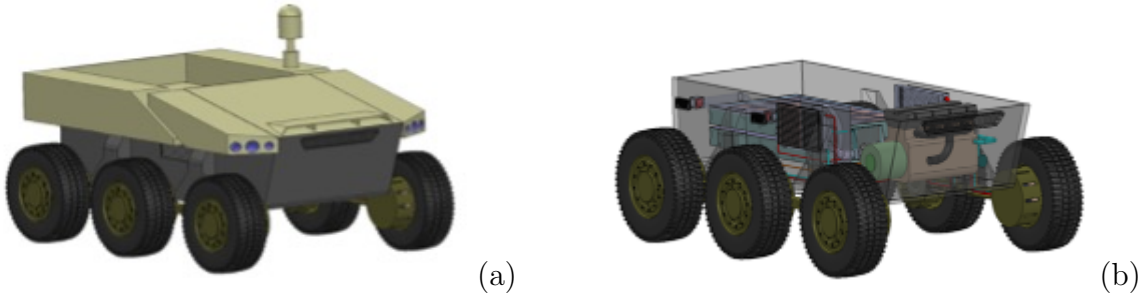

(a) (b)

Figure 4.2: Six wheeled autonomous military ground vehicle – (a) featuring in-hub electric propulsion with hybrid thermal management system; and (b) system architecture with platform removed.

bon fibers have been introduced to pure metallic materials (e.g., aluminum, copper, etc.) which resulted to advanced composite materials with improved thermal and mechanical properties. For instance, the in-plane thermal conductivity of aluminum-carbon composite could reach 700 W/mK while the aluminum thermal conductivity is around 200 W/mK [30].

Two-phase heat transfer devices, including heat pipes, thermosyphon, etc., are recognized due to their outstanding effective thermal conductivity, simplicity in geometry, and unique flexibility in structure. The effective thermal conductivity of a 30mm-diameter 1m-long copper rod can be 90 times higher than a copper rod of the same size [36]. Two-phase passive devices have been designed and developed in different configurations for various applications and heat transfer capabilities. The integration of heat pipes in vehicle cooling applications, including electric motor and battery pack thermal management systems, have been investigated with the aid of computational simulations and experimental investigations. The results illustrated that heat transfer capabilities of passive cooling solutions are still limited to low to moderate heat generating applications.

A vehicle cooling system's energy efficiency may be further enhanced with inte-

gration of a hybrid thermal management system which emphasizes on passive cooling methods as well as active cooling solutions. The integration of hybrid thermal management using high thermal conductivity two-phase passive devices for electric motor cooling applications have been computationally investigated and experimentally explored [42, 59, 60]. The research gap is to design an innovative thermal management system which includes multiple passive heat rejection pathways coupled with a computer-controlled supplementary liquid system within a thermal bus concept. The inclusion of passive heat transfer devices and high effective thermal conductivity materials offers a cooling solution which accommodates increasing thermal loads while enabling a silent sentry operation mode with no energy consumption. During the passive mode of operation, a relatively large portion of the heat is moved to the ambient surroundings through two-phase passive devices.

The remainder of the paper is organized as follows. Section 4.2 explains the hybrid cooling system strategy the with thermal bus concept and a cradle designed for electric motor cooling. The cooling system architecture is demonstrated in Section 4.3. The experimental results are discussed and explored in Section 4.4. Conclusions may be found in Section 4.5.

4.3 Electric Motor Cooling System Strategies

Electric and hybrid vehicles typically contain AC electric motors in the powertrain system for propulsion. In conventional electric motors, a wire wound stator draws current to meet the load demand. Heat is generated when current passes through the stator winding structure as well as frictional effects due to rotating parts. The heat generation rate varies depending on the road profile and driving conditions. To ensure proper performance, the excess heat must be dissipated to the

ambient surroundings to maintain the motor within the prescribed temperature limits. The heat has been traditionally removed through conventional cooling systems which offer coolant flow across the external shell or air flow around the stator windings. However, these methods generally require considerable fan and pump operation which consumes electrical power. Overcooling and overheating are thermal challenges which may occur.

In some instances, the electric motor's heat generation may be low to moderate which reflects a stationary or constant speed driving condition. On the other hand, hill climbing, or sudden accelerations will produce relatively large amounts of heat. A properly designed passive cooling system offers cooling for various motor operating modes, but the demand for high heat rejection necessitates the integration of a liquid cooling system. The novel thermal management system features parallel heat transfer pathways which maintain the motor's temperature within prescribed limits while minimizing the cooling system energy consumption. Figure 4.3 illustrates an in-hub electric motor with passive and active cooling pathways.

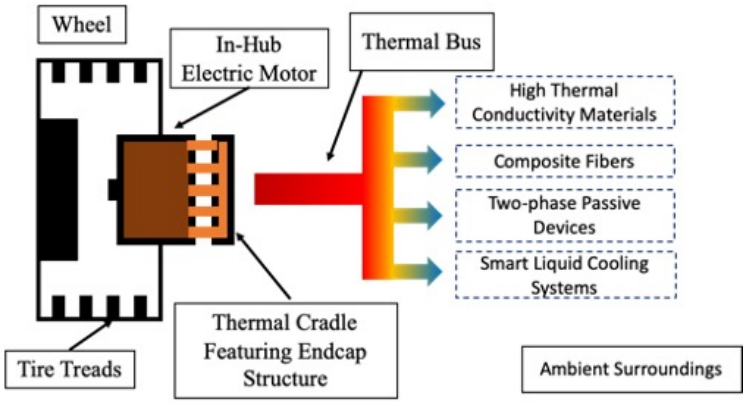

Figure 4.3: Heat flow for electric motor to environment via multiple thermal pathways including passive and active solutions.

Electric motors are offered in different configurations, sizes, and efficiencies.

Regardless, the generated heat must be efficiently removed from the motor structure. A high thermal conductivity surface area, which thermally interfaces the electric motor with the cooling system or "Cradle" is designed to transfer heat away from the shell. This heat is moved to a separate heat exchanger(s) using passive and/or active cooling. The pathways must feature adequate flexibility so that they can fit within a compact structure. For instance, military vehicles restrict air flow due to armor and other blast integration hardware. A flexible thermal bus allows heat to travel from the motor source to remote heat exchangers located along the outer surfaces. The bus features passive cooling solutions (e.g., carbon fibers, heat pipes, thermosyphon, composites) with no external power requirements for low and moderate heat rejection needs. A compact computer-controlled liquid cooling system can be supplied to the bus for large heat removal instances. The liquid cooling system's energy consumption can be minimized by using a supervisory control algorithm to regulate the pump and fan operating cycles with respect to the electric motor's operating temperature.

The heat exchanger finally dissipates the heat to the ambient surroundings. The heat rejection may occur through either natural convection or forced convection depending upon the heat dissipation requirements. The passive and active cooling system may share a common heat exchanger or attach to multiple separated heat exchangers at different locations. The heat exchanger(s) may feature multiple fan assemblies with variable speed AC motors for further minimization of electrical power consumption using a non-linear control algorithm.

4.4 Electric motor Cooling System Experiment

A complete bench top electric motor cooling system featuring passive and active cooling pathways is designed and built. Figure 4.4 displays the experimental set

that is constructed to determine the hybrid cooling system thermal behavior. An emulated electric motor is used to supply heat input to the system. The cooling system contains cradle, thermal bus, and heat exchangers to efficiently remove the excess heat with minimum energy consumption. The designs of the emulated electric motor and hybrid cooling system's components are explained in the following subsections.

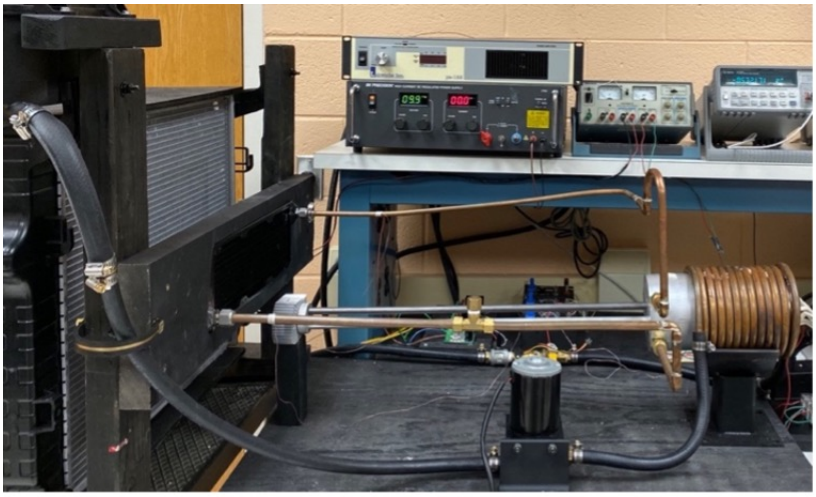

Figure 4.4: Bench top experimental set up constructed for electric motor hybrid cooling system featuring parallel heat rejection pathways.

4.4.1 Electric Motor Thermal Load

To emulate the heat generation by an electric motor, heater cartridges are placed in a radial fashion in an aluminum block. The heat input is supplied using six 700W cartridge heaters. The aluminum cylinder represents the motor shell. The electric power to the cartridge heater powers are computer-controlled to simulate different driving profiles for various wheel torques and speeds. Figure 4.5 shows the configuration of the fabricated electric motor shell which is 10cm diameter and 16cm long aluminum block.

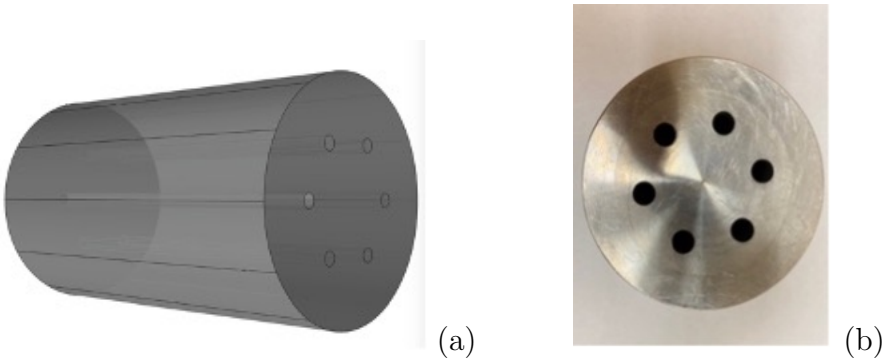

(a) (b)

Figure 4.5: Emulated electric motor used to supply input heat to the cooling system using cartridge heaters – (a) perspective graphical view; and (b) top experimental view.

4.4.2 Cradle

The electric motor is enclosed with a thin shell "cradle," including endcap, which transmits the internal heat to the cooling system. The assembly is comprised of a 15.2cm outer diameter aluminum cylinder and a 15.2cm outer diameter cylindrical end-cap structure as shown in Figs. 4.6(a) and 4.6(b). The endcap features two holes on a circular surface and internal fluid passages for interfacing with the thermal bus. The effective thermal conductivity of the cradle is significantly promoted with integration of capillary heat pipes per Fig. 4.6(c). Finally, a copper pipe is coiled around the lateral surface of the cradle where the liquid circulation is supplied. The prototype cradle design is illustrated in Fig. 4.6(d). Thermal interface materials (e.g., thermal paste) may be used to enhance the thermal contacts between the emulated electric motor and cradle.

The enclosed heat pipes are two-phase passive devices with high effective thermal conductivities and flexible structures. Heat pipes are typically composed of a sealed enclosure containing of a wick structure saturated with a small amount of working fluid such as water, acetone, ammonia, etc. The working fluid is chosen with

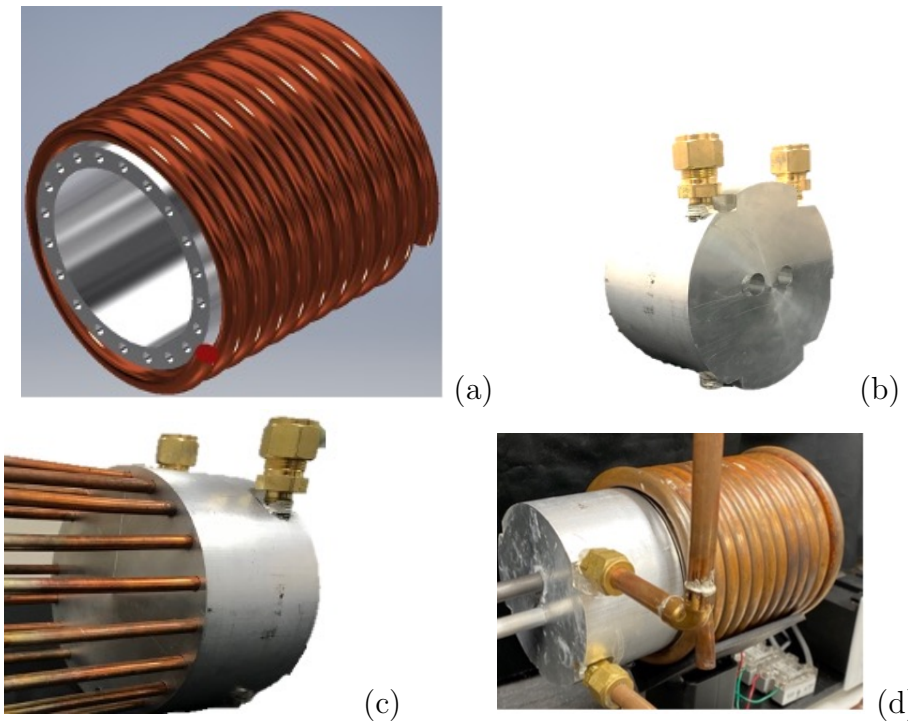

Figure 4.6: Cradle - (a) structure with featuring liquid jacket; (b) front view - endcap; (c) back view – end cap with embedded capillary heat pipes; and (d) complete prototype .

respect to the required operating temperature. A heat pipe has evaporator and condenser sections connected through an adiabatic section. The heat, externally applied to the evaporator, vaporizes the liquid accumulated in the wick structure. The resulting vapor pressure drives the vapor towards the condenser through the adiabatic section. The vapor releases the latent heat of vaporization and turns back to the liquid phase. Then, the condensate travels back to the adiabatic section towards the evaporator through the wick structure due to the capillary pressure created across the wick. This is a continuous process as long as a sufficient capillary pressure is created across the wick structure.

4.4.3 Hybrid Thermal Bus

Heat transfer between the cradle and the heat exchanger(s) occurs via conduction and convection. The hybrid thermal bus includes three passive heat transfer pathways combined with a compact computer-controlled liquid cooling system. The passive cooling solutions include high thermal conductivity material, carbon fiber, and thermosyphon. The thermal bus is thermally insulated on its lateral surface. The bench top scale experiment enables a 60cm heat transfer length between the thermal load and the heat exchangers, as shown in Fig. 4.7, with the thermal insulation cover removed.

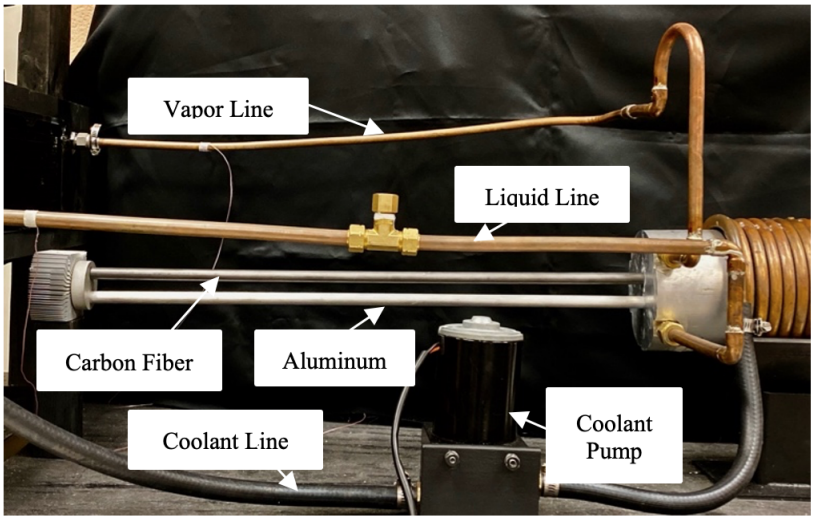

Figure 4.7: Hybrid cooling system concept featuring hybrid thermal bus with insulation cover removed.

4.4.3.1 Thermosyphon (TS)

The Thermosyphon is a gravity aided two-phase passive device which offers extraordinary thermal conductivity. This natural circulation closed loop system is partially filled with a working fluid. The working fluid is passively circulated between

a heating section, known as the evaporator, and a cooling section, known as the condenser. To ensure the liquid return, the condenser must be situated slightly above the evaporator assembly. A design consideration is the filling ratio of the working fluid properties which significantly influences the thermal performance. Several experimental and numerical studies have been conducted to investigate the effects of different operating parameters on thermal performance [61]. The integration of loop heat pipes in a thermal bus based thermal management system was also explored mathematically [60].

A complete closed loop thermosyphon, including evaporator and condenser components, has been designed and built as shown in Fig. 4.7. The loop contains distilled acetone with a filling ration of 50%. The internal fluid passages within the cradle serve as the thermosyphon evaporator assembly which transfers the heat to the working fluid. The heat initially increases the subcooled liquid up to the boiling point where phase change begins. The vapor travels the vapor line towards the heat exchanger due to buoyancy-driven motion of bubbles originating from the cradle surface area. The working fluid may release the latent and sensible heat while flowing through the heat exchanger. The condensate is then returned back the endcap due to gravity. Three individual variable speed DC fans (1.26W) are attached to the heat exchanger for enhanced convective heat transfer.

4.4.3.2 Carbon Fibers (CF)

Exceptional thermal characteristics and unique mechanical properties of carbon fibers (e.g., carbon nanotubes, vapor-grown fibers) offer another solution for improved thermal management. Carbon-based composites may feature enhanced thermal conductivity, stability, structure flexibility, and strength associated with weight reduction [58].

As proof of concept, the designed thermal bus has integrated a 1.27cm-diameter 60cm-long carbon rod to conduct the heat to a heat sink as shown in Fig. 4.7. The thermal conductivity of the carbon rod varies as a function of temperature. Along the length of the rod, at room temperature, the thermal conductivity is predicted to be approximately 140W/mK. However, the thermal conductivity decreases as the temperature increases until it reaches a minimum of approximately 40W/mK at 2000°C.

The directional heat transfer rate, $\frac{dQ_x}{dt}$, through the carbon rod may be expressed as

$$\frac{dQ_x}{dt} = -k_x(T)A\frac{dT}{dx} \tag{4.1}$$

where $k_x(T)$ denotes the temperature dependent thermal conductivity in x-direction and A is the heat transfer cross-sectional area. The temperature differential with respect to x becomes $\frac{dT}{dx}$.

4.4.4 High Thermal Conductivity Materials (AL)

Conduction is the primary mode of heat transfer in low heat generating applications such as on-board electronics. The benefit of a passive solution is high reliability, low maintenance cost, and no moving components. The effectiveness of the conductive heat transfer is determined by the conductive heat transfer surface area, length, temperature gradient, and thermal conductivity. Conduction is commonly used in thermal management due to the minimal cost and implementation requirements.

A 1.27cm-diameter 60cm-long aluminum rod is implemented in the thermal bus structure. The rod is thermally interfaced with the endcap on one end and attached to the heat sink on the other end as shown in Fig. 5.7. The resistance of

the thermal interface between endcap and rods is decreased using a thermal paste.

4.4.5 Smart Liquid Cooling Systems

Traditional liquid cooling systems are typically composed of a water pump, mechanical thermostat valve, radiator, and fan(s). The proposed compact hybrid thermal management system features a smart liquid cooling system which offers on-demand cooling for minimized energy consumption. A computer-controlled 12-volt DC pump, for reduced total weight and size, provides a flow rate of 20 GPM (gallon per minute) while drawing up to 6 amps under normal operating conditions. The operation cycles of the radiator fan(s) and the coolant pump is then minimized with respect to the electric motor core temperature using classical control theories. The temperature and current measurements are recorded on a computer through a National Instrument data acquisition system, NI-6211, and the data is monitor and analyzed on LabView.

4.4.5.1 Heat Exchanger Dynamics

The transported heat may be dissipated to the ambient surroundings through individual heat exchangers. The concentrated heat conducted through the aluminum and carbon rods share a compact finned heat sink. A cross flow heat exchanger has been integrated in the thermosyphon to cools down the working fluid. Three 10cm DC fans are attached to the heat exchanger to supply up to 2m/s forced air flow.

Further, the supplementary liquid cooling system employs a separate radiator assembly which transfers the thermal energy from the circulating coolant to the ambient environment. This radiator also features two AC fans (110volt, 0.5Amp) which supply air flow across the heat transfer surface area should the ram air become


(a)

(b)

Figure 4.8: Heat exchangers arranged in a parallel configuration – (a) thermosyphon; and (b) liquid cooling heat exchanger.

inadequate. The operation cycles of the AC and DC fans are optimized with respect to the cooling demands. This strategy maintains the heat load's temperature while minimizing energy consumption. Figure 4.8 displays the heat exchangers arranged in a parallel configuration.

4.5 Results and Discussion

The designed bench top scale hybrid cooling system has been assembled in a laboratory. A complete set of experimental testing has been conducted to describe the thermal behavior of the cooling system subject to a steady-state input thermal load and a time-dependent load profile. This smart cooling system is programmed to regulate the electric motor's operating temperature, T_H, between 65°C to 75°C. The ambient temperature is maintained at approximately $T_\infty = 22$°C during the experiments.

The experimental investigation involves the evaluation of the emulated electric motor thermal performance. Figure 4.9 provides the temperature response of the emulated electric motor before and after the cradle structure is attached. The thermal

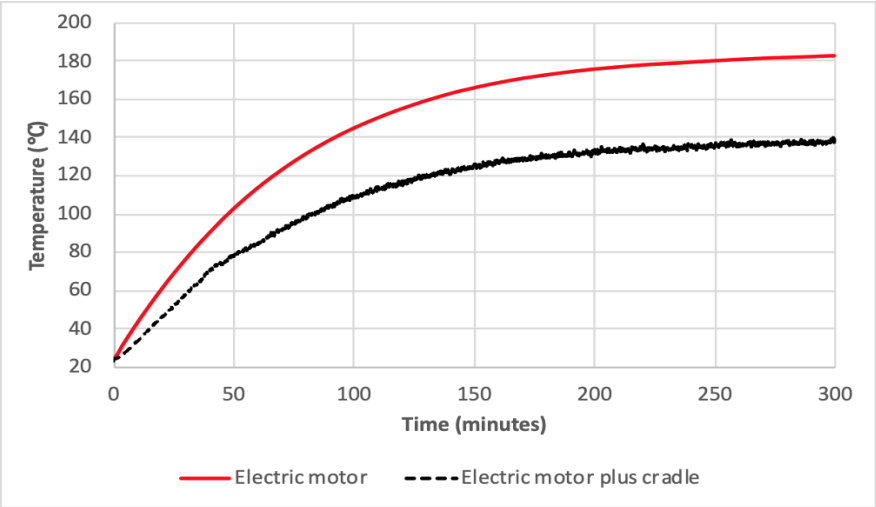

Figure 4.9: Baseline - Temperature response of emulated 160VA electric motor; time constants of 110 minutes and 76 minutes for the emulated motor by itself and emulated motor attached to cradle – Free convection on cradle lateral surface.

behavior of the emulated electric motor with 160W heat generating rate (for a 98% efficient electric motor, 160W heat generation corresponds to a shaft load of 8kW electric motor) is shown as a function of time. The steady-state condition is reached after 5 hours of operation with a 110-minute of time constant at a temperature of 185°C . The temperature response is then measured with the cradle installed while the identical input heat is continuously applied by the motor. As a result, the temperature falls to 140°C with a lower time constant of 76 minutes. This drop in the final temperature is due to the additional thermal capacitance and the natural convection heat transfer which occurs through the cradle lateral surface.

Each cooling pathway is then supplied to the cradle one at a time and the thermal behaviors of the electric motor and the cooling systems are analyzed. First, the performance of the thermosyphon subject to 160VA heat is studied. Figure 4.10 shows the temperatures of the electric motor, evaporator, and condenser outlet as a function of time. The generated heat flows towards the cradle endcap which contains

Test No.	System Configurations				T_{max} (℃)	τ (min)	Cooling Actuators	
	TS	CF	AL	Liquid			Power Usage (kJ)	Energy Usage (W-hr)
1	Free	-	-	-	78	58.7	0	0
2	Forced	-	-	-	72	31.6	0.79	0.22
3	-	X	-	-	101	75.8	0	0
4	-	-	X	-	95	67	0	0
5	-	X	X	-	98	73.7	0	0
6	Free	X	X	-	78	48	0	0
7	Forced	X	X	-	72	-	0.68	0.19
8	Free	X	X	X	72	-	0	0
9*	Free	X	X	X	75	-	41.3	11.5

Table 4.1: Experimental test matrix to explore thermal response of cooling system methods subject to the 160VA emulated motor (Tests 1-9) and varying thermal load of 200-3000 W (Test 9*)

the working fluid, acetone, in liquid phase. The motor's temperature rises rapidly from 22°C to 75°C which vaporizes the working fluid at approximately 60°C . The vapor travels the vapor line due to buoyancy-driven motion of bubbles toward the heat exchanger. Once the vapor reaches the heat exchanger, it releases the latent heat and returns back to the liquid phase. The vaporization continuously increases the pressure of the vapor line until the pressure becomes sufficient to passively drive the liquid back to the evaporator through the liquid line. Once the circulation begins, the temperature of the liquid line sharply increases (t = 100s) until it reaches steady-state at t $\bar{2}$30s. The effect of the fan operation on the heat exchanger's performance is demonstrated by applying forced convection at t = 240s. As illustrated, the temperature of the liquid line drops significantly after 5 seconds of fan operation and then rapidly returns to the steady-state condition after approximately 100 seconds. This results in 6°C and 2°C temperature drops at the evaporator and electric motor, respectively. The free and forced heat transfer regions are shown in Fig. 4.10.

The cooling capacity of the complete passive cooling system, including thermosyphon, carbon, and high thermal conductivity material, is examined. Figure 4.11 displays the responses of the 160VA emulated electric motor, cradle, and heat sink

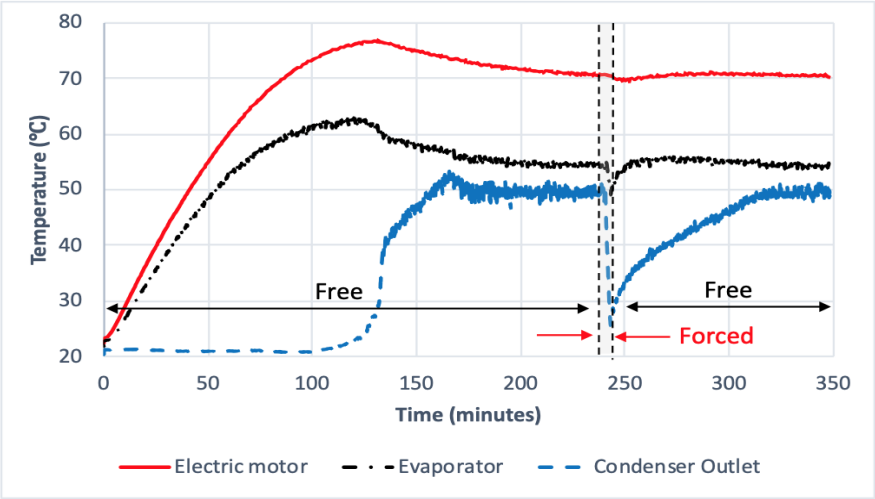

Figure 4.10: Tests 1 and 2 - Temperature response of evaporator, condenser inlet and condenser outlet of thermosyphon subject to 160VA steady-state input heat - Forced cooling regions are shaded with gray.

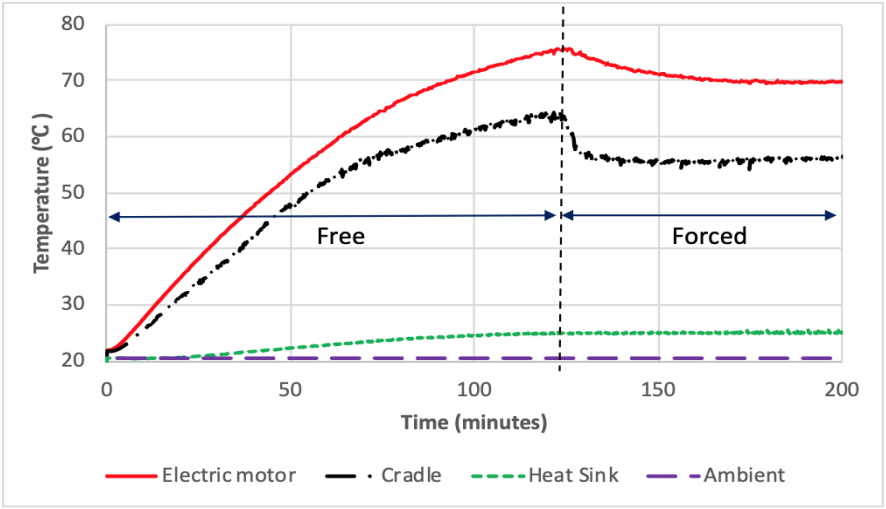

Figure 4.11: Tests 6 and 7 - Temperature response of the passive cooling system subject to the 160VA electric motor.

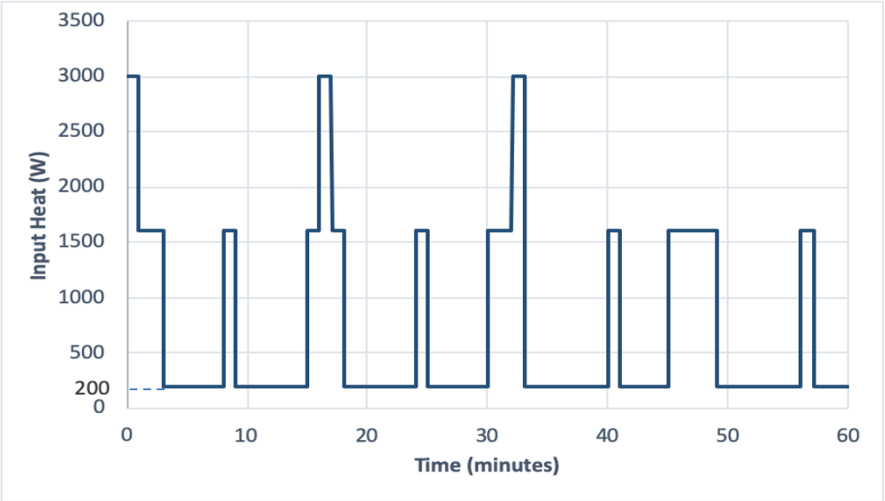

Figure 4.12: Test 9 - Electric motor heat generation rate as a function of time

attached to the carbon and aluminum rods. The results illustrate that the complete passive cooling system cannot maintain the motor's temperature below 75°C which is the maximum operating temperature. The forced convection is supplied to the heat exchangers at t=125s through the attached optional fans. The electric motor's temperature reduces down to 72°C during the fan operation where the operating conditions are met Likewise, the thermal performance of each cooling pathway is evaluated and summarized in Table 4.1.

The experimental investigation is continued to predict the thermal performance of the developed hybrid cooling system for the time-dependent input heat shown in Fig. 4.12. This load profile may represent the generated heat through an in-hub electric motor of a platooning ground vehicle. The heat generation initially remains at 3kW (e.g., 150kW shaft load for 98% efficient motor) for 1 minutes which may correspond to vehicle acceleration cycles. The remaining variation of heat generation could be related to instantaneous vehicle speed and applied torque. The simulated heat load profile is supplied to the electric motor for test 9.

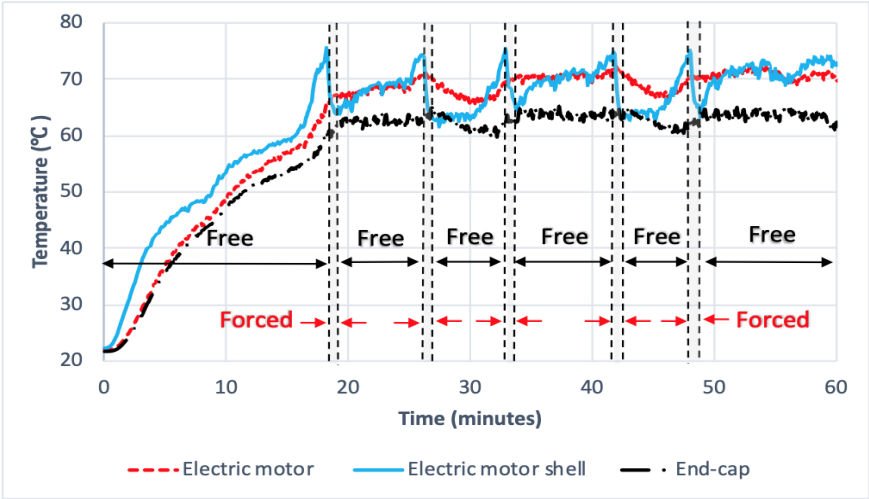

Figure 4.13: Test 9 - Thermal response of emulated motor interfaced with the completed hybrid cooling system subject to transient heat continuously applied

The thermal behavior of the complete hybrid cooling system subject to the time-dependent input load is described. Temperature measurements are conducted on the electric motor, motor shell, and endcap. Figure 4.13 shows the temperature responses with respect to the transient heat input. In this configuration, the thermal load is primarily dissipated to the ambient environment through the passive heat rejection pathways. Once the operating temperature violates the prescribed operating temperature range ($T_{max} = 75°C$), the ethanol glycol circulation begins. The computer-controlled liquid cooling system operating cycles is regulated using classical control theories. The coolant is circulated continuously between the evaporator and radiator assembly until the electric motor's temperature reduces to the lower temperature limit ($T_{min} = 65°C$). The results illustrate that the hybrid cooling strategy is able to secure the electric motor's operating temperature between 65°C to 75°C with minimum reliance on the active cooling operation. The liquid cooling energy consumption in 1 hour of operation is 41.3kJ is equivalent to 11.5Wh. This means

that the hybrid cooling system energy consumption is reduced up to 93% while the heat rejection needs are managed through the passive cooling systems.

4.6 Conclusion

The emphasis on autonomy and fuel efficiency in the next generation of military ground vehicles necessitates the integration of electric motors with battery pack in the propulsion system. This study experimentally investigates the thermal behavior of an electric motor hybrid cooling system subject to several inputs with different configurations. The innovative electric motor thermal management system features a hybrid thermal bus composed of multiple passive cooling pathways coupled with a computer-controlled liquid cooling system. This provides an alternative pathway which enables on-demand cooling, silent sentry operation, and component downsizing while reducing energy consumption. The results demonstrate that the designed hybrid cooling system can maintain the electric motor's temperature within the prescribed range while offering up to 93% energy saving for a light load condition. However, the results may not represent the global optimal energy efficiency. Therefore, future work includes the development of a mathematical model which represents the proposed cooling system architecture to formulate an optimization problem for maximized energy efficiency.

Chapter 5

An Innovative Electric Motor Cooling System for Hybrid Vehicles - Model and Test

5.1 Abstract

Enhanced electric motor performance in transportation vehicles can improve system reliability and durability over rigorous operating cycles. The design of innovative heat rejection strategies in electric motors can minimize cooling power consumption and associated noise generation while offering configuration flexibility. This study investigates an innovative electric motor cooling strategy through bench top thermal testing on an emulated electric motor. The system design includes passive (e.g., heat pipes) cooling as the primary heat rejection pathway with supplemental conventional cooling using a variable speed coolant pump and radiator fan(s). The integrated thermal structure, "cradle", transfers heat from the motor shell towards an end plate for heat dissipation to the ambient surroundings or transmission to

an external thermal bus to remote heat exchanger. A complete lumped parameter numerical modelling was implemented to estimate the thermal behavior of the corresponding electric motor cooling system. Experimental and numerical results compare the temperature, heat flux, and cooling power measurements. For 250VA thermal load applied, the hybrid heat rejection strategy could save up to 33% of the power consumption while the operating condition is secured. Higher thermal loads can be handled through the combined passive and active pathways with minimum power consumption. Based on these findings, integrated electric motor cooling merits attention for further investigation through field testing, scaling, and utilization in other applications.

5.2 Introduction

Improved performance, durability, mobility and reliability have increased the interest in propulsion system electrifications in military ground vehicles. Military vehicles can be as small as an autonomous vehicles or as big as large trucks. A mid size six wheeled autonomous military ground vehicle is shown in Fig. 5.1 [62]. Propulsion systems in hybrid vehicles typically include electric motors in parallel or series with combustion engines. Electric motor windings typically carry up to 90 amperes which generate a significant amount of waste heat. Heat dissipation is even more challenging in military vehicles due to their complex configuration, excessive operating conditions, unique working environments, and protective armor. The heat needs to be carried off through an advanced thermal management system, which secures operating temperatures within prescribed limits with minimum power consumption, noise generation, maintenance cost, and weight.

The emphasis on the minimization of energy consumption in the next gener-

Figure 5.1: Six wheeled autonomous military ground vehicle.

ation of combat vehicles demands an innovative hybrid cooling system which offers improved fuel efficiency, design flexibility, and compact structure while the safety of soldiers is secured. A solution may feature passive cooling strategy along with a computer controlled conventional liquid cooling system to dissipate the generated heat to the ambient environment. The computer-controlled hybrid cooling system strategy offers a tool to regulate the electro-mechanical actuator operating cycles which further minimizes the energy consumption during low, moderate and high heat dissipating demands. Figure 5.1 displays an autonomous military ground vehicle platform which may feature hybrid cooling system for improved fuel efficiency.

Passive cooling strategies have been previously studied for improved heat dissipation rates in automotive applications. Enhanced passive heat transfer rate may be achieved through heat transfer surface area expansion and/or integration of high thermal conductivity materials. Different fin structures may be incorporated for enlarging heat transfer surface areas, although unlimited surface expansion faces serious

design issues due to the space limitation. High thermal conductivity materials, carbon fibers, two-phase passive devices, etc. have been integrated in thermal management systems for further improved heat transfer rates [17,31–33,63]. Two phase heat transfer devices, including heat pipes and thermosyphons, are passive devices which offer high effective thermal conductivity to transfer relatively large amounts of heat for fairly long distances with no external power needed [16]. Heat pipes with different configurations and thermal capabilities have been well-studied [36]. Heat pipes have been used in different cooling system architectures for improved thermal management systems including military vehicles [41, 64, 65].

For large heat generating applications, conventional liquid cooling systems have been well-developed. In such systems, the heat generating components are in liquid communication with a heat exchanger. The coolant is circulated throughout the system to move the heat from heat sources to the ambient surroundings. In recent developments, mechanical components have been replaced with electro mechanical actuators. Tao [13, 14] applied a non-linear control algorithm to optimize the electro-mechanical actuator operation time for reduced energy consumption. Shoai-Naini et al. [44, 60] has numerically explored hybrid thermal management systems with integration of heat pipes coupled with a conventional liquid cooling system. The performance of a heat pipe-based electric motor cooling system with an attached centrifugal fan has been computationally investigated [66].

In this study, the integration of hybrid cooling system for electric motor applications will be examined. The proposed hybrid cooling strategy offers a passive heat rejection pathway combined with a computer controlled liquid cooling system. The passive cooling system configuration is composed of multiple capillary heat pipes which passively transfer the heat to a finned structure heat exchanger with no energy consumption. For promoted convective heat transfer rate, a centrifugal fan is placed

in the middle of the heat sink. Along with the passive cooling, a computer controlled liquid cooling system is provided for high heat rejection demands. The remainder of the paper is organized as follows. Section 5.3 describes the proposed hybrid cooling strategy in detail. The corresponding mathematical model for the complete hybrid cooling system is presented in Section 5.4. Then, the findings are validated through a set of bench top experimental tests presented in Section 5.5. Finally, Section 5.6 includes the conclusion.

5.3 Cooling System Description

Propulsion system electrification has increased the demand for innovative electric motor cooling systems which operate with high efficiency and minimum energy consumption. Electric vehicle drive systems and accompanying battery packs are typically recognized as the primary heat generating sources in electric vehicles. The heat generation usually ranges over low to high with respect to operating conditions. The generated heat must be routed towards the ambient surroundings to maintain the system's prescribed temperature. Low to moderate heat generation rates usually correspond to stationary conditions or low speed driving profiles. In this case, a high-performance passive cooling system may be sufficient to dissipate the associated thermal energy with no external power consumption. However, passive cooling pathways usually suffer from lack of high heat transfer capabilities.

Passive cooling limited heat transfer effectiveness necessitates the integration of a supplementary conventional liquid cooling system in the proposed vehicle cooling system for high heat dissipation scenarios. The proposed thermal management system features a passive heat rejection pathway along with a computer controlled conventional liquid cooling system to efficiently satisfy the cooling demands over a

wide range of heat generation instants. The liquid cooling system operating cycles may be optimized based on a supervisory control algorithm for minimal energy consumption and maximized cooling system efficiency. This heat is typically dissipated to the ambient surroundings or transferred to a heat recovery system. To avoid overheating, the heat generated during operation should be efficiently transmitted out of the motor housing through a high conductive thermal mechanism, or "cradle". The cradle's optimized surface area offers low thermal resistance to provide a high thermal conductivity pathway between the heat source and a thermal bus for heat transportation or an attached heat exchanger for heat dissipation to the ambient environment.

The flexible thermal bus may be designed for short or long-distance heat transportation. A passive thermal bus may be composed of high thermal conductivity materials or two-phase passive devices to efficiently transfer the heat. The thermal properties including high thermal conductivity, diffusivity, and low thermal expansion may significantly influence the thermal energy transmission. An effective thermal bus may feature multiple heat rejection pathways for different heat rejection scenarios along with some fluid passages for fluid flows that significantly increase the thermal capability of the cooling system. This process is essentially associated with an exceptional convective heat transfer coefficient induced by absorbing/releasing sensible and latent heat.

The transported heat must be dissipated to the ambient surroundings; typically a high efficiency heat exchanger with an electric fan. The thermal efficiency of the heat exchanger is typically characterized by the effective heat transfer surface area, thermal conductivity, and the convective heat transfer co-efficient. The surface area of the heat exchanger is maximized for any particular applications with respect to space limitations. The thermal conductivity of the heat exchanger is further limited due

to manufacturing costs, total weight, and operating conditions. Improved convective heat transfer coefficient may significantly increase the heat dissipation to the ambient surroundings. Convective heat transfer coefficients and effective heat transfer surface areas are typically maximized with integration of different fin designs, including, but not limited to, plain, wavy, and louvered fins, and/or optimization of fin spacing. Enhanced convective heat transfer coefficients may be achieved by introducing forced convection to the radiator, which increases air flow running through the fin arrays.

The complete electric motor cooling system architecture is conceptually shown in Figure 5.2. The generated heat is primarily dissipated to the ambient environment though the passive cooling system, composed of multiple heat pipes extending within the cradle structure on one side, and attached to a finned structure heat sink assembly on the other side. An optional centrifugal fan is then placed in the middle of the heat sink structure for enhanced convective heat transfer rate as necessary. In addition to the passive cooling system, a complete conventional liquid cooling system is supplied to the electric motor through a cooper coil wrapped around the external surface area of the main cradle structure for increased heat rejection capabilities during high heat rejection demands. The cradle structure surface, including the copper coil, is completely covered by insulation materials to channel the heat. Therefore, the generated heat is only shared between the passive and active cooling systems while there is no direct heat dissipation to the ambient surroundings through the cradle structure.

5.4 Mathematical Model

The proposed hybrid cooling system is modelled using a lumped parameter approach to estimate the thermal performance for various driving profiles. Figure 5.3

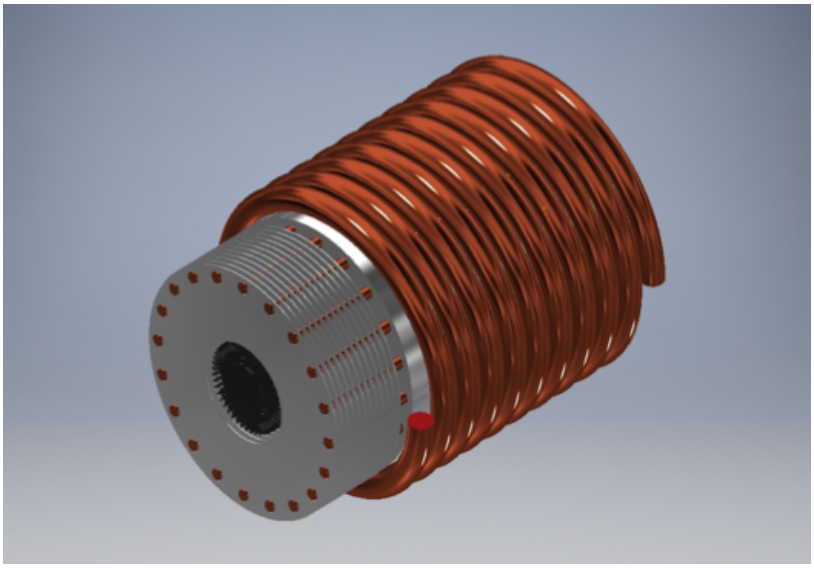

Figure 5.2: Compact cooling system for an electric motor with the insulating protective cover removed.

illustrates a schematic diagram for the proposed hybrid cooling system thermal nodal network. This hybrid system features a passive heat rejection pathway combined with a conventional liquid cooling system. The power consumption is calculated based on the active cooling fan and water pump electrical power specifications. The cooling system is interfaced with an emulated electric motor through a high thermal conductivity cylindrical cradle structure that brings the contact to the electric motor housing. The heat is dissipated to the ambient surroundings via two separate heat exchangers; a heat sink and a radiator.

The passive cooling system features a load bus which transfers the thermal energy to the heat sink for dissipating to the ambient. The thermal bus mechanism consists of multiple capillary heat pipes with the evaporator sides extending inside the cradle structure and the condenser sides extending outside the cradle. The heat pipes are placed equally spaced in a radial pattern within the cradle wall. A series of fins is added to the heat pipes' condenser sections for enhanced heat dissipation. A

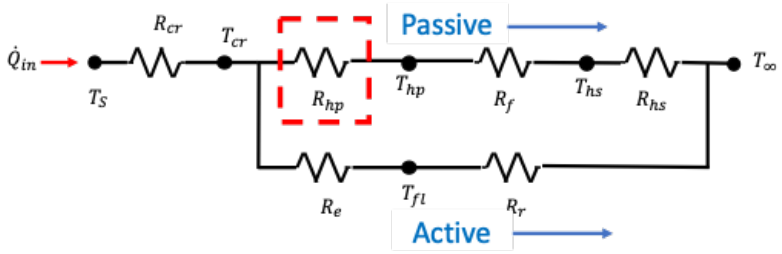

Figure 5.3: Thermal nodal network for hybrid cooling system.

centrifugal fan may be placed in the center of the heat sink to promote forced convection if needed. Capillary heat pipes typically offer high effective thermal conductivity, low weight, and compact thermal bus structures for short distance heat transmission.

A standard active cooling system is incorporated for high heat rejection scenarios. The heat is transferred to the coolant through a helically coiled copper tube, referred to as a "water jacket", wrapped around the periphery of cradle structure. The heat is then dissipated to the ambient through a radiator with an attached fan for forced convective heat transfer. The system circulates the coolant using a water pump while the associated flow rate may be measured by a flow meter.

5.4.1 Cradle

A significant amount of heat is produced within the electric motor housing as current flows through the winding structure. Traditional cooling systems typically offer air flow across the external shell or coolant flow within the shell. Water, ethylene glycol or oil flows around the periphery of the stator. The integration of hybrid cooling in electric motor applications necessitate an alternative thermal contact mechanism that provides high thermal conductivity thermal interfaces for both passive and active cooling pathways.

The cradle design includes an aluminum hollow cylinder that offers a hybrid

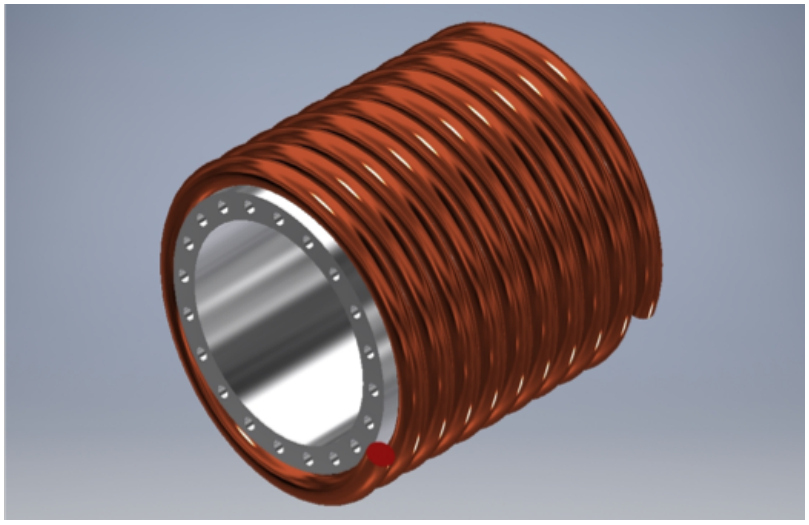

Figure 5.4: Hybrid cradle design featuring heat pipe holes and wrapped copper tubing for coolant circulation.

thermal contact for the motor housing interface (Refer to Figure 5.4). There are twenty holes, evenly spaced, within the wall for the passive thermal bus interfaced with the heat pipe evaporators. The coolant may be supplied to the electric motor through a copper pipe tubing of 1/2" diameter helically coiled around to the lateral surface of the cradle structure. The cradle structure, including the spring coil, is well-insulated to avoid heat dissipation to the cradle surroundings. However, the insulation material and the insulating protective cover are not shown in figure 5.4 to emphasis on the demonstration of e-motor cradle structure.

The temperature profile over the cradle may be modeled as a hollow cylinder with two boundary conditions. For one-dimension, steady state condition, with no internal heat generation, the cradle temperature, T_{cr}, may be written as

$$\frac{1}{r}\frac{\delta}{\delta r}\left(kr\frac{\delta T}{\delta r}\right) = 0 \tag{5.1}$$

$$T_{cr}(r) = C_1 ln\big(\frac{r}{r_1}\big) + C_2 \tag{5.2}$$

where C_1 and C_2 are constants, k denotes the thermal conductivity, and $_1$ indicates the inner cylinder radius. The complete Nomenclature List may be found in the Appendix.

The boundary conditions include a surface temperature specification at the inner radius, $r = r_1$, which may be expressed as

$$T_{cr}(r_1) = T_s \tag{5.3}$$

A heat flux condition may be imposed at the outer surface. The heat flow, q , is continuous between the cylinder and the fluid,$r = r_2$, so that

$$q = -k\frac{\delta T_c}{\delta t} = h(T_{cr}(r_2) - T_{fl}) \tag{5.4}$$

where h is the convective heat transfer coefficient, $T_f l$ denotes the coolant temperature, and r_2 represents the outer radius of the cylinder where the cradle is interfaced with the coolant.

Finally, the expression for the cradle's temperature distribution, $T_{cr}(r)$, becomes

$$T_{cr}(r) = \left(\frac{T_s - T_{fl}}{\frac{k}{hr_2} + ln\big(\frac{r_2}{r_1}\big)}\right) ln\left(\frac{r}{r_1}\right) + T_s \tag{5.5}$$

The temperature profile over the cradle structure, T_{cr}, may be calculated when the heat transfer is associated with conduction and convection. The cradle thermal

resistance, R_{cr}, may be modeled using two resistances in series so that

$$R_{cr} = \frac{L_{cr}}{k_{cr}A_{cr}} + \frac{1}{h_{cr}A_{cr}} \tag{5.6}$$

where terms L_cr, k_cr, A_cr, and h_cr denote the cradle length, thermal conductivity, heat transfer surface area, and convective heat transfer coefficient.

5.4.2 Heat Pipes

Heat pipes are two-phase passive devices with exceptional thermal conductivity, long lasting durability, structure flexibility, and minimal temperature drop along the structure. They usually contain a small amount of working fluid (e.g., water, acetone, ammonia). Once the heat is applied to one end of the pipe, the working fluid, accumulated in the wick structure, is vaporized. The resulting vapor pressure moves the vapor towards the other end, condenser, where the latent heat of vaporization is released, and the vapor returns back to the liquid phase. Then, the liquid passively travels back to the evaporator section through the wick due to the capillary pressure. The latent heat of vaporization is continuously transferred from the evaporator to the condenser section as long as the capillary pressure, created across the wick structure, is adequate for flow circulation within the pipe. Heat pipes can be of any size and configuration. The thermal behavior of capillary forced heat pipes interfaced within the electric motor shell was computationally modeled and studied [17]. Figure 5.5 conceptually displays the design of the cradle with the heat pipes installed.

The thermal performance of heat pipes is typically characterized with respect to their configurations, diameters, total lengths, working fluid thermal properties, wall and wick structure materials, etc. Capillary pressure, required to run the liquid flow throughout the heat pipe, is created within the wick structure. The wick structure

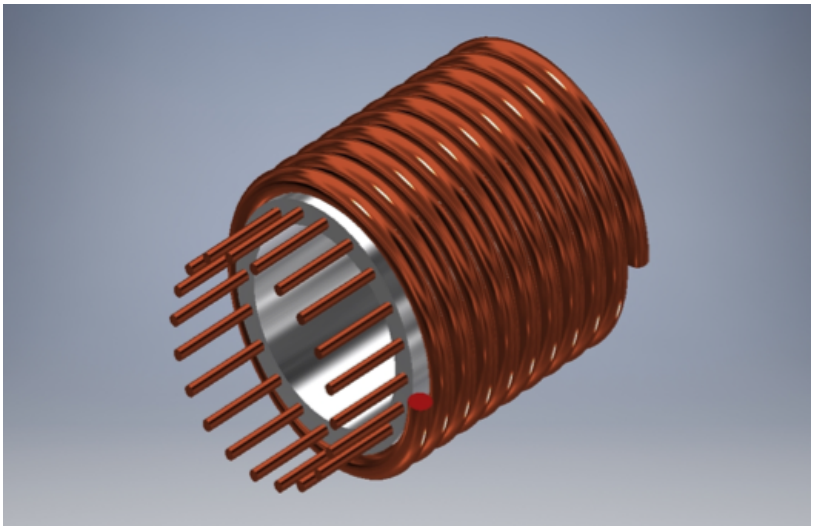

Figure 5.5: Cradle structure with embedded heat pipes inserted to form radial pattern before addition of circular fins.

usually contains a porous material which can be characterized by the porosity and permeability. The capillary pressure, P_c, must be large enough to overcome the frictional pressure losses occurring during the evaporation-condensation process or

$$\Delta P_c > \int_{L_{ef}} \frac{\delta P_v}{\delta x} dx + \int_{L_{ef}} \frac{\delta P_l}{\delta x} dx + \Delta P_{PC,e} + \Delta P_{PC,c} + \Delta P_g \tag{5.7}$$

where ΔP_c)is the capillary pressure created within the wick structure, $\frac{\delta P_v}{\delta x}$ is the sum of inertial and viscous pressure drop occurring in vapor phase due to vapor flow, and $\frac{\delta P_l}{\delta x}$ is the sum of inertial and viscous pressure drop occurring in the liquid phase. The symbol $\Delta P_{PC,e}$denotes the pressure gradient across the phase transmission in the evaporator, $\Delta P_{PC,c}$ represents denotes the pressure gradient across the phase transmission in the evaporator, andΔP_g is the static pressure drop due to gravity. The terms $\Delta P_{PC,e}$and $\Delta P_{PC,c}$ are neglected to simplify the mathematical description based on operating conditions.

The thermal behavior of capillary forced heat pipes may be simplified using

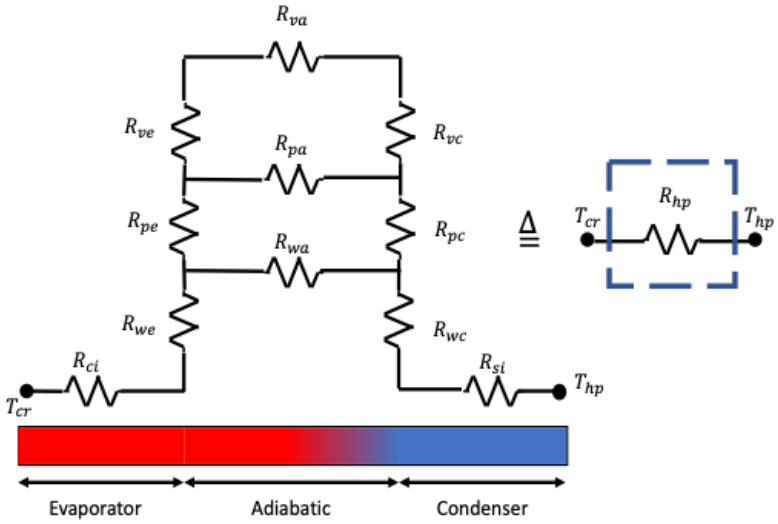

Figure 5.6: Thermal nodal network associated with a capillary heat pipe and simplified notations.

the lumped parameter analysis. The thermal nodal network, shown in Figure 5.6, corresponds to a round heat pipe interfaced with a heat source and a heat sink.

The thermal resistance of the heat pipe, R_{hp}, may be expressed as

$$R_{hp} = \frac{T_{cr} - T_{hp}}{q_{hp}} \tag{5.8}$$

where T_hp represents the heat pipe operating temperature and q_hp is the heat is being transferred. The corresponding thermal performance of the capillary forced heat pipe may be estimated as

$$R_{hp}^{-1} = \left[R_{ci} + R_{we} + R_{pe} + R_{ve} + \frac{1}{\frac{1}{R_{va}} + \frac{1}{R_{pa}} + \frac{1}{R_{wa}}} + R_{wc} + R_{pc} + R_{vc} + R_{si} \right]^{-1} \tag{5.9}$$

In this expression, R_{we}, R_{pe}, and R_{ve} represent the thermal resistance of the wall,

wick, and vapor in the evaporator. Similarly, R_{wc}, R_{pc}, and R_{vc} denote the thermal resistance of the wall, wick, and vapor in the condenser. Further, R_{va}, R_{pa}, and R_{wa} indicate the vapor, wick structure, and the wall thermal resistances in the axial direction, respectively.

The external contact thermal resistance at the evaporator interface, R_{ci}, may be stated as

$$R_{ci} = \frac{R'_e}{\pi d_0 L_e} \tag{5.10}$$

where $R_e^{'}$ is the contact resistance, d_o is the inner diameter of the pipe, and L_e denotes the evaporator length. The contact thermal resistance at the condenser interface, R_{si}, may be expressed as

$$R_{si} = \frac{R'_c}{\pi d_0 L_c} \tag{5.11}$$

where L_c indicates the condenser length and $R_c^{'}$ is the contact resistance between the heat pipes and the heat sink.

The radial conduction resistance in cylindrical coordinate, R_w, becomes

$$R_w = \frac{ln(\frac{d_{wo}}{d_{wi}})}{2\pi L_w k_w} \tag{5.12}$$

where d_{wo} and d_{wi} represent the inner and outer diameters of the pipe, L_w is length, and k_w corresponds to the thermal conductivity of the pipe.

The thermal conduction for the wick structure in radial direction, R_p, may be written

$$R_w = \frac{ln(\frac{d_{po}}{d_{pi}})}{2\pi L_p k_p} \tag{5.13}$$

where d_{pi} and d_{po} are the inner and outer diameters of the wick structure. Lastly, L_p represents the length, and k_p is the wick thermal conductivity.

The adiabatic thermal resistance, $R_v a$, may be expressed as

$$R_w = \frac{T_v(P_{ve} - P_{vc})}{\rho_v h_{fg} q} \tag{5.14}$$

where T_v is the vapor temperature, $P_v e$ and $P_v c$ indicate the vaper pressures in the evaporator and condenser. Note that the thermal resistance at the liquid-vapor interfaces, $R_v e$ and $R_v c$, as well as the adiabatic vapor chamber, $R_v a$, are negligible due to this small values.

The equivalent thermal resistance, $R_h p$, may be reduced to the expression

$$R_{hp}^{(} - 1) = (R_{we} + R_{pe} + R_{wc} + R_{pc})^{(} - 1) \tag{5.15}$$

5.4.3 Heat Exchanger

The cooling system design requires a high efficiency heat exchanger which significantly enhances the heat dissipation to the ambient surroundings. The heat dissipation can be raised by expanding the effective heat transfer surface area, increasing the convective heat transfer coefficient, and/or integrating high effective thermal conductivity materials. A properly designed heat exchanger may feature a fan to compensate the lower convective coefficient if ram-air becomes insufficient (e.g., a low speed driving mode or stationary conditions). The proposed electric motor hybrid cooling system offers two separate heat exchangers. One is a circular finned heat sink structure attached to the back side of the electric motor with as associated fan in the center. The second heat exchanger is a standard ground vehicle radiator assembly for active cooling.

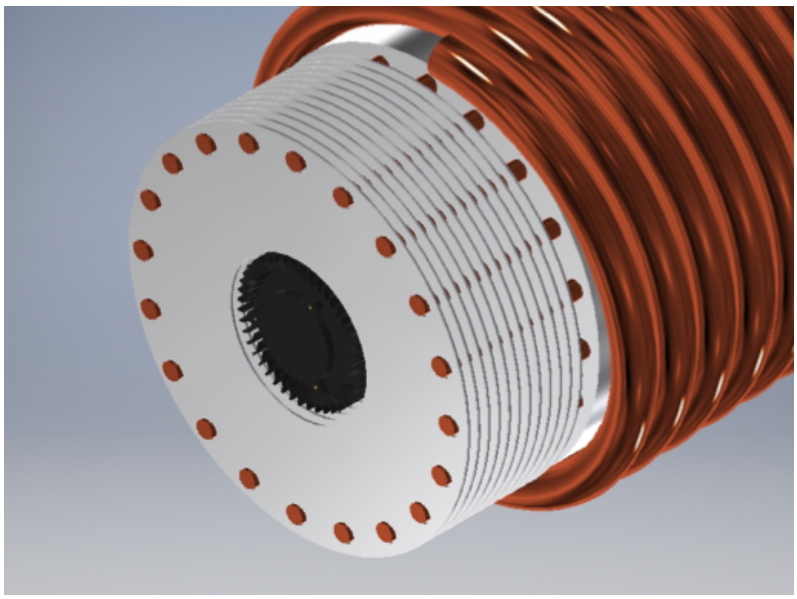

Figure 5.7: Electric motor cooling system with attached finned heat sink and optional centrifugal fan for forced convection.

Figure 5.7 illustrates the complete passive cooling system design, including the finned heat sink with the attached fan for greater heat dissipation. Adding fins extends the heat transfer surface area and consequently, increases convective heat transfer coefficient of the system. The system features multiple circular fins mounted on the outer ends of the embedded heat pipes. When properly designed, passive free convection cooling may be able to maintain the electric motor operating temperature should the ram air intake be sufficient, or heat generation is low. However, a centrifugal fan, placed in the center of the heat exchanger, provides forced convection if needed based on a supervisory control algorithm.

Natural convection heat transfer significantly depends on effective heat transfer surface area and convective heat transfer coefficient. During the natural convection mode, the flow between the fins is induced by the buoyancy effect as the fin surface temperatures exceed the ambient temperature (refer to Figure 5.8). The optimum fin

spacing consideration yields to the maximum convective heat transfer coefficient with respect to the lengths of the adjoining vertical plates. The optimum vertical plate spacing, S_{op}, may be expressed as

$$S_{op} = 3.24 L_f Re_L^{-1/2} Pr^{-1/4} \tag{5.16}$$

where L_f represents the fin length while $Re_L$and Pr denote the Reynolds number and Prandtl number.

The heat conducted to the fins may be modeled as a thermal resistance as follows

$$R_f = \frac{L_f}{k_f A_f} \tag{5.17}$$

where R_f is the conductive thermal resistance, k_f denotes the thermal conductivity of the fins, and A_f is the thermal interface surface area.

The convective heat transfer coefficient is calculated based on the Nusselt number which represents the dimensionless temperature gradient at the fin surface. The Nusselt number, Nu_s, for vertical oriented plates may be written as [67]

$$Nu_s = \frac{1}{24} Ra_s \left(\frac{S_{op}}{L}\right) \left(1 - e^{-\frac{35}{Ra_s \left(\frac{S_{op}}{L}\right)}}\right)^{0.75} \tag{5.18}$$

The flow motion between the adjoining vertical plates is governed by a balance between the viscous forces and buoyancy known as Rayleigh number. The Rayleigh number, Ra_s, for vertical plates can be expressed as

$$Ra_s = \frac{g \beta \Delta T S_{op}^3 \rho_a}{\alpha \mu} \tag{5.19}$$

where g is gravity, β represents the thermal expansion coefficient, Δ T is the temperature difference between the fin surface and the air, ρ_a denotes the air local density, α is the thermal diffusivity, and μ indicates the air viscosity. The free convective heat transfer coefficient, h_{fr}, can be stated as

$$h_{fr} = \frac{Nu_s k_A}{S_{op}} \tag{5.20}$$

where k is the thermal conductivity of the air with respect to the ambient and the fin surface temperatures.

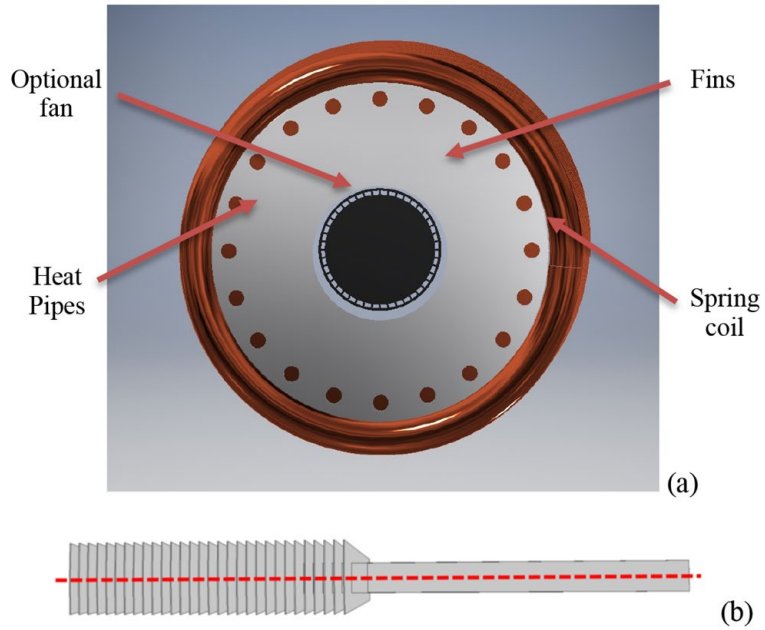

Figure 5.8: Hybrid cooling concept with heat pipes– (a) end view of system with heat pipe tips in contact with final circular fins; and (b) one heat pipe with plain finned heat sink assembly.

The forced convective heat transfer coefficient, Nu_b, acting upon the fins may

be expressed as [68]

$$Nu_b = \frac{1}{\left(\frac{Re_L Pr}{2}\right)^3} + \frac{1}{\left(0.644 Re^{0.5} Pr^{0.33} \sqrt{1 + \frac{3.65}{\sqrt{Re_L}}}\right)^3} \tag{5.21}$$

The Prandtl number, Pr, can be calculated as

$$Pr = \frac{\mu c_{p,A}}{k_A} \tag{5.22}$$

where $c_{p,A}$ denotes the specific heat of air.

The Reynolds number, used in Eq. (21), becomes

$$Re_L = \frac{\rho_a v_a S_{op}^2}{\mu L_f} \tag{5.23}$$

where v_A is the air flow velocity. The forced convection coefficient, h_{fo}, can be calculated by

$$h_{fo} = \frac{Nu_b K_f}{S_{op}} \tag{5.24}$$

The heat dissipation from the heat exchanger, q_o, to the ambient surroundings is governed by the convection heat transfer equation which can be expressed as

$$q_o = hA_{hs}(T_\infty - T_{hs}) \tag{5.25}$$

where h can be either the free or forced convective coefficient depending upon the fan operation cycle, and T_∞corresponds to the ambient temperature. The corresponding

convective thermal resistance for the heat sink, R_{hs}, may be stated as

$$R_{hs} = \frac{1}{hA_{hs}} \tag{5.26}$$

5.4.4 Conventional Cooling System

Hybrid ground vehicles typically utilize conventional liquid cooling systems to dissipate the generated heat to the ambient surroundings. A standard cooling system consists of a water pump, radiator, and a thermostat. Models for liquid cooling systems are typically composed of heat load-to-coolant heat exchanger (e.g., water jackets) and coolant-to-ambient surroundings heat rejection pathways (e.g., radiators). Electric motor cooling systems typically provide cooling passages around the periphery of the stator windings designed for heat dissipation through the coolant (e.g., water ethylene glycol, oil) circulation. There is a thermostat which regulates the heat exchange between the heat source/radiator/ambient and the coolant to maintain the heat load within a specified temperature range.

The designed cradle structure features a helically coiled tube supplied around the periphery of the emulated electric motor housing. This provides a convective heat transfer interface between the cradle outer surface area and the coolant. The exterior of the apparatus is assumed to be well insulated so that the dissipated heat is transferred to the coolant. The local convective heat transfer of spring coil heat exchangers depends on their configurations. The peripherally averaged Nusselt number, Nu_D, for constant wall temperature boundary condition is expressed as [69]

$$Nu_D = \left[\left(3.66 + \frac{4.434}{a}\right)^3 + 1.153\left(\frac{Re_D(\frac{D}{C})^{1/2}}{b}\right)\right]^{3/2} \tag{5.27}$$

where $a = 1 + \left[\frac{927(\frac{C}{D})}{Re_D^2 Pr}\right]$ and $b = 1 + \left[\frac{0.477}{Pr}\right]$ while D and C are constants evaluated based on the spring coil heat exchanger dimensions.

The averaged convective heat transfer coefficient, $\overline{h}$, may be calculated as

$$\overline{h} = Nu_D \frac{k_e}{d_e} \tag{5.28}$$

The convective thermal resistance, R_e, due to the heat transfer occurred between the coolant and the cradle may be stated as

$$R_e = \frac{1}{\overline{h} A_e} \tag{5.29}$$

where A_e is the coil thermal contact surface area.

The system dissipates the absorbed thermal energy to the ambient surroundings through a single pass flow radiator with the fan assembly. The radiator performance may be characterized with the inlet and outlet fluid temperatures, effective heat transfer surface area, and the overall heat transfer coefficient. Calculation of the overall heat transfer coefficient for heat exchangers is not straight forward. However, it can be estimated through experimental temperature measurements for a selected radiator. The heat transfer between the heat exchanger structure and the surroundings is assumed to be negligible so that the overall heat transfer between the hot and cold fluid is conserved so that

$$q_c = q_A \tag{5.30}$$

where q_c represent the amount of the heat released by the coolant throughout the radiator. The heat dissipated to the ambient surroundings due to the air motion, q_A,

induced by the fan assembly, becomes

$$q_A = m_A A c_{p,A}(T_{Ai} - T_{Ao}) \tag{5.31}$$

where T_{Ai} and T_{Ao} are the air temperatures at the inlet and outlet of the heat exchanger while $c_{p,A}$ represents the specific heat of air. They can be simply measured using two thermocouples at the air intake and air outtake of the radiator. The term m_A represent the air flow rate which may be calculated

$$m_A = \rho_A v_A A_A \tag{5.32}$$

where ρ_A, v_A, and A_A represent the density, velocity and the heat transfer surface area, respectively. The air velocity, $v_a ir$, can be measured experimentally using an anemometer in the laboratory.

The amount of the heat released through the coolant due to the fluid flow within the radiator may be evaluated as

$$q_c = m_c c_{p,c}(T_{ci} - T_{co}) \tag{5.33}$$

where m_c is the coolant flow rate induced by the water pump, $c_{p,c}$ represents the coolant specific heat, and T_{ci} plus T_{co} denote the coolant temperatures at the inlet and outlet of the radiator. The coolant flow rate, and the temperatures are obtained through experimental testing measurements using a flow meter. The radiator convective thermal resistance, R_r, may be estimated as

$$R_r = \frac{1}{m_c c_{p,c}} \tag{5.34}$$

A summary of the parameters used in the numerical simulation, MATLAB/Simulink,

is presented in Table 5.1.

Symbol	Value	Unit	Symbol	Value	Unit
A_A	7e-2	m^2	L_{Cr}	0.01	m
A_{cr}	6.3e-2	m^2	L_e	0.135	m
A_e	4.7e-2	m^2	L_f	4e-4	m
A_f	2.5e-2	m^2	L_p	7.5e-4	m
A_{hs}	0.43	m^2	L_w	7.5e-4	m
$c_{\rho,A}$	1000	J/kg.K	$\dot{m}_A$	4.6	m/s
$c_{\rho,c}$	4200	J/kg.K	$\dot{m}_c$	1.1	m/s
d_e	1e-2	m	m_{cr}	2.05	kg
d_{pi}	3e-3	m	m_s	4.8	kg
d_po	4.5e-3	m	n	17	-
d_{wi}	4.5e-3	m	R_{pc}	6.11e-3	K/W
d_{wo}	6e-3	m	R_{pe}	2.94e-3	K/W
g	9.81	m/s^2	R_{wc}	1.53e-3	K/W
h	15	W/m^2K	R_{we}	7.37e-4	°C
k_A	2.6e-2	W/mK	S_{op}	4e-3	m
k_cr	205	W/mK	T_o	24	°C
k_e	400	W/mK	T_{ref}	60	°C
k_f	205	W/mK	T_∞	22	°C
k_p	200.3	W/mK	v_A	5	m/s
k_w	400	W/mK	ρ_A	1.225	kg/m^3
L_c	6.5e-2	m	β	3.4e-3	k^{-1}

Table 5.1: Summary of the model parameters used in the numerical simulation.

5.5 Experimental System

The hybrid cooling system numerical findings are validated through a complete set of bench top scale thermal testing in the laboratory. The components required to set up the hybrid cooling system are manufactured with the same dimensions and specifications as designed and simulated in the mathematical model. The cooling system is interfaced with an emulated electric motor which add the desired heat to the system. Integration of the emulated electric motor simplifies the regulation

of the heat generation in laboratory. The emulated electric motor is a cylindrical aluminum block which is 0.1m in diameter and 0.16m in length. Six cartridge heaters are embedded in a radial pattern, equally spaced, within the block for uniformed heat distribution. Figure 5.9(a) illustrates the schematic of the aluminum block with the heaters installed.

The emulated electric motor is interfaced with the cooling system through the cradle structure. The manufactured cradle is shown in Figure 4.9(b). The cradle is an aluminum hollow cylinder that accommodates the e-motor structure. The microscopic gap between the electric motor and the cradle structures is filled up with thermal paste for improved thermal contact. Twenty holes, equally spaced, are then machined within the cradle wall that provides room for heat pipe placements. 0.15m of the heat pipes are inserted within the cradle wall while the remaining is left out to serve as the condenser. The active cooling system is then supplied to the cradle structure through a thin-wall copper tubing attached to the lateral surface.


(a)

(b)

(c)

Figure 5.9: Experimental test bench components – (a) Emulated electric motor with six heater cartridges, (b) cooling system structure, and (c) graphical display of data acquisition screen.

Passive is the primary heat rejection pathway in the system. The heat is carried out of the cradle through the heat pipes. A finned structure heat sink is then attached to condenser section of the heat pipes for extended heat transfer surface area. The heat sink features a centrifugal fan for enhanced heat dissipation to the

ambient surroundings. Ram air intake is supplied to the system through a three-phase variable speed AC blower located near the heat sink. The excess heat is then dissipated to the ambient surroundings through the computer controlled liquid cooling system. The water pump and radiator fan operating cycles are regulated based on the emulated electric motor temperature readings PID algorithm. The signals, including temperatures and current measurements, are recorded on a computer through a data acquisition system and analyzed on National Instrument Lab-View using NI-6211 data acquisition system as shown in Figure 5.9(c).

The performance of the proposed hybrid cooling system is investigated for different heat loads between 90VA to 750VA heat. The thermal response of the cooling system is studied through different experimental test configurations. The corresponding test matrix is summarized in Table 5.2. First, the thermal performance of each individual cooling system is investigated for different load profiles. Next, the complete hybrid system efficiency is explored for various thermal loading scenarios.

5.6 Numerical and Experimental Results

A complete electric motor hybrid cooling system, including passive and active cooling strategies, is designed and numerically modeled. The cooling system thermal performance is then validated through a set of bench top scale thermal testing on an emulated electric motor. The generated heat is transported from the motor through the cradle that routes it towards the hybrid cooling system. The passive cooling is the primary heat rejection pathway which is composed of multiple capillary forced heat pipes incorporated within the cradle structure. The pipes transfer the generated heat to the heat sink where the heat is dissipated to the ambient surroundings. For large heat dissipation demands, a computer controlled conventional liquid cooling

system is supplied to the electric motor through a helically coiled tube attached around the periphery of the cradle. When properly designed, the cooling system must regulate the electric motor operating temperature between 50°C to 60°C. The ambient temperature is T_{∞}=22°C with a maximum motor operating temperature of T_{max}=60°C.

The thermal response of the emulated electric motor subjected to steady state heat input is initially investigated with no cooling supplied. Figure 5.10 displays the thermal response of the motor subject to 160VA heat. The motor temperature exceeds 185°C after 4 hours with time constant of 54 minutes. Next, the aluminum housing is placed within the cradle structure and the temperature response of the emulated electric motor is recorded to determine the combined transient thermal response. As expected, slower heat and lower temperatures were observed due to the increased thermal capacitance and outer surface area of the complete assembly.

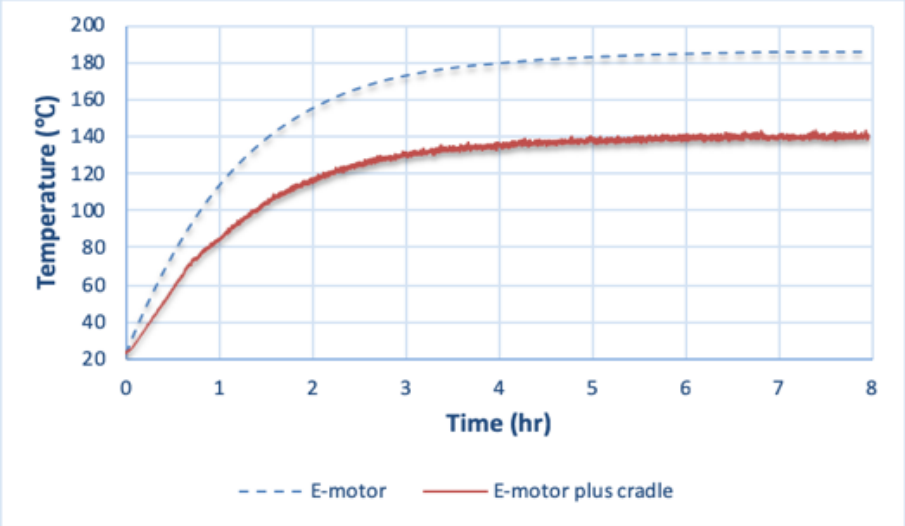

Figure 5.10: Test #0 (baseline) - Temperature response of emulated 160VA electric motor; time constants of 54 minutes and 48 minutes for the e-motor and electric motor plus cradle.

The heat pipe-based system is then applied to the emulated motor. The heat

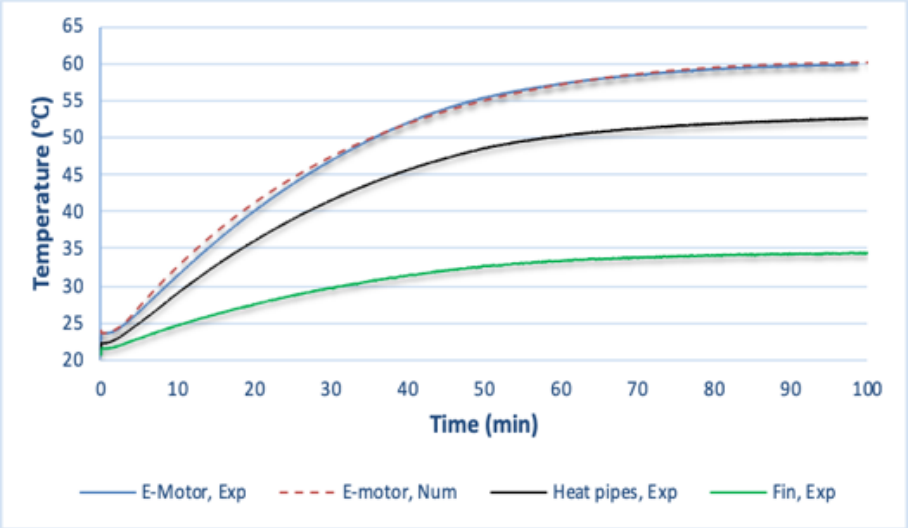

Figure 5.11: Test #2 – Experimental and numerical temperature responses of the system with emulated electric motor interfaced to heat pipe forced convection.

can be transported to the finned structure sink through twenty heat pipes embedded within the cradle. Figure 5.11 shows the experimental and numerical temperature response of the emulated motor, thermal bus, and heat sink subjected to 160VA heat while only the forced air convective cooling strategy is supplied. The experimental and numerical results show that passive cooling system could cool down the electric motor temperature down to 59 where the electric motor operating condition is secured. The load's temperature should never violate the prescribed operating temperature limits which is set to T_{ref}.

To maintain the temperature during high heat generating instances, the conventional liquid cooling system is coupled with the heat pipe cooling method. A classical controller is employed to minimize the water pump and radiator fan operating cycles. The operating cycles is regulated with respect to the e-motor's operating temperature to avoid over-cooling or overheating. The controller is programmed so that the conventional liquid cooling is actuated once the e-motor reaches to T_{ref}.

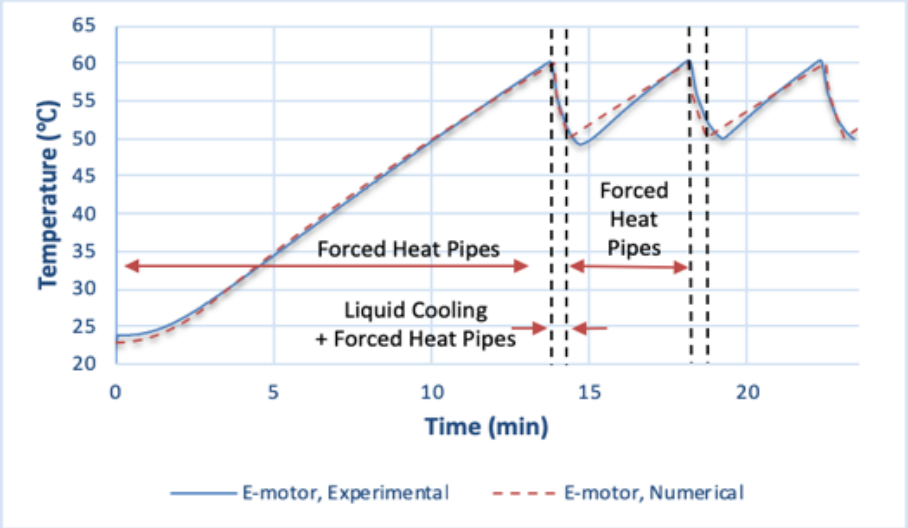

Figure 5.12: Test #5 - Thermal response of emulated motor interfaced with heat pipe forced convection and liquid convective cooling system subject to 500VA heat continuously applied.

Once the temperature reaches to T_{ref}, the excessive heat is dissipated through the coolant circulation between the evaporator and radiator until the e-motor cools down to T_{ref}-10°C. This is a continues cycle as long as an excessive heat is added to the cooling system. This strategy will secure the electric operating conditions with minimum energy consumption required for running the water pump and fan. Figure 5.12 displays the numerical and experimental temperature responses of the electric motor subject to 500VA heat (Test #5). The heat is initially removed through the passive cooling strategy until the electric motor temperature reaches to T_{ref} at t=13.2 (min). This is the point where the conventional liquid cooling system kicks in and reduce the temperature down to T_{ref}-10°C at t= 13.8 (min). The numerical model developed in Section 3 for the electric motor hybrid cooling is also validated through bench top testing. As shown in Figure 5.12, the numerical and experimental results differ by approximately 5% but have the same trends throughout the transient response as demonstrated by the close tracking. Consequently, the mathematical

model can serve as an engineering design tool for cooling system configuration and component sizing studies.

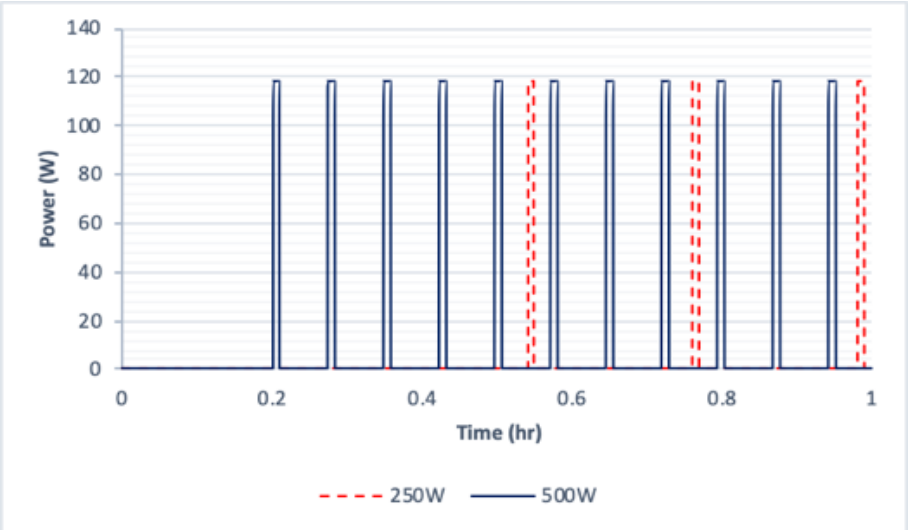

Figure 5.13: Test Nos. 3 and 5 - Cooling system power consumption associated with the 250VA (dashed line) and 500VA (solid line) applied thermal loads.

Figure 5.13 displays the electric motor cooling system power consumption subject to 250VA and 500VA continuous heat inputs as function of time. These results illustrate that the conventional liquid cooling system operates more frequently to maintain the motor temperature within the allowed rating temperature as the heat input to the cooling system grows. However, the discrete operating cycle for the pump and fan actuators should be observed which is due to the presence of the parallel heat pipe cooling pathway.

The power consumption by the cooling system's actuators is listed in Table 5.2. Figure 5.14 displays the relationship between heat pipe thermal transport capabilities and the system energy consumption. The free and forced convective based heat pipe solution consumes minimal energy but remains limited to the 160VA for the laboratory experiment. However, the hybrid cooling architecture scales readily to

Test No.	Heat Input (VA)	System Configurations			T_{max} (°C)	Time Constant (min)	Heat Flux (W/m^2)	Cooling	
		Heat Pipe		Liquid Cooling				Power Consumption (KJ)	Energy Consumption (W-hr)
		Free Convection	Forced Convection						
0	160	-	-	-	185	54	-	-	-
1	160	X			92	38	88	0	0
2	160		X		55	29	160	21.6	6.0
3	250		X	X	60	-	-	32.3	8.9
4	250			X	60	-	-	49.7	13.3
5	500		X	X	60	-	-	66.7	18.5
6	750		X	X	60	-	-	103.8	28.8

Table 5.2: Experimental test matrix to explore thermal response of cooling system methods

accommodate larger heat loads with cyclical operation of the pump and fan. In Table 5.2, the time constants for the free and forced convection of air and liquid are listed to provide insight into the overall transients.

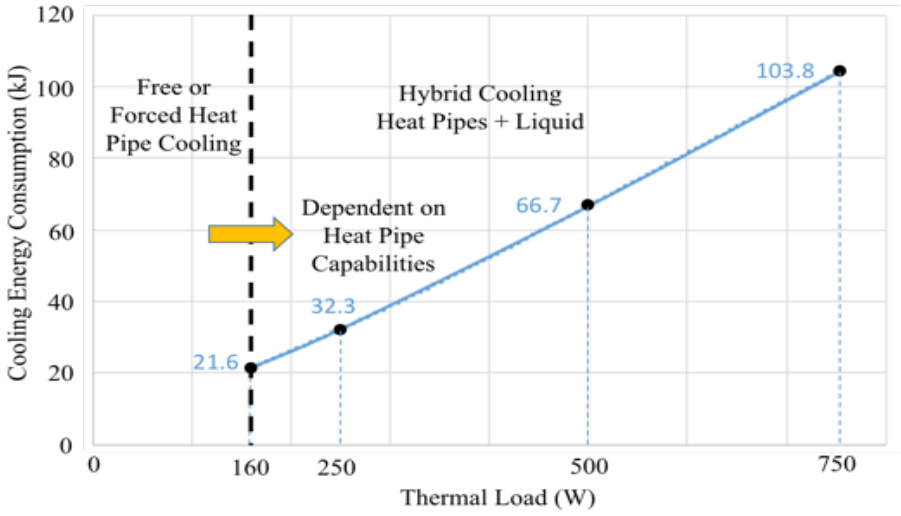

Figure 5.14: Hybrid cooling system energy consumption as a function of thermal heat load which indicates design opportunity for sizing heat pipes.

The heat pipe cooling system thermal pathway effectiveness may be further investigated through experimental heat flux measurements. A heat flux measurement technique, using heat flux sensors, signal amplifiers, and a data acquisition system, has been previously applied to thermal fluid systems [70]. To evaluate the heat pipe

thermal capabilities, heat flux sensors are carefully placed between the cradle outer surface area and the copper tubing. As discussed, the emitted heat could exit the cradle structure through the heat pipes and/or the coolant. In the laboratory, the heat pipes are first removed so that the heat only leaves the cradle towards the copper tubing. This allows the total amount of heat transferred to the copper coils to be estimated. Second, the passive cooling structure, including the heat pipes, fins, and the fan assembly, is added to the cradle. Now, the heat may be shared between the heat pipe pathways where the heat is moved towards the heat sink and the copper coil. The heat flux measurement is then repeated at the same location. The experiment yields the heat flux difference between these two configurations and offers insight into the thermal transport process. Figure 5.15 displays the heat flux removed through the pipe cooling system subject to a 90VA heat load. The heat pipes remove approximately 50% of the heat flux while the remainder moves towards the coolant pathway. The heat flux magnitude measured with 160VA thermal load applied is reported in Table 5.2.

5.7 Conclusion

Military ground vehicle propulsion systems require a flexible thermal management option to accommodate aggressive operating cycles, harsh ambient conditions, and demanding designs. A novel hybrid cooling system, featuring passive and active cooling system strategies, has been proposed to optimize cooling system energy consumption. The passive cooling system consists of multiple capillary forced heat pipes which reject the heat to the ambient environment through an attached finned structure heat sink. A supplementary computer- controlled conventional liquid cooling system is then supplied to the electric motor for excessive heat dissipation demands. This

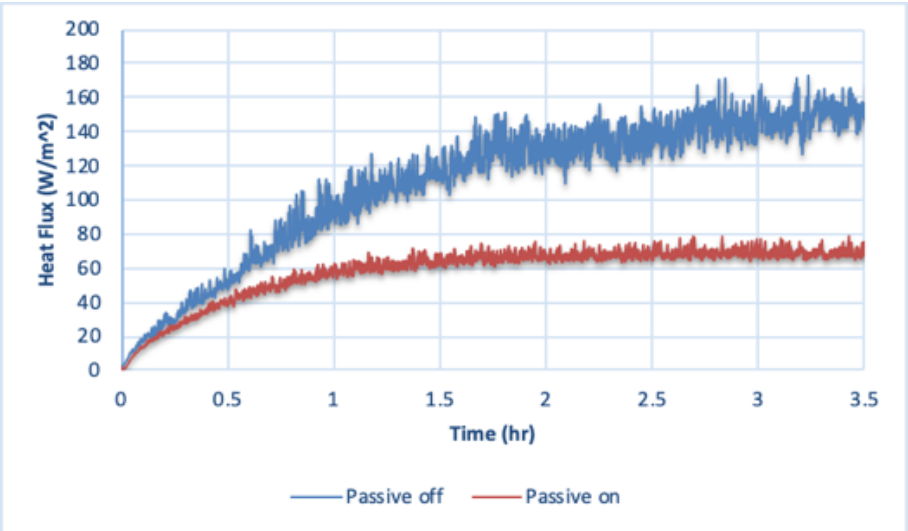

Figure 5.15: Heat flux measurements conducted on cradle outer surface area with heat pipes on (red line) and heat pipes removed (blue line): difference illustrates the amount of the flux removed by heat pipes subject to a 90VA applied load.

hybrid system is numerically modeled using a lumped parameter approach across the multiple thermal pathways. The developed mathematical model is validated through bench top experimental testing for several heat inputs and configurations. The results indicate that the cooling system can maintain electric motor temperatures within the target limit with reduced cooling systems actuator operation. The proposed hybrid cooling system could save up to 33% of the energy consumption while 250VA thermal load is applied. Future work includes refining the thermal management model, optimizing system parameters, and integrating real-time supervisory control algorithm for further minimized energy consumption.

Chapter 6

Multi-Objective Design Optimization of an Electric Motor Thermal Management System for Autonomous Vehicles

6.1 Abstract

The integration of electric motors into ground vehicle propulsion systems requires the effective removal of heat from the motor shell. As the torque demand varies based on operating cycles, the generated heat from the motor windings and stator slots must be rejected to the surroundings to ensure electric machine reliability. In this paper, an electric motor cooling system design will be optimized for a light duty autonomous vehicle. The design variables include the motor cradle volume, the number of heat pipes, the coolant reservoir dimensions, and the heat exchanger size while the cost function represents the system weight, overall size, and performance.

The imposed requirements include the required heat transfer per operating cycle (6, 9, 12kW) and vehicle size, component durability requirement, and material selection. The application of a nonlinear optimization package enabled the cooling system design to be optimized. Through numerical studies, a 50% reduced overall mass could be achieved for a 12kW heat generating scenario while the operating conditions are secured. These findings establish a design tool for multiple pathway cooling systems in electric motor propelled vehicles.

6.2 Introduction

Automobile industries, aerospace manufacturers, and robotic companies are moving fast towards electrification to achieve improved sustainability, reduce carbon emissions, and lower maintenance cost. On top of these, the United States currently requires importing an enormous amount of crude oil from unstable regions to satisfy domestic needs, which is a potential threat to the U.S national security. One sustainable solution is to replace traditional internal combustion engines with high-efficiency electric motors with battery packs to propel vehicles, from small robots to large trucks [71].

The integration of electric drive platforms offers higher power density, improved durability, enhanced fuel efficiency, and extended mission range while providing a quiet sentry mode of operation. In some instances, there is still a need for a hybrid powertrain system which includes a diesel engine besides an electric propulsion system to handle heavy-duty cycles. Besides these advantages, an advanced electric propulsion system could enable autonomy for the next generation of combat vehicles. This paradigm shift in military mobility requires an advanced thermal management system which can maintain the heat-generating components within their prescribed

operating temperature ranges while minimizing cooling system power consumption, overall size, and weight.

Current vehicles widely use liquid cooling systems for heat removal purposes. The traditional cooling methods contain several mechanical and electrical components, including water pumps, radiators, thermostats, fans, etc. Besides these components, a coolant is circulating between the radiator and the heat-generating devices to regulate the operating temperatures. Conventional liquid systems are well-established; however, these components' sizes are typically over-estimated to ensure the heat loads operating conditions during peak load operations [72]. An oversized cooling system may occupy immoderate space under the hood, leading to an unnecessary weight addition to the vehicle. This means a lot of energy consumption which may be saved to extend the electric range via electrification of targeted subcomponents.

Conduction and free convection heat transfer modes may be used to dissipate the heat with no external power. The passive heat transfer used to be enhanced by extending the heat transfer surface area or using high thermal conductivity materials. However, there is always a space limitation that restricts the heat transfer surface area. In recent developments, the integration passive methods (e.g., heat pipes, thermosyphons, phase change materials. etc.) has become popular for vehicle thermal management systems [65, 73–75]. Two phase passive devices are closed systems containing a small amount of working fluid, which continuously circulates between the evaporator and condenser sections as long as a temperature differential exists. These heat transfer devices feature exceptional heat transfer capabilities and outstanding structure flexibility, could offer an attractive, lightweight thermal management solution for vehicle applications [36, 76]. Passive devices' structure can be optimized with respect to the vehicle design configuration to maximize the performance while

minimizing the overall system size and weight [77].

Passive methods are typically applicable to energy systems where the heat generation is low to moderate. Therefore, a supplemental liquid cooling solution may be incorporated besides a passive cooling system to efficiently handle low, medium and high heat rejection loads. This strategy is known as "hybrid cooling" [60]. The integration of a hybrid cooling strategy for electric vehicle applications has been investigated in several numerical and experimental studies [59, 64, 78]. An advanced hybrid cooling system may integrate passive heat rejection pathways in parallel with a computer-controlled liquid cooling system. In this method, passive is the primary mode of heat transfer, while the fluid cooling system enables on-demand cooling for high heat generating instances. The computer-controlled liquid cooling system's energy consumption has been reduced with the regulation of actuator's operating time using non-linear control algorithms [57, 79].

The results demonstrate that hybrid cooling solutions could effectively impact the cooling system's energy consumption for different driving scenarios. However, these studies did not investigate the optimization of the cooling design parameters on the power usage and the total weight. Further improvement in autonomous vehicle cooling system energy efficiency, design configuration, and system weight may be achieved with optimization of the cooling system design parameters for a low-duty to heavy-duty application [80, 81]. This study aims to optimize a hybrid cooling system structural design using a nonlinear optimization approach. The design variables include the electric motor cradle dimensions, thermal bus size, and heat exchanger effective surface area. The cost function is comprised of the system weight, size, and performance while the required amount of heat transfer capabilities and space limitations serve as constraints. The optimized solution will satisfy the power demands and reduce the vehicle's costs due to fuel consumption and maintenance issues.

The remainder of this paper is organized as follows. Section 6.2 presents the hybrid cooling system architecture, including a "cradle," a "thermal bus," and heat exchangers. The design parameters are described in Section 6.3 where the optimization problem is formulated. Section 6.4 includes a discussion and numerical results. Finally, conclusions are presented in Section 6.5.

6.3 Hybrid Cooling System Strategies

An advanced autonomous vehicle carries several heat-generating electrical and electromechanical components, including electric motors, battery packs, and on-board electronics (refer to Fig. 6.1). The electric motor is generally recognized as the primary heat-generating component within the electric propulsion system. A significant amount of heat is produced due to the electrical and mechanical losses. The heat loss may be estimated with respect to the electric motor efficiency, instantaneous speed, and applied torque. This means that the electric motor heat generation rate basically depends on the road profile, driving scenario, and operating condition. To ensure an efficient electric motor operation, the excessive heat must be removed appropriately to maintain the temperature within a certain operating temperature range during the normal operation for reliable performance and enhanced durability. Conventional electric motors typically use a fan to blow air across a shell or a traditional liquid cooling system that circulates the coolant around the stator. The traditional methods generally require significant pump and fan operations, which increase the cooling system power consumption and noise generation.

In recent developments, the efficiency of electric motors has considerably improved. This means that the electric motor heat generation rate may be low to moderate in most instances, such as constant speed or idle mode of operating. How-

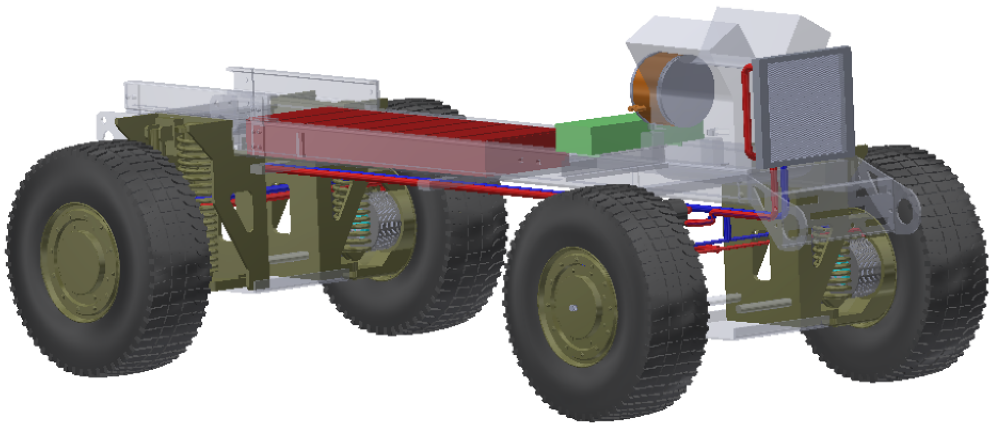

Figure 6.1: Autonomous military ground vehicle platform - A four wheeled chassis featuring in-hub electric propulsion with hybrid thermal management system.

ever, a relatively large amount of heat may be produced if a large amount of torque or sudden acceleration is required. A properly designed cooling system must offer different cooling modes, including passive and smart active solutions, to regulate the electric motor's temperature during the low, moderate, and high heat rejection needs with minimum power consumption while its structure occupies minimal space and adds minimum weight to the vehicle. Figure 6.2 demonstrates the hybrid cooling strategy that may apply to an in-hub electric motor.

Regardless of the electric motor power rating, size, and configuration, the electric motor cooling system must be thermally interfaced with the electric motor shell and/or the stator windings to collect the heat effectively. The integration of the hybrid cooling system requires an innovative thermal interface "cradle" that can effectively share the passive and active cooling systems. The heat moves to a flexible thermal bus which carries the heat to a remote heat exchanger. The hybrid thermal

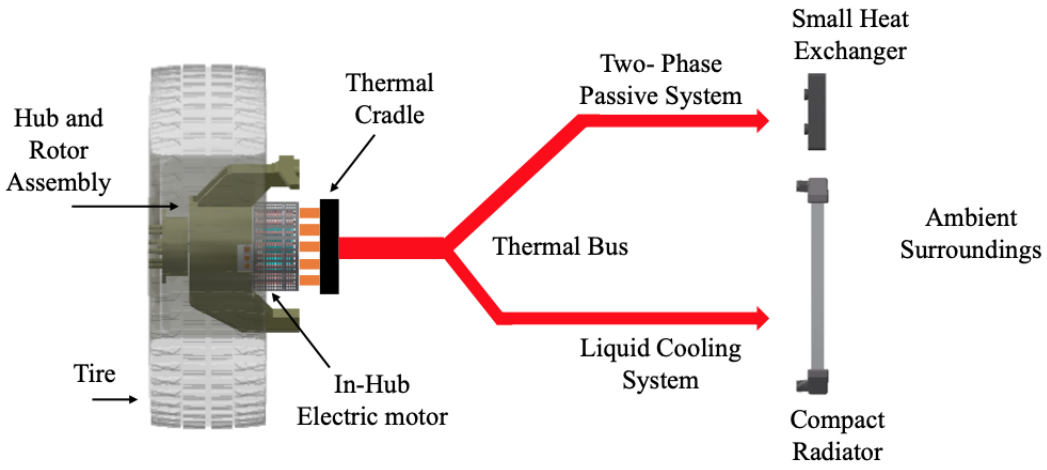

Figure 6.2: Hybrid cooling system configuration for a small size autonomous vehicle featuring in-hub electric motors.

bus incorporates a passive cooling pathway beside a complete computer-controlled liquid cooling system offering on-demand cooling. The smart liquid cooling system may contain a variable speed water pump with a controller programmed to regulate the operation with respect to the heat rejection demands.

Sometimes the heat needs to travel through very restricted pathways to reach the ambient surroundings. For instance, military ground vehicles sometimes restrict the ram air from flowing into the hood due to the vehicle's unique configuration and extraordinary operating conditions. This could be even more challenging if minimization of the thermal signature is required. Therefore, the thermal bus structure must be compact and flexible to carry the heat towards any direction with minimum sensitivity to gravity. The heat eventually dissipates to the ambient surroundings through the radiator(s). The cooling system may integrate a single radiator for the passive and active cooling systems or an induvial radiator for each cooling mode. This de-

pends on the required heat transfer capabilities and space limitations. The operation of the fan(s) may be regulated to reach further minimization in power consumption. Figure 6.3 graphically illustrates the hybrid cooling system prototype designed for in-hub electric motors.

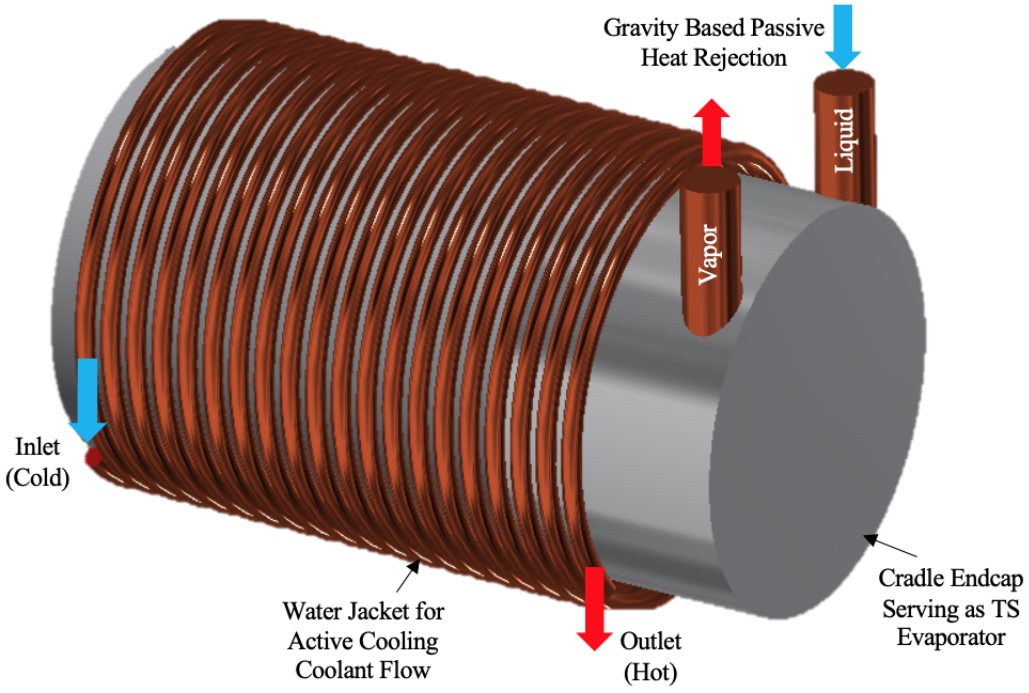

Figure 6.3: Hybrid electric motor cradle architecture for the hybrid cooling system.

6.4 Mathematical Model of Cooling System

The proposed hybrid cooling system incorporates a gravity aided two-phase closed-loop thermosyphon system for passive heat rejection. The thermosyphon is a sealed (under vacuum) closed loop system that effectively transfers heat between the

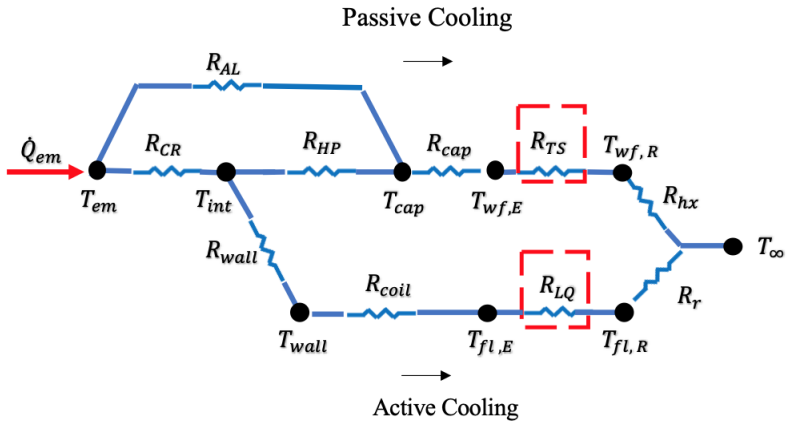

Figure 6.4: Thermal nodal network corresponding the hybrid cooling system featuring passive and active cooling methods.

evaporator and the heat exchanger. The heat initially vaporizes the working fluid through the evaporator. The vaporized working fluid travels the vapor line using the pressure created due to the temperature difference between the evaporator and condenser. The vapor releases the latent heat and turns back to the liquid phase in the condenser. The liquid is then moved back to the evaporator through the liquid line using gravity. To ensure the liquid return, the condenser must be placed slightly above the evaporator. This closed loop system offers exceptional effective thermal conductivity due to continuous evaporation-condensation during the heat transfer process within the system. The weight addition associated with the integration the two-phase passive device is minimal as it requires a relatively small amount of working fluid to operate.

This study implements a lumped parameter approach to model the cooling system mathematically. This model contains several thermal resistances representing the thermal behavior of the cradle, the thermal bus, and the heat exchangers. Figure 6.4 displays the thermal nodal network corresponding to the hybrid cooling

system. The model is used to set up the optimization problem and define the design parameters. The design parameters are discussed in the following subsections.

6.4.1 Cradle

The electric motor thermally interfaces with the cooling system with a thermal structure called "cradle." Figure 6.5 schematically illustrates a cradle design in the electric motor enclosed within a hollow cylinder with an endcap. The effective thermal conductivity of the cradle structure is enhanced with the integration of capillary heat pipes. Note the configuration of the heat pipes embedded within the cradle wall. The purpose of the heat pipes is to significantly increase the heat transfer to the endcap. The endcap structure features a built-in fluid passage which serves as an evaporator for the thermosyphon. The liquid cooling is supplied to the cradle through a copper pipe coiled around the cradle structure's external surface. This component is referred to as a "water-jacket." The contact thermal resistance between the components can be minimized once thermal paste is applied.

The cradle design parameters include the wall thickness, the number of heat pipes, the thermosyphon evaporator size, and the water jacket volume. The thermal contact resistance between the components is assumed to be negligible in this study. Figure 6.6 illustrates the 1-D thermal model representing the complete cradle thermal behavior.

The electric motor heat loss, $\dot{Q}_{loss}$, represents the overall heat loss due to the current circulation, $\dot{Q}_{ind}$, bearing motions , $\dot{Q}_{fr}$, and heat from outside world, $\dot{Q}_o$ while it may be expressed as

$$\dot{Q}_{loss} = \dot{Q}_{ind} + \dot{Q}_{fr} + \dot{Q}_o \tag{6.1}$$

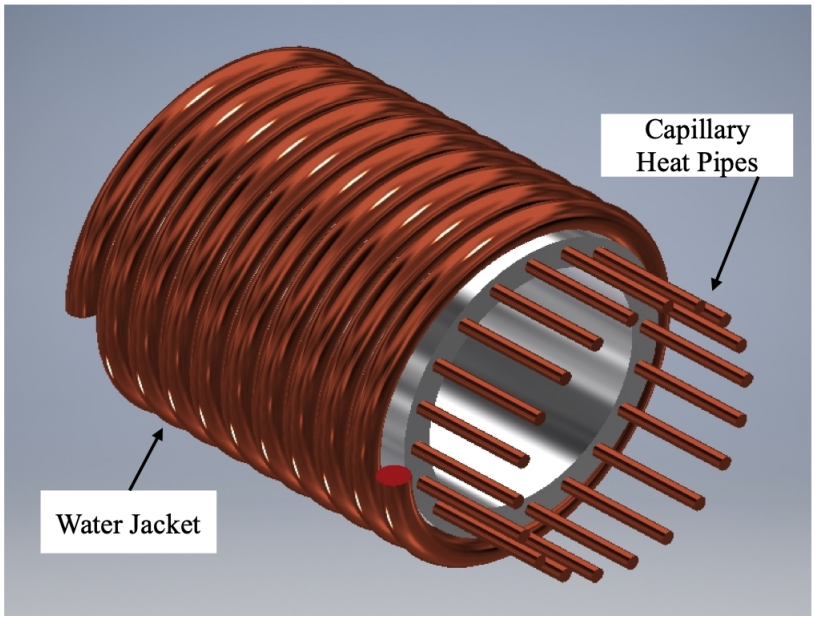

Figure 6.5: Cylindrical cradle structure with embedded capillary heat pipes in the wall and water jacket on the lateral surface.

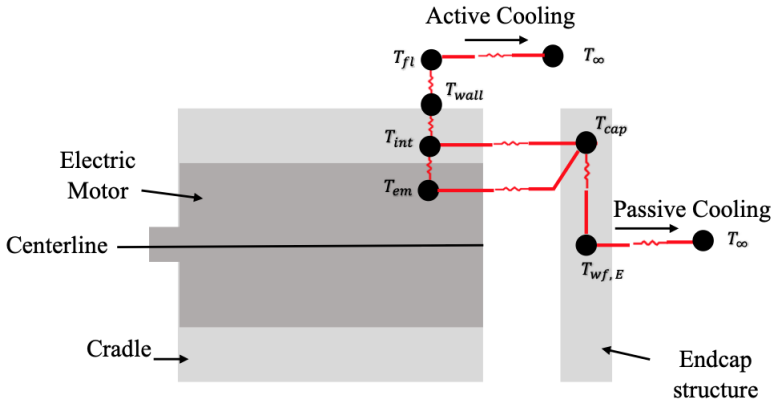

Figure 6.6: 1D representative thermal nodal network for the cradle structure.

The heat initially moves in radial and axial directions towards the cylindrical cradle and the endcap.

The governing thermal equation for electric motor surface temperature, T_{em}, becomes

$$C_{em}\frac{T_{em}}{dt} = \dot{Q}_{loss} - \frac{T_{em} - T_{cap}}{R_{AL}} - \frac{T_{em} - T_{int}}{R_{CR}} \tag{6.2}$$

where C_{em} is the heat capacity of the electric motor. The terms T_{cap} and T_{int} represent the endcap and cradle temperatures, respectively. The axial thermal resistance towards the endcap, R_{AL}, may be expressed as

$$R_{AL} = \frac{L_{AL}}{k_{AL}A_{AL}} \tag{6.3}$$

where L_{AL}, A_{AL}, and k_{AL} denote the endcap effective length, heat transfer surface area, and thermal conductivity, respectively. Similarly, the heat flow in the radial direction is modeled using a thermal resistance, R_{CR}, determined as

$$R_{CR} = \frac{\ln \frac{r_{int}}{r_{em}}}{2\pi L_{CR}k_{CR}} \tag{6.4}$$

where the termsr_{em}, L_{CR}, and k_{CR} represent the cradle inner radius, length, and thermal conductivity, respectively. The radial distance between the heat pipes and the center-line, r_{int}, and may be calculated as

$$r_{int} = \frac{r_{em} + r_{po}}{2} \tag{6.5}$$

where r_{po} denotes the circular cradle outer radius. The centerline is defined at the center of the electric motor as shown in Fig. 6.6. From the T_{int} node the heat can move further in the radial direction towards the coil via conduction and in the

axial direction towards the endcap using the capillary heat pipes. The interior cradle temperature, T_{int}, may be expressed as

$$C_{int}\frac{T_{int}}{dt} = \frac{T_{em} - T_{int}}{R_{CR}} - \frac{T_{int} - T_{cap}}{R_{HP}} - \frac{T_{int} - T_{wall}}{R_{wall}} \tag{6.6}$$

where C_{int} is the cylindrical cradle heat capacity and T_{wall} denotes the cradle exterior surface temperature. The symbol R_{wall} denotes the conductive thermal resistance in the axial direction and may be written as

$$R_{CR} = \frac{\ln \frac{r_{po}}{r_{int}}}{2\pi L_{CR} k_{CR}} \tag{6.7}$$

where L_{CR} is the cradle length. The thermal resistance of capillary heat pipes, R_{HP}, is well-established [82] and is expressed as

$$R_{HP} = \frac{R_s R_{fg}}{R_s + R_{fg}} \tag{6.8}$$

where R_s denotes the thermal resistance of the heat pipe shell and R_{fg} represents the thermal response of the phase change thermal resistance. The term, R_s, may be estimated with respect to the heat pipe configuration as

$$R_s = \frac{L_{eff}}{k_s A_s} \tag{6.9}$$

where L_{eff}, A_s, and k_s denote the heat pipe length, shell heat transfer surface area in the axial direction, and shell thermal conductivity, respectively. The diameter and the length of the heat pipes are denoted by D_{hp} and L_h. The thermal resistance due to the working fluid circulation within the heat pipe,R_{fg}, may be written as

$$R_{fg} = R_{we} + R_{pe} + R_{wc} + R_{pc} \tag{6.10}$$

where the terms R_{we}, R_{pe}, R_{wc}, and R_{pc} represent the thermal resistances of the walls and the wicks at the evaporator and condenser sections.

The endcap temperature, T_{cap}, may be determined from the heat transfers between the electric motor-endcap and cylindrical cradle-endcap and endcap-working fluid, so

$$C_{cap}\frac{dT_{cap}}{dt} = \frac{T_{em} - T_{cap}}{R_{AL}} + \frac{T_{int} - T_{cap}}{R_{HP}} - \frac{T_{cap} - T_{wf,E}}{R_{cap}} \tag{6.11}$$

where C_{cap} and R_{cap} are the endcap heat capacity and thermal resistance, respectively. The term, $T_{wf,E}$, denotes the thermosiphon's evaporator temperature. The convective heat transfer between the endcap and the working fluid within the reservoir may be modeled as a convective thermal resistance, R_{cap}, so that

$$R_{cap} = \frac{t_{cap}}{k_{cap}A_e} \tag{6.12}$$

where A_e is the effective heat transfer surface area between the cap and the thermosyphon's evaporator. The terms, t_{cap} and k_{cap}, denote the thermosyphon evaporator wall thickness and the evaporator thermal conductivity, respectively. The effective heat transfer surface area and may be written as

$$A_e = 2\pi r_{pa} L_{pa} \tag{6.13}$$

where r_{pa} and L_{pa} represent the radius and the length of the built-in passage for the working fluid circulation in the endcap. The working fluid, in this case acetone, collects the heat and passively circulates between the evaporator and condenser using the gravity force.

The working fluid mass flow rate may be calculated using the energy balance at

the evaporator. Assuming that the evaporator always contains liquid and vapor and the vapor temperature variation within the evaporator and vapor line is negligible, the heat transfers to the liquid-vapor line within the evaporator and the energy balance becomes

$$\frac{T_{em} - T_{cap}}{R_{AL}} + \frac{T_{int} - T_{cap}}{R_{HP}} = \dot{m}_w l_v + \dot{m}_w \; c_{p,w} \left(T_{wf,E} - T_{wf,R}\right) \tag{6.14}$$

where l_v is the specific heat of vaporization, $c_{p,w}$ is the working fluid specific heat, and the working fluid's temperature at the heat exchanger is denoted by $T_{wf,R}$. Equation (6.14) may be simplified and the working fluid mass flow rate, $\dot{m}_w$, may be expressed as

$$\dot{m}_w = \frac{\frac{T_{em} - T_{cap}}{R_{AL}} + \frac{T_{int} - T_{cap}}{R_{HP}}}{c_{p,w} \left(T_{wf,E} - T_{wf,R}\right) + l_f} \tag{6.15}$$

Improved heat transfer capabilities and reduced weight reduction may be achieved by embedding capillary heat pipes within the cradle. Therefore, the cradle contains a number of heat pipes that fit within the wall, N, as

$$N = \frac{2\pi r_{int}}{D_{hp} + s} \tag{6.16}$$

where the term s represents the minimum spacing that must exist between each heat pipe due to the manufacturing limitations.

6.4.2 Thermal Bus

The thermal bus structure includes the vapor and liquid lines carrying the working fluid in the thermosyphon and the pipes for coolant circulation for the active cooling method. The evaporator temperature, $T_{wf,E}$, may be determined by the heat

transfer between the endcap and the condenser so that

$$C_{TS,E}\frac{dT_{wf,E}}{dt} = \frac{T_{cap} - T_{wf,E}}{R_{cap}} - \frac{T_{wf,E} - T_{wf,R}}{R_{TS}} \tag{6.17}$$

where $C_{TS,E}$ is the heat capacity of the evaporator. The thermal resistance between the evaporator and condenser due to the working fluid circulation, R_{TS}, may be written as

$$R_{TS} = \frac{1}{\dot{m}_w c_v} \tag{6.18}$$

where c_v is the heat capacity of the acetone in the vapor phase.

The excess heat may be removed through the active cooling system. The conventional liquid system provides a constant coolant flowrate to move the heat between the water-jacket and the radiator. The temperature of the cradle wall,T_{wall}, becomes

$$C_{wall}\frac{dT_{wall}}{dt} = \frac{T_{int} - T_{wall}}{R_{wall}} - \frac{T_{wall} - T_{fl,E}}{R_{coil}} \tag{6.19}$$

where the C_{wall} denotes the heat capacity of cradle wall and the term R_{coil} represents the coil thermal resistance.

Similarly, the temperature of the coolant within the water jacket, $T_{fl,E}$, may be written as

$$C_{LQ,E}\frac{dT_{fl,E}}{dt} = \frac{T_{wall} - T_{fl,E}}{R_{coil}} - \frac{T_{fl,E} - T_{fl,R}}{R_{LQ}} \tag{6.20}$$

where $C_{LQ,E}$ is the heat capacity of water jacket and the coolant inside. The symbol $T_{fl,R}$ represents the temperature of coolant at the radiator. The thermal resistance

due to the conduction heat transfer through the coil, R_{coil}, may be presented as

$$R_{coil} = \frac{\ln \frac{r_{inn}}{r_{po}}}{2\pi L_{CR} k_{cu}} \tag{6.21}$$

where the term r_{inn} represents the distance between the interior coil and the centerline. The convective thermal resistance due to the operation of the liquid cooling system, R_{LQ}, may become

$$R_{LQ} = \frac{1}{\dot{m}_{LQ} c_f} \tag{6.22}$$

where the terms $\dot{m}_{LQ}$ and c_f represent the coolant mass flow rate and the specific heat capacity. The flow rate is a function of the coolant velocity, V_{LQ}, the coolant density, ρ_{LQ}, and the passage surface radius, r_{LQ}, such that

$$\dot{m}_{LQ} = \rho_{LQ} \pi {r_{LQ}}^2 V_{LQ} \tag{6.23}$$

6.4.3 Heat Exchangers

The transmitted heat is eventually dissipated to the ambient surroundings through the passive heat exchanger and a compact radiator with a fan assembly. The working fluid temperature at the passive heat exchanger, $T_{wf,R}$, may be expressed as

$$C_{TS,R} \frac{dT_{wf,R}}{dt} = \frac{T_{wf,E} - T_{wf,R}}{R_{TS}} - \frac{T_{wf,R} - T_{\infty}}{R_{hx}} \tag{6.24}$$

where $C_{TS,R}$ is the heat capacity of the heat exchanger. The term R_{hx} represents the thermal resistance of the passive heat exchanger and it may be written as

$$R_{hx} = \frac{1}{\eta_{TS} \dot{m}_{hx} c_{p,a}} \tag{6.25}$$

where the terms η_{TS} and $c_{p,a}$ denote the efficiency of the thermosyphon heat exchanger and the air specific heat capacity. The air mass flow rate, $\dot{m}_{hx}$, may be expressed as

$$\dot{m}_{hx} = \rho_a L_{hx} W_{hx} V_{ram} \tag{6.26}$$

where ρ_a and V_{ram} represent the air density and the velocity of the ambient air hitting the heat exchanger due to ram air effect and/or the fan operation. The length and width of the heat exchangers are denoted by the terms $L_{hx}$and W_{hx}. On the liquid side, the coolant temperature at the radiator, $T_{fl,R}$, may be derived with respect to the ambient temperature, T_∞, such that

$$C_{LQ,R}\frac{dT_{fl,R}}{dt} = \frac{T_{fl,E} - T_{fl,R}}{R_{LQ}} - \frac{T_{fl,R} - T_\infty}{R_r} \tag{6.27}$$

where $C_{LQ,R}$ is the heat capacity of the radiator of the liquid system. Lastly, the thermal resistance of the radiator, R_r, may be determined as

$$R_r = \frac{1}{\eta_r \dot{m}_r c_{p,a}} \tag{6.28}$$

where η_r is the efficiency of the radiator and it is estimated experimentally. The air mass rate running through the radiator structure, $\dot{m}_r$, may be calculated as

$$\dot{m}_r = \rho_a L_r W_r V_r \tag{6.29}$$

where the symbols L_r and W_r are the radiator length and width, while V_r is the air velocity through the radiator.

The overall thermal resistance of the cooling system, R_T, may be expressed as

$$R_T = \frac{T_{em} - T_\infty}{\dot{Q}_{loss}} \tag{6.30}$$

6.5 Optimization Problem

The nonlinear hybrid cooling optimization problem, solved using the MATLAB Fmincon package, enables the design for light weight combat vehicles. The system design vector $x^* = (t_{cap}, r_{LQ}, r_{pa}, r_{po}, W_{hx}, W_r)$ includes the thermosyphon evaporator wall thickness, liquid cooling system pipe radius, passive system pipe radius, cradle outer radius, and the heat exchanger and radiator widths. Given this design vector, the optimization problem can be stated as

$$minJ(x^*) \tag{6.31}$$

$$subject\ to\ G(x^*, U)\ and\ H(x^*, U) \tag{6.32}$$

where $J(x^*)$ denotes the cost function to be minimized. The terms $G(x^*, U)$ and $H(x^*, U)$ represent nonlinear equality and inequality constraints with U denoting the input heat.

In this study, the cost function considers the mass of the cooling system components such that

$$M_T = M_{cr} + M_{tb} + M_{hx} + M_r \tag{6.33}$$

where M_{cr} is the cradle mass, M_{tb} denotes the thermal bus mass and M_{hx} and M_r represent the heat exchanger and radiator masses. Expanding these respective terms and substituting into Eq. (7.31) results in

$$J(x^*) = \rho_{AL}[\pi L_{CR}(r_{po}^2 - r_{pi}^2) - (N L_h \frac{\pi D_{hp}^2}{4})] + \rho_{AL}[\pi r_{po}^2 (L_{AL} + 2(t_{cap}))] + \rho_{cu}[2\pi r_{LQ} L_{coil}(r_{inn} - r_{po}] + \rho_{AL}[(H_{hx} L_{hx} W_{hx} + H_r L_r W_r)] + \rho_{LQ}[\pi {r_{LQ}}^2 L_{LQ} + H_r L_r W_r] + \rho_{ac}[\pi {r_{LQ}}^2 L_{ac}] \quad (6.34)$$

where ρ_{LQ} is the coolant density, L_{LQ} denotes the total length of the liquid system tube filled with the coolant, and L_{ac} is the length of the thermosyphon liquid return containing the working fluid.

The single imposed nonlinear constraint becomes

$$H(x^*), U) = \Delta T - R_T \dot{Q}_{loss} \quad (6.35)$$

whereΔT is the maximum allowed temperature difference between the electric motor and the ambient surroundings. In this study, $\dot{Q}_{loss}$ is assigned to be U.

The optimization problem calls the cooling system simulation, Eqs. 7.11 – 7.30, to calculate the electric motor thermal response for the applied heat loads based on the design vector values introduced in the minimization process. The system parameter values are summarized in Table 6.1.

6.6 Numerical Results and Discussion

The proposed electric motor cooling system is designed and simulated for three heat rejection rates: 6kW, 9kW, and 12kW. These heat generation rates correspond to a 85% efficient electric motor shaft loads of 40kW, 60kW, and 80kW. The six design parameters, initial conditions, and lower plus upper bounds are summarized Table 6.2. The lower bound of the cradle wall's thickness is set to accommodate the heat pipes internally while the rigidity of the structure is secured.

The thermal response of the baseline cooling system subject to 12kW heat input is shown in Fig. 6.8(a) which includes the dynamic responses of the electric motor,

Symbol	Value	Units	Symbol	Value	Units
c_{al}	900	J/kg.K	L_{LQ}	10	m
c_{cu}	385	J/kg.K	L_{pa}	25.4	cm
$c_{p,a}$	1000	J/kg.K	L_{pa}	10	m
c_v	1290	J/kg.K	L_r	50	cm
$c_{p,w}$	1550	J/kg.K	L_w	0.5	cm
$D_{hp,w}$	4.5	mm	r_{inn}	r_{po}+0.1	cm
D_{hp}	6.3	mm	r_{em}	5	cm
k_{ac}	0.18	W/m.K	s	2	mm
k_{al}	237	W/m.K	t_{hx}	1	cm
k_{cu}	400	W/m.K	v_{LQ}	0.5	m/s
k_s	400	W/m.K	v_r	2	m/s
k_w	200	W/m.K	v_{ram}	1	m/s
L_{ac}	0.1	m	ρ_a	1.2	kg/m^3
L_{Al}	5	cm	ρ_{al}	2700	kg/m^3
L_{coil}	2	m	ρ_c	997	kg/m^3
L_{cr}	15.2	cm	ρ_{cu}	8960	kg/m^3
L_{eff}	4.5	cm	ρ_{LQ}	1000	kg/m^3
l_f	518	kJ/kg	$\rho_{w,g}$	2.2	kg/m^3
L_h	20	cm	$\rho_{w,l}$	750	kg/m^3
$L_{hp,c}$	5	cm	Pr	2.4	-
$L_{hp,e}$	14	cm	μ	3.1e-4	N.s/m^2
L_{hx}	40	cm	ΔT	40	°C

Table 6.1: Summary of model parameters with values

endcap, cradle, water-jacket, heat exchanger, and radiator. The results demonstrate that the electric motor's operating temperature increases exponentially and violates the allowed operating temperature range with the initial conditions. The total mass of the corresponding cooling system is approximately 52kg.

The specifications of the UQM power phase 145 are used in the numerical simulation [83]. This electric motor must be maintained at 65°C during steady state operation to avoid overheating. The initial cooling system components and the ambient temperatures are 25°C. Accordingly, the difference between the ambient tem-

Symbol (units)	Initial Conditions	Lower Bound	Upper Bound
r_{LQ} (mm)	8.5	4	13
r_{pa} (mm)	7.5	3	10
r_{po} (mm)	85	70	100
t_{cap} (mm)	2.5	2	5
W_{hx} (mm)	260	20	500
W_r (mm)	350	50	650

Table 6.2: Initial values of the design parameters with their lower and upper bounds

perature and the electric motor peak temperature, ΔT, should never exceed 40°C. The initial conditions correspond to the sizes of the baseline cooling system, shown in Fig. 6.7, built for experimental testing and mathematical model validation purposes in the laboratory.

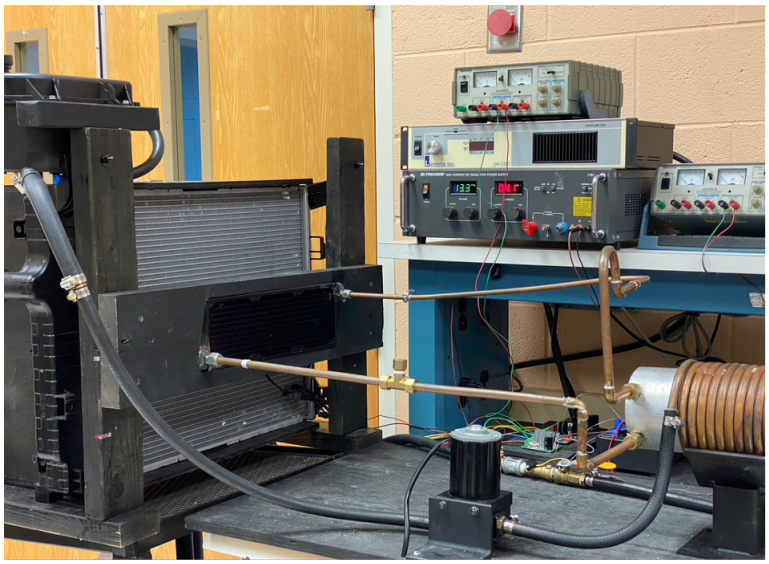

Figure 6.7: Bench top experimental setup - Complete electric motor cooling system featuring active and passive heat rejection pathways.

The optimized values for three heat generation rates are summarized in Table

6.3. It begins with the optimization of the hybrid cooling system subject to 6kW continuous heat load. The results demonstrate that this amount of heat loss can be securely managed, while the cooling system's mass is reduced down to 11kg. The optimized cooling system features a cradle structure with 6cm outer radius. The collected heat is transferred to a 20cm x 39.8cm x 2cm radiator via forced convection through a 1.01cm radius tube. On the passive side, the evaporator wall thickness is 2mm. The heat passively travels a 1cm inner radius pipe to reach a 20cm x 17.5cm x 2cm heat exchanger.

Design Variables (units)	**Thermal Load**			Multipliers (12 kW) $(\lambda_{l_1}, \lambda_{u_1})$
	Low (6kW)	**Medium (9kW)**	**High (12kW)**	
r_{LQ}(mm)	7.7	9.6	11.1	0.02, 2.5
r_{pa}(mm)	8.4	9.2	10	0.02, 21.36
r_{po}(mm)	70.4	70	70	464.3, 5e-3
t_{cap}(mm)	2	2	2	134.8, 0.06
W_{hx}(mm)	87.4	134	246	0.01, 7.8e-4
W_r (mm)	229	367	480	4e-4, 0.01

Table 6.3: Optimized design parameters for three different operating conditions; (a) Low, 6kW; (b) Medium, 9kW; and (c) High, 12kW, and the Lagrange multipliers for the 12kW simulation

For the 9kW heat input, a larger cooling system is required to maintain the electric motor's operating temperature at 65°C). The simulation shows the mass is reduced down to 14.5kg which is 72% lighter than the baseline system. The optimized length for the radiator and heat exchanger are 367mm and 134mm. A 9.6mm radius tube provides the adequate coolant flow rate between the cradle and the radiator in the active cooling system. Besides, the thermosyphon requires an evaporator with a 2mm wall thickness, and 9.2mm radius circular passage.

The thermal behavior of the cooling system subject to the 12kW power is

investigated and the proper sizes of the components are found for minimal weight addition to the vehicle. Figure 6.8(b) shows the temperature of the electric motor, cradle, endcap, water-jacket, heat exchanger, and radiator. The simulation results demonstrate that the optimized hybrid cooling system's overall weight is reduced to approximately 18kg. This means the proper selection of component sizing could reduce approximately 50% of the cooling system's weight, while accommodating a continuous 12kW of heat dissipation.

The optimized system features a compact 60mm outer diameter cradle, a 200mm x 480mm x 20mm radiator, and a 20mm x 246mm x 20mm heat exchanger. A 11.1mm radius tube provides the required coolant mass flow rate in the active cooling system. On the passive side, the optimized evaporator passage radius size becomes 10mm. The evaporator wall thickness remains at the lower bound, 2mm, which creates the lowest possible thermal resistance between the electric motor and the working fluid. Besides, the outer radius of cradle reduces to 60mm which minimizes the overall weight and thermal resistance at the same time. Note that this radius size fits 33 capillary heat pipes inside the cradle wall.

In terms of computational costs, the array of nonlinear inequality constraints can be converged in a couple of hours using a regular core-i7 desktop computer. This study considers steady state types of operation while the developed mathematical model can be used to optimize the design parameters subject to several time-dependent driving cycles for a higher computational cost compensation. Figure 6.9 shows the value of nonlinear inequality constraint at every iteration. The results show that this nonlinear optimization process is completed in less that approximately 200 iterations.

The impact of each design variable on the objective function is evaluated through a sensitivity analysis using the Lagrangian Duality method [84] for the hybrid

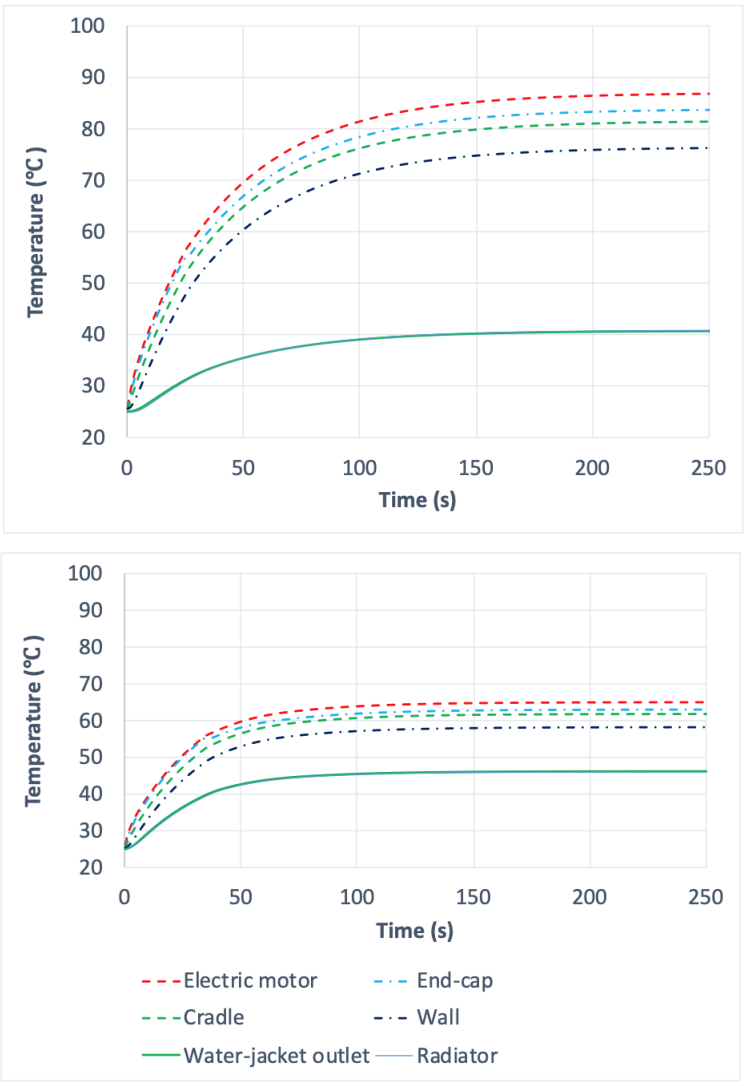

Figure 6.8: Temperature response of hybrid cooling system subject to 12kW heat continuously applied; (a) Baseline system with initial design variables; and (b) Optimized cooling system.

cooling system subject to 12kW heating power. Lagrange multipliers, shown by the term λ_i, and also known as dual multipliers or shadow prices, are indicators that demonstrate the partial derivatives of the objective function with respect to each constraint at the optimal solution [85, 86]. The constraints with nonzero Lagrange are recognized as active or binding at optimality. This study quantified the influence of design parameters, x^*, on the objective function using Lagrange multipliers at the lower and upper bound constraints. The Lagrange multipliers at the upper bound constraints,λ_{u_i}, and the lower bound constraints, λ_{l_i}, are calculated for 12kW heat input scenario using MATLAB and summarized in Table 6.3.

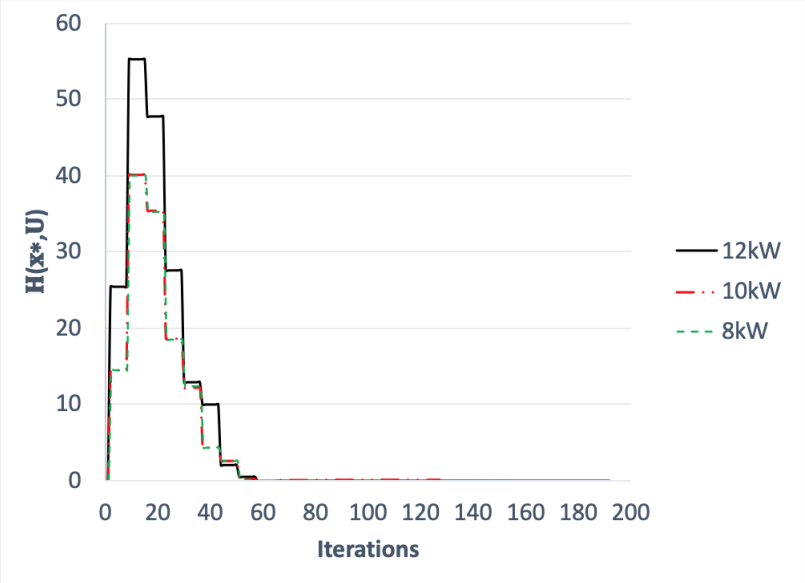

Figure 6.9: Nonlinear inequality constraint values at each iteration.

In this sensitivity analysis, the Lagrange multiplier's higher absolute value indicates the higher tendency of the objective function to violate the corresponding constraint. Thus, it can be concluded that the priority is to decrease the thicknesses of the cradle wall, r_{po}, and evaporator wall, t_{cap}, should the design configuration allow. In addition, increasing the evaporator passage radius, r_{pa}, will provide a larger heat

transfer surface area to transfer heat to the working fluid while it does not increase the system's weight significantly. This analysis shows the rest of the design parameters, including r_{LQ}, W_{hx}, and W_r are properly adjusted to manage a 12kW heat loss while the electric motor's thermal demands are satisfied.

6.7 Conclusion

Military ground vehicles are progressing toward electric motor propulsion systems with rechargeable battery packs. This paradigm shift reduces the reliance on fossil fuels while enabling silent autonomous operation for enhanced combat capabilities. This study optimizes a multiple pathway electric-motor cooling system. The electric motor cradle size, coolant reservoir, and heat exchanger dimensions are the design variables, while the cost function includes the system weight. The constraints correspond to a medium-size vehicle undergoing a standard operating cycle for heat rejection requirements. A nonlinear optimization method is implemented to find the optimal design. This numerical study demonstrates a reduced overall weight has been achieved for light-duty to medium-duty type of applications. This method can be used as a design tool to find minimum hybrid cooling system weight with respect to the electric motor pick temperature, heat rejection demands, and operating conditions

Chapter 7

A Model Reference Adaptive Controller for an Electric Motor Thermal Management System in Autonomous Vehicles

7.1 Abstract

Technological advancements and growth in electric motors and battery packs enable vehicle propulsion electrifications, which minimize the need for fossil fuel consumption. The mobility shift to electro motors creates a demand for an efficient electric motor thermal management system that can accommodate heat dissipation needs with minimum power requirements and noise generation. This study proposes an intelligent hybrid cooling system that includes a gravity aided passive cooling solution coupled with a smart supplementary liquid cooling system. The active cooling system contains a radiator, heat sink, variable frequency drive, AC fan, DC pump,

and real time controller. A complete nonlinear mathematical model is developed using a lumped parameter approach to estimate the optimum fan and pump operations at each control interval. Four different control strategies, including nonlinear model predictive controller, classical PI control, sliding mode control, and stateflow, are developed, and their performance is compared. The experimental results demonstrate that the nonlinear model predictive control method is the most effective strategy, which reduces the cooling system fan power consumption by 73% for only a 5% increase in the pump power usage compared to classical control for a specific 60 minute driving cycle.

7.2 Introduction

Emphasizing reducing combat vehicle fossil fuel consumption, maintenance costs, and noise generation has made the U.S Army consider innovative technologies for the next generation of combat vehicles [54]. Considering the fact that relying on fossil fuels on a battlefield could be a potential threat to U.S. national security, electrified propulsion system could be a sustainable solution to enhance the security, reliability, and survivability of the soldiers. Vehicle electrification also enables autonomy and improves vehicle mobility and durability. In vehicle electrification, a high-efficiency electric motor with battery packs replaces traditional diesel engines with high fuel consumption and heat generation rates. Vehicles could also feature a hybrid propulsion system that includes single or multiple electric motors incorporated with a diesel engine in a series or parallel configuration for applications requiring a large amount of torque [87]. This evolution creates a demand for an advanced thermal management system that dissipates the generated heat properly and maintains the heat load(s) within their prescribed operating temperature range(s) with minimal

external power needs [88]. Depending on the heat dissipation needs, a passive, active, or hybrid cooling system may be used to control the heat load's operating temperature [73, 89–92]. Figure 7.1 graphically shows passive, active, and hybrid cooling regions where the cooling solutions are located.

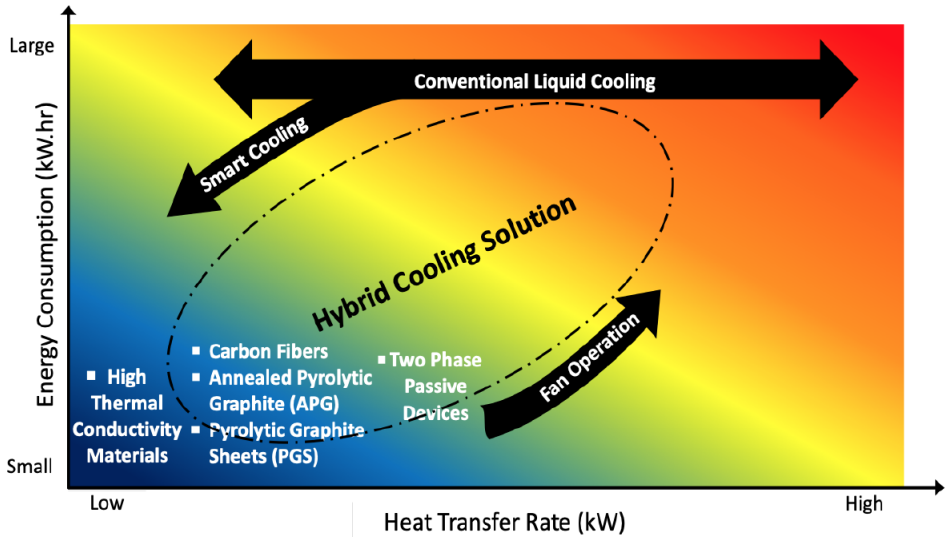

Figure 7.1: Hybrid heat rejection for medium load under moderate ambient conditions.

Current practices include conventional cooling methods supplying coolant or airflow across the heat load housing for large heat dissipating needs [8]. Traditional cooling systems contain several mechanical and electrical components (e.g., coolant pump, fan assembly, radiator, wax-based thermostat, etc.) to dissipate the heat to the ambient surroundings. While these methods generally offer adequate cooling capacity, immoderate fan and pump operations can cause considerable electrical power usage, which can be saved to extend the vehicle's mission range. Besides, the cooling systems may suffer from a lack of precise temperature tracking system for temperature-sensitive applications. Relatively high noise generation, significant weight addition, and large space requirements are the other major drawbacks associated with these

cooling techniques.

In recent developments, electro-mechanical actuators (e.g., variable position thermostat valve), servo motors, variable speed pump and fan, and advanced transducers replace the old-fashioned components in traditional liquid cooling systems. This advancement creates an opportunity to regulate the cooling system's operation based on heat rejection demands through linear and non-linear control algorithms [14, 93, 94]. This strategy, known as smart cooling, could ensure the heat loads' operating temperature with reduced power consumption.

On the other hand, passive cooling systems may be implemented for low heat-rejecting applications. Traditional passive cooling systems, relying on conduction and/or free convection heat transfer modes, eliminates the need for external power source for heat transfer. They usually contain no moving parts, which reduces the risk of failure, maintenance cost, and noise generation. However, the absence of a convective heat transfer coefficient and space restrictions limit the passive cooling capacity. Recent passive cooling innovations could offer several effective solutions that improve cooling systems' thermal performance while saving precious electrical power usage. They include, but are not limited to, high thermal conductivity composite fibers, advanced phase change materials, and two-phase passive devices [95–101] Two phase passive devices (e.g., heat pipes, thermosyphon, etc.) became an attractive solution for thermal management of applications with low to moderate heat dissipating requirements. Heat pipes are closed loop systems which contain an evaporator and a condenser with a small amount of working fluid. This natural closed loop system uses the potential of the latent heat of vaporization to provide a passive circulation between the evaporator and condenser. Two phase passive devices could offer extraordinary thermal conductivity, outstanding structure flexibility, and long-lasting durability. The thermal conductivity of heat pipes can be up to 100 times higher

than a same size copper pipe [36]. The integration of heat pipes for low to moderate heat generation applications (e.g., electric motors, battery packs, electronics, etc.) has been numerically and experimentally investigated [75, 79, 90].

Recent studies demonstrate a hybrid thermal management configuration which integrates passive cooling systems coupled with a smart liquid cooling system. The hybrid strategy is suitable for applications in which the load's heat generation rate varies significantly during the operation such as electric propulsion systems. The heat generation rate of an electric or hybrid propulsion system depends on the driving cycle, road profile, and ambient conditions. In an advanced hybrid cooling strategy, the primary mode of heat transfer is generally passive while a computer-controlled liquid cooling system offers on demand cooling should the electric motor's temperature becomes excessive [42, 59, 60, 102]. This study aims to develop a nonlinear model predictive control for a hybrid thermal management system which maintains the electric motor's temperature with reduced power consumption. The developed controller is experimentally validated, and the cooling system power consumption is calculated.

The remainder of this paper is organized as follows. Section 7.2 explains the proposed hybrid cooling system architecture. The corresponding mathematical model for the hybrid cooling is developed in Section 7.3. Section 7.4 demonstrates the nonlinear controller designs, and the experimental results are discussed in Section 7.5. Conclusions may be found in Section 7.6.

7.3 Cooling System Architecture

This study designs and develops an advanced hybrid cooling system for an electric six-wheeled autonomous military vehicle featuring six in-hub electric motors, shown in Fig. 7.2. The cooling system incorporates a complete closed loop passive

system besides an advanced liquid cooling system. The liquid cooling system consists of a variable speed coolant pump, radiator fan, and a radiator assembly. The pump and fan operating cycles are computer-controlled using a nonlinear model predictive control algorithm to maintain the electric motor's operating temperature at the target temperature with maximum efficiency.

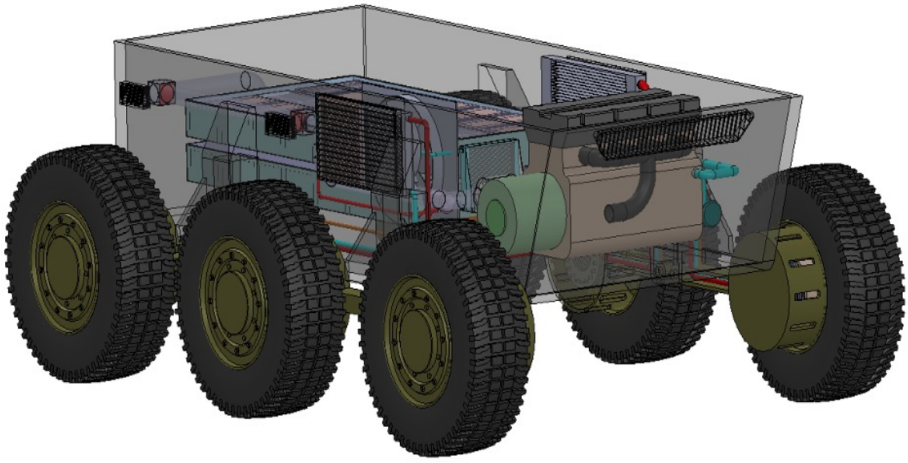

Figure 7.2: Autonomous military ground vehicle – Six wheeled chassis featuring in-hub electric propulsion.

The heat generation rate of electric motors may vary depending on the amount of current running through the stator winding. The current is induced by the torque applied on the wheels and it varies based on the driving cycles and operating conditions. The hybrid cooling system offers a sustainable passive heat rejection pathway which continuously removes heat to the ambient surroundings. The passive cooling system can handle low to moderate heat rejection instances including constant speed driving conditions and stationary modes of operation. In addition, a computer controlled liquid cooling system is supplied to the electric motors for excessive heat rejection demands. For instance, a large amount of torque may be required for high hill climbing or abrupt changes in a road profile. Figure 7.3 graphically displays the

cooling system configuration for the six wheeled autonomous vehicle.

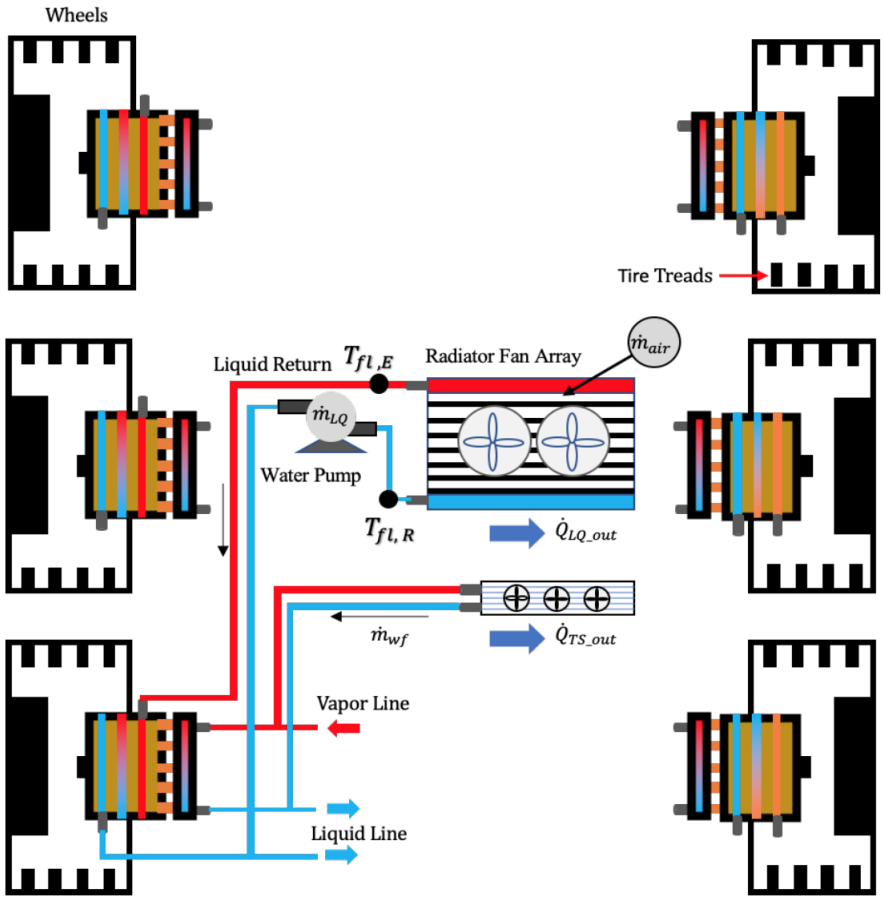

Figure 7.3: Hybrid cooling system configuration for a six-wheel autonomous vehicle featuring in-hub electric motors.

The integration of the hybrid cooling system requires an advanced thermal interface that effectively transfers the generated heat to the cooling system. The thermal interface, shown in Fig. 7.4, is called the "Cradle" hereinafter. The cradle structure contains an aluminum hollow cylinder and an attached endcap structure. The components are fastened together using multiple capillary heat pipes embedded within the cradle wall. The heat pipes, distributed in a radial fashion, improve the effective thermal conductivity of the cradle. The electric motor is then enclosed

within the cradle. The heat transfer occurs in both radial and axial directions from the electric motor to the cradle. The attached endcap serves as an evaporator for the passive system. It features a built-in passage which contains the working fluid. The heat applied to the endcap raises the working fluid's temperature up to the boiling point where it turns to vapor and leaves the cradle. The liquid cooling system is supplied to the cradle through a copper pipe coiled around the structure. Should the electric motor's temperature become excessive, the coolant pump starts operating at a proper speed; it circulates the coolant between the coil and the radiator to dissipate the heat to ambient surroundings.

Modern combat vehicles require a significant amount of power to support the power train, on-board electronics, sensors, and communication systems. This power creates a large amount of heat that needs to be rejected safely while hiding from infrared detector. The proposed cooling system features a compact thermal bus structure which routes the heat through restrictive pathways where even airflow is limited. The heat travels the thermal bus to reach heat exchangers. The thermal bus can be thermally insulated so that minimal heat transfer occurs along the structure to the ambient surroundings. This concept may minimize thermal signature should infrared thermal imagining be blocked.

The thermal energy eventually moves to two remote heat exchangers that dissipate the heat to the ambient environment. The heat exchangers are arranged in series or in parallel based on the vehicle configuration. The active cooling system radiator features a variable speed AC fan assembly. Should the ram air be insufficient, forced convective heat transfer is applied. The cooling system's efficiency depends on the operation of the coolant pump and radiator fan which require external electric power for operation. The goal is to minimize the operation of the active components while the electric motor's temperature is securely maintained within the prescribed

operating rage.

7.4 Mathematical Model

A complete mathematical model is developed to estimate the hybrid cooling system's performance featuring passive and active cooling strategies. This model may be used to estimate the thermal behavior of the electric motor, thermal interface, thermal bus, and heat exchangers for different operating cycles and ambient conditions. The electric motor's heat generation rate is simulated as a function of vehicle speed and the applied torque to the wheels. The thermal model of the hybrid cooling system is explained in the following subsections. The electric motor generates heat due to the friction loss, $\dot{Q}_{fr}$, associated with bearing motions, induction loss,$\dot{Q}_{ind}$, due to the current circulation, and heat from the outside world, $\dot{Q}_o$, and it may be written as

$$\dot{Q}_{em} = \dot{Q}_{ind} + \dot{Q}_{fr} + \dot{Q}_o \tag{7.1}$$

The generated heat is initially transferred to the endcap structure and electric motor shell. The shell shares the collected heat between the passive and active cooling systems. The heat may travel towards the passive endcap structure through the embedded heat pipes while the remainder heat is received by the active cooling system picks through the copper pipe coiled around the shell. The electric motor thermal management system is mathematically modeled using the lumped parameter approach. The thermal nodal network corresponding to the electric motor cooling system architecture is shown in Fig. 7.4. The high-level diagram represents the thermal resistance of the components and introduces the system states. The thermal

resistances depend on the system's thermal properties and architecture.

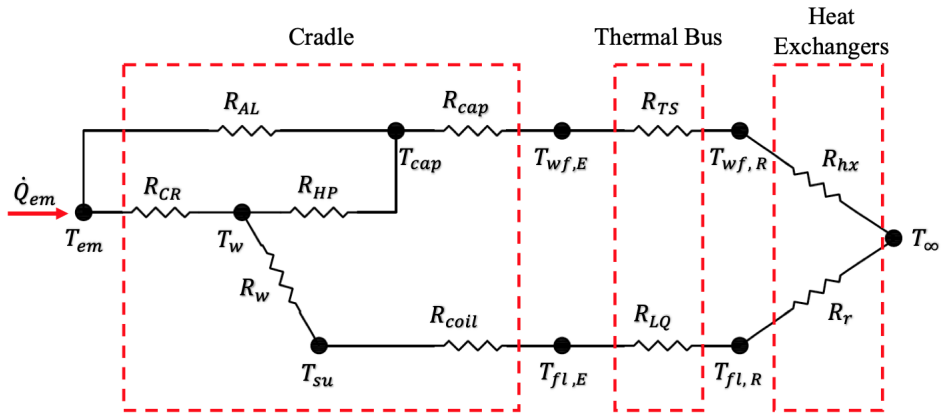

Figure 7.4: Nodal thermal network for the hybrid cooling system featuring the cradle, thermal bus, and dual heat exchangers.

7.4.1 Cradle

The cradle is also mathematically modeled using the lumped parameter approach. It includes a couple of thermal resistances, in parallel and series fashion, that represent the conductive and convective heat transfers occurring within the cradle. The cradle thermal nodal network representing the proposed cradle structure is shown in Fig. 7.5.

The electric motor is enclosed in the cylindrical cradle structure while the cap is thermally attached to the top of the electric motor housing. Therefore, the energy balance at the electric motor may be driven as

$$C_{em}\frac{T_{em}}{dt} = \dot{Q}_{em} - \frac{T_{em} - T_{cap}}{R_{AL}} - \frac{T_{em} - T_w}{R_{CR}} \tag{7.2}$$

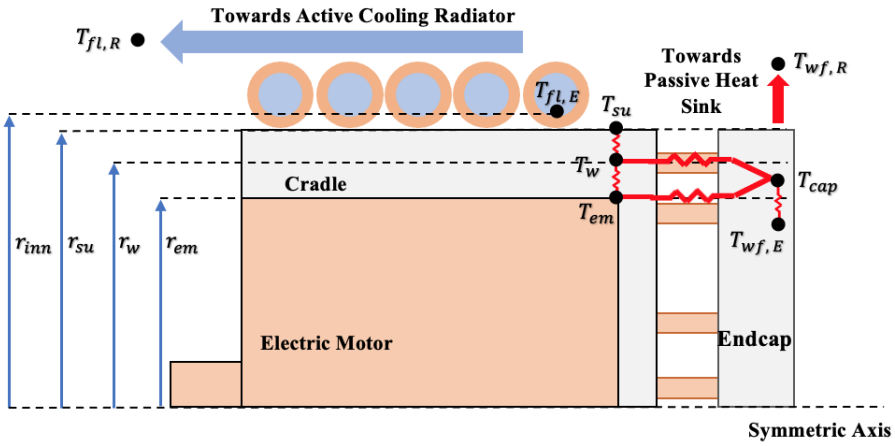

Figure 7.5: Electric motor and cradle cross-section area which illustrates the one-dimensional representations of the thermal nodal diagrams.

where the terms T_{em}, T_{cap}, and T_w denote the electric motor, endcap, and cradle wall temperatures while R_{AL} and R_{CR} are thermal resistances of the endcap and the cylindrical cradle structure. Also, the symbol C_{em} represents electric motor heat capacity. The endcap thermal resistance endcap, R_{AL}, becomes

$$R_{AL} = \frac{L_{AL}}{k_{AL} A_{AL}} \tag{7.3}$$

where L_{AL} represents the length of heat transfer between electric motor and the endcap, the term A_{AL} denotes the endcap heat transfer surface area, and the term k_{AL} is the aluminum thermal conductivity. The thermal resistance between the electric motor surface area and the cradle wall, R_{CR}, may be written as

$$R_{CR} = \frac{\ln \frac{r_w}{r_{em}}}{2\pi L_{CR} k_{AL}} \tag{7.4}$$

where r_{em} denotes the electric motor radius, and r_w represents the distance between

the motor center-line and the embedded heat pipes, and the height of the cylindrical cradle is denoted by L_{CR}.

The heat transferred to the wall continues in a radial direction towards the outer surface area and moves in an axial direction to the endcap. Therefore, the wall temperature, T_w, becomes

$$C_w \frac{T_w}{dt} = \frac{T_{em} - T_w}{R_{CR}} - \frac{T_w - T_{cap}}{R_{HP}} - \frac{T_w - T_{su}}{R_w} \tag{7.5}$$

where C_w is the wall heat capacity, T_{su} represents the outer surface area's temperature. The terms R_{HP} and R_w represent the heat pipe and wall thermal resistances. The thermal resistance of the wall in the cylindrical coordinate system may be determined as

$$R_w = \frac{\ln \frac{r_{su}}{r_w}}{2\pi L_{CR} k_{AL}} \tag{7.6}$$

where r_{su} denotes the cylinder outer radius. The heat pipe thermal resistance, R_{HP}, has been well established [103] it is expressed as

$$R_{HP} = \frac{R_s R_{fg}}{R_s + R_{fg}} \tag{7.7}$$

where R_s denotes the shell's thermal resistance, and R_{fg} is the phase change thermal resistance and it may be determined as

$$R_{fg} = R_{we} + R_{pe} + R_{wc} + R_{pc} \tag{7.8}$$

where the terms R_{we}, R_{pe}, R_{wc}, and R_{pc} represent the thermal resistances of the walls and the wick structures at the evaporator and condenser sections. The thermal

resistance of the shell is expressed as

$$R_s = \frac{L_{eff}}{k_s A_s} \tag{7.9}$$

where L_{eff}, k_s, and A_s represent the heat pipe effective length, thermal conductivity, and heat transfer surface area, respectively.

The transferred heat vaporizes the working fluid filling the endcap. The resulted vapor creates a pressure difference across the evaporator and a remote heat exchanger. The endcap design includes a built-in passage that always contains a working fluid. The heat is then conducted through the evaporator wall and reaches the working fluid. Therefore, the endcap temperature, T_{cap}, may be written as

$$C_{cap}\frac{dT_{cap}}{dt} = \frac{T_{em} - T_{cap}}{R_{AL}} + \frac{T_w - T_{cap}}{R_{HP}} - \frac{T_{cap} - T_{wf,E}}{R_{cap}} \tag{7.10}$$

where C_{cap} represents the endcap heat capacity and $T_{wf,E}$ is the working fluid's temperature in the evaporator. The evaporator wall thermal resistance, R_{cap}, may be expressed as

$$R_{cap} = \frac{\ln \frac{r_w}{r_{ev}}}{2\pi L_{cap} k_{AL}} \tag{7.11}$$

where r_{ev} is the distance between the thermosyphon evaporator from the centerline, and L_{cap} represents the perimeter of the endcap.

The temperature of the exterior surface area may be determined based on the heat conducted in the radial direction from the cradle to the exterior surface area and the heat moving to the coolant through the attached coil. Therefore, the cradle

exterior surface area's temperature, T_{su}, may be driven as

$$C_{su}\frac{dT_{su}}{dt} = \frac{T_w - T_{su}}{R_w} - \frac{T_{su} - T_{fl,\ E}}{R_{coil}} \tag{7.12}$$

where C_{su} represents the heat capacity and R_{coil} denotes the thermal resistance of the coil and it may be modeled as a conductive thermal resistance such that

$$R_{inn} = \frac{\ln \frac{r_{inn}}{r_{su}}}{2\pi L_{CR} k_{cu}} \tag{7.13}$$

where k_{cu} denotes the coil thermal conductivity, and r_{inn} is the distance between the coil interior surface and the centerline.

7.4.2 Thermal Bus

$$\frac{T_{em} - T_{cap}}{R_{AL}} + \frac{T_{int} - T_{cap}}{R_{HP}} = \dot{m}_w l_v + \dot{m}_w\ c_{p,w}\left(T_{wf,E} - T_{wf,R}\right) \tag{7.14}$$

where l_v is the specific heat of vaporization, $c_{p,w}$ is the working fluid specific heat, and the working fluid's temperature at the heat exchanger is denoted by $T_{wf,R}$. Equation (14) may be simplified and the working fluid mass flow rate, $\dot{m}_w$, may be expressed as

$$\dot{m}_w = \frac{\frac{T_{em} - T_{cap}}{R_{AL}} + \frac{T_{int} - T_{cap}}{R_{HP}}}{c_{p,w}\left(T_{wf,E} - T_{wf,R}\right) + l_f} \tag{7.15}$$

Improved heat transfer capabilities and reduced weight reduction may be achieved by embedding capillary heat pipes within the cradle. Therefore, the cra-

dle contains a number of heat pipes that fit within the wall, N, as

$$N = \frac{2\pi r_{int}}{D_{hp} + s} \tag{7.16}$$

where the term s represents the minimum spacing that must exist between each heat pipe due to the manufacturing limitations.

7.4.3 Thermal Bus

The thermal bus structure includes a vapor and liquid line for the closed-loop passive system, and a fluid supply line, and a fluid return line for the active cooling systems. The pipes are separated with an insulating material so that the heat transfer between the tubes are minimal. On the passive side, the applied heat to the working fluid vaporizes the working fluid. Once the pressure difference between the evaporator and the heat exchanger becomes sufficiently large, the vapor can travel the vapor line and reach the heat exchanger. Therefore, the energy balance for the passive heat rejection pathway becomes

$$C_{TS,\ E}\frac{dT_{wf,E}}{dt} = \frac{T_{cap} - T_{wf,E}}{R_{cap}} - \frac{T_{wf,E} - T_{wf,\ R}}{R_{TS}} \tag{7.17}$$

where $C_{TS,\ E}$ is the evaporator heat capacity and $T_{wf,\ R}$ denotes the heat exchanger's temperature. The thermal resistance of passive system, R_{TS}, depends on the mass flow running between the evaporator and the heat exchanger and it may be written as

$$R_{TS} = \frac{1}{\dot{m}_w\ c_{v,w}} \tag{7.18}$$

where $c_{v,w}$ is the acetone specific heat and $\dot{m}_w$ denotes the working fluid mass flow

rate. The mass flow rate may be determined from the energy balance at the evaporator. Assuming that the endcap is always contains a mixture of working fluid liquid and vapor, and the vapor temperature variation along the liquid and vapor lines is negligible, energy balance becomes

$$\frac{T_{em} - T_{cap}}{R_{AL}} + \frac{T_{int} - T_{cap}}{R_{HP}} \; = \dot{m}_w l_v + \; \dot{m}_w c_{p,w} \left(T_{wf,E} - T_{wf,R}\right) \tag{7.19}$$

where l_v denotes acetone's latent heat of vaporization, and $c_{p,w}$ is the acetone specific heat in the liquid phase. The mass flow rate, $\dot{m}_w$, may be written as

$$\dot{m}_w = \; \frac{\frac{T_{em} - T_{cap}}{R_{AL}} + \frac{T_{int} - T_{cap}}{R_{HP}}}{c_{p,w} \left(T_{wf,E} - T_{wf,R}\right) + \quad l_v} \tag{7.20}$$

In addition, the thermal bus incorporates a liquid cooling system. The temperature of the coolant at the water-jacket, $T_{fl,E}$, may be determined as

$$C_{LQ,E} \frac{dT_{fl,E}}{dt} = \; \frac{T_{su} - T_{fl,E}}{R_{coil}} - \frac{T_{fl,E} - T_{fl,R}}{R_{LQ}} \tag{7.21}$$

where $C_{LQ,E}$ denotes the water-jacket heat capacity and $T_{fl,R}$ is the coolant temperature running through the radiator. The overall thermal resistance of the liquid cooling system may be expressed as

$$R_{LQ} = \frac{1}{\dot{m}_{LQ} c_f} \tag{7.22}$$

where $\dot{m}_{LQ}$ and c_f represent the coolant mass flow rate and the specific heat capacity. The coolant mass flow rate may be determined as

$$\dot{m}_{LQ} = \; \rho_{LQ} A_{LQ} V_{LQ} \tag{7.23}$$

where the symbols ρ_{LQ}, A_{LQ}, and V_{LQ} represent and the coolant density, the coolant tube surface area, the coolant velocity which is experimentally estimated as

$$V_{LQ} = \sum_{i=0}^{1} \propto_i v^i{}_{c,LQ} \tag{7.24}$$

7.4.4 Heat Exchangers

The two-phase passive system releases the latent and sensible heat of the working fluid to the ambient through a heat sink and returns the cooled liquid to the evaporator using gravity. The working fluid temperature at the heat sink,$T_{wf,E}$, may be expressed as

$$C_{hx}\frac{dT_{wf,R}}{dt} = \frac{T_{wf,E} - T_{wf,\ R}}{R_{TS}} - \frac{T_{wf,R} - T_{\infty}}{R_{hx}} \tag{7.25}$$

where R_{hx} denotes the overall heat exchanger thermal resistance, C_{hx} is the heat exchanger heat capacity, and T_{∞} represents the ambient air temperature. The thermal resistance of the heat sink assuming that acetone enters the heat sink is determined as

$$R_{hx} = \frac{1}{h_{hx}A_{hx}} \tag{7.26}$$

where h_{hx} represents the convective heat transfer coefficient, and A_{hx} is the heat transfer surface area between the working fluid and the heat sink. Similarly, the energy balance at the active radiator may be written as

$$C_r\frac{dT_{fl,R}}{dt} = \frac{T_{fl,E} - T_{fl,R}}{R_{LQ}} - \frac{T_{fl,R} - T_{\infty}}{R_r} \tag{7.27}$$

where $T_{fl,R}$ denotes radiator's temperature, C_r is the heat capacity, and $R_{\ r}$ is the

radiator's effective thermal resistance. The radiator convective thermal resistance is calculated based on the convective heat transfer coefficient, $h_r(t)$. The coefficient is estimated through the NTU method with real time temperature measurements at the radiator inlets and outlets. Therefore, the variable thermal resistance of the radiator may be formulated as

$$R_r = \frac{1}{h_r\,(t)\;\; A_r} \tag{7.28}$$

where the A_r denotes the average radiator heat transfer surface area between the radiator and the air. The air flow rate hitting the radiator structure, $\dot{m}_a$, may be determined as a function of the average air velocity, V_a, as

$$\dot{m}_a = \;\rho_a A_r V_a \tag{7.29}$$

where ρ_a is the air density and A_r represents the heat transfer surface area to the ambient air. The ram air effect is neglected in this study and the air velocity is determined experimentally based on the applied voltage to the AC fan frequency drive, $v_{c,a}$, as

$$V_a = \sum_{i=0}^{1} \beta_i {v^i}_{c,a} \tag{7.30}$$

7.4.5 Nonlinear Controller Design

Four control strategies will be developed and applied to the hybrid cooling system for electric motor temperature tracking under a specific driving profile. When properly designed, the actuators operating time is minimized while the electric motor's operating temperature is secured about the specified set point value. The energy

consumption of the hybrid cooling system only attributes to the fan and pump operations when the liquid cooling system is activated. This control strategies provides on demand cooling by switching between passive and hybrid cooling modes to minimize the system power consumption.

This study considers only one of the in-hub electric motors as the heat generating component for setting up the optimization problem and modeling the nonlinear controllers. Thus, Eqs. (7.1) through (7.29) may be rearranged in a compact nonlinear form $\dot{\bar{x}} = f(x, u)$ for $x \in R^{8\times 1}$.

$$\dot{\bar{x}} = \begin{pmatrix} -\frac{x_1 - x_3}{C_{em}R_{AL}} - \frac{x_1 - x_2}{C_{em}R_{CR}} + \frac{Q_{em}}{C_{em}} \\ \frac{x_1 - x_2}{C_w R_{CR}} - \frac{x_2 - x_3}{C_w R_{HP}} - \frac{x_2 - x_6}{C_w R_{coil}} \\ \frac{x_1 - x_3}{C_{cap}R_{AL}} + \frac{x_2 - x_3}{C_{cap}R_{HP}} - \frac{x_3 - x_4}{C_{cap}R_{cap}} \\ \frac{x_3 - x_4}{C_{TS,\ E}R_{cap}} - \frac{x_4 - x_5}{C_{TS,\ E}R_{TS}} \\ \frac{x_4 - x_5}{C_{hx}R_{TS}} - \frac{x_5 - T_\infty}{C_{hx}R_{hx}} \\ \frac{x_2 - x_6}{C_{su}R_w} - \frac{x_6 - x_7}{C_{su}R_{coil}} \\ \frac{x_6 - x_7}{C_{LQ,E}R_{coil}} - \frac{x_7 - x_8}{C_{LQ,E}R_{LQ}} \\ \frac{x_7 - x_8}{C_r\ R_{LQ}} - \frac{x_8 - T_\infty}{C_r R_r} \end{pmatrix} \tag{7.31}$$

where $x = [T_{em}\ \ T_w\ \ T_{cap}\ \ T_{wf,E}\ \ T_{wf,R}\ \ T_{su}\ \ T_{fl,E}\ \ T_{fl,R}]^T$ and $u = [\ \dot{m}_{LQ}\ \dot{m}_a\ Q_{em}\ \ T_\infty]$. The electric motor heat generation rate depends on the vehicle driving profile and the ambient temperature is not controllable. Therefore, they both may be regarded as measured disturbances. The coolant mass flow rate, $\dot{m}_{LQ}$, and the air flow rate, $\dot{m}_a$ are controllable which are considered as manipulated variables in this problem.

The controller design begins with the development of a nonlinear MPC controller which requires this problem to be converted to a nonlinear optimization problem with a quadratic cost function and constraints [104]. Therefore, Eq. (31) is

discretized with a sample rate of τ and it may be written as

$$x\left(k+1\right)=x\left(k\right)+f(x\left(k\right),u\left(k\right))\tau \tag{7.32}$$

where the terms k and k+1 are the current and next time steps. Similarly, the control input vector at the current time step may be expressed as

$$u\left(k\right)=[\dot{m}_{LQ}(k)\quad \dot{m}_{a}(k)\quad Q_{em}(k)\quad T_{\infty}(k)] \tag{7.33}$$

The input sequence, U_k, from time step k to k+p-1 may be defined as

$$U_{k}=[u(k)\quad u(k+1)\quad ...\quad u(k+p-1)] \tag{7.34}$$

where p is the preselected prediction horizon. Applying restrictions to the difference of the input sequences between adjacent time steps can avoid excessive changes in the coolant and air changes such that

$$\Delta U_{k}(i)=\begin{cases} U_{k}\left(i\right)-U_{k-1}\left(1\right) & \text{ı}=1 \\ U_{k}\left(i\right)-U_{k-1}\left(i-1\right) & 1<i<p \end{cases} \tag{7.35}$$

The electric motor's temperature at time step $k+1$ may be rearranged and solved using Eq. 27 as

$$x_{1}\left(k\right)=[1\ 0\ 0]\left(x\left(k-1\right)+f\left(x\left(k-1\right),u\left(k-1\right)\right)\ \tau\right) \tag{7.36}$$

The quadratic cost function, J, becomes

$$J_{k}=Q(T_{set}-x_{1}(k))^{2}+R(\Delta U_{k}(i))^{2} \tag{7.37}$$

where T_{set} represents the prescribed operating temperature set point temperature for the electric motor and the terms Q and R are the weights for temperature tracking and input change rate. The overall cost function starting from time step k within the prediction horizon, P, may be formulated as

$$J_{k\to k+p-1} = \sum_{i=1}^{p} Q(T_{ref} - \bar{x}_1(k+i))^2 + R(\Delta U_k(i))^2 \tag{7.38}$$

The developed nonlinear model predictive controller integrated sequential quadratic programming algorithm. Therefore, the optimum control input sequence, $U_{k,opt}$, leading to the minimum value for the cost function can be solved as

$$U_{k,opt} = \arg\ min\ J_{k\to k+p-1}(U_k) \qquad subject\ to\ U_{min} \leq U_k \leq U_{max} \tag{7.39}$$

where the vectors $U_{min} \in R^{p\times 1}$ and $U_{max} \in R^{p\times 1}$ denote the minimum and maximum input signal sequences and may be written as $U_{min} = [\dot{u}_{min}]^T$ and $U_{max} = [\dot{u}_{max}]^T$.

The performance of nonlinear model predictive control algorithm is compared classical PI, non-linear sliding mode control (SMC), and state flow (SF) methods to regulate the heat load's operating temperature with minimum cooling system power consumption. The proportional and integral gains are selected using a MATLAB toolbox and summarized in Table 7.1.

Next, a sliding mode controller is created to regulate the operation of the liquid cooling system [105]. Considering the nonlinear dynamic system presented by Eq. (29), the system's output is the electric motor's operating temperature such that

$$y = x_1 \tag{7.40}$$

The output tracking error, e, may be defined as

$$e = T_{set} - y(t) \tag{7.41}$$

where y(t) denotes the system's output. The sliding surface, S, is chosen to be linear function being a function of tracking error and its first derivative and it may be expressed as

$$S(t) = \dot{e} + ce \tag{7.42}$$

where c is a positive number and may be found in Table 7.1. The goal is to design a controller that drives the sliding surface to zero which derives the tracking error to zero.

The fourth controller is developed using a Stateflow control algorithm which switches between "ON" and "OFF" modes when the input signal crosses the threshold between T_c and T_{set}.

7.5 Experimental Results and Discussion

A bench top scale hybrid cooling system has been designed and fabricated in the laboratory, refer to Fig. 7.6, so that the performance of four real time controllers can be evaluated. The experimental system is capable of transferring heat between the electric motor and the remote heat exchangers using passive and active cooling channels. The experiment considers heat loads between 200W ¡Q_{em}¡ 3kW during a 60-minute drive cycle.

The electric motor is emulated using six AC cartridge heaters distributed in a radial fashion within the cylindrical aluminum block. The heaters are computer-

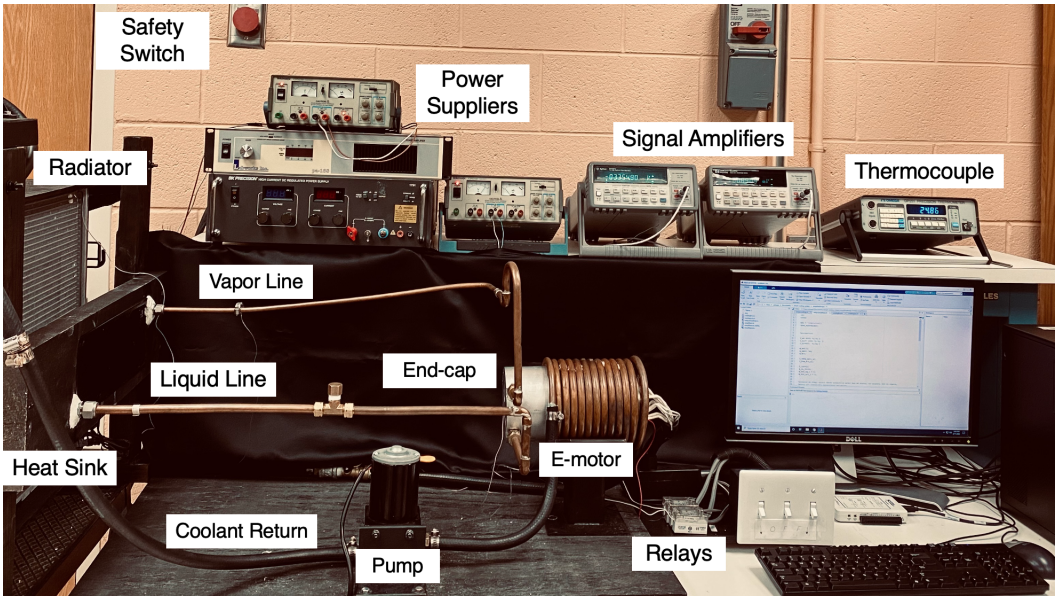

Figure 7.6: Bench top experimental setup designed for electric motor cooling system featuring passive and active systems.

controlled which enable the simulation of several steady-state and time-dependent driving cycles using an Arduino board, three relays, and a rheostat. The system design parameters and control variables are summarized in Table 7.1.

The room temperature is maintained at T_∞ =23°C during the tests. The components' initial temperatures are set at the ambient temperature. The bench top system features a passive gravity-aided thermosyphon, and an active liquid cooling system. The thermosyphon was filled with 25% acetone to water mixture to ensure the availability of evaporator working fluid. The liquid system includes a radiator, coiled evaporator, coolant, DC pump, a VFD fan, and the controller. Five T-type thermocouples measure the electric motor and cradle metals, ambient, thermosyphon evaporator, and radiator inlet fluids. A USB-6211 National Instrument data acquisition measures the signals and generates control signals. An AC and DC current meter measures the actuators' power consumption.

Symbol	Value	Units	Symbol	Value	Units
A_{AL}	81	cm^2	L_{CR}	15.2	cm
A_{LQ}	1.26	cm^2	L_{eff}	4.5	cm
A_{hx}	0.06	cm^2	l_v	534	kJ/kg
A_r	0.3	m^2	p	6	s
A_s	0.1	m^2	P	500	-
c	1.5	-	r_{em}	5	cm
$c_{p,w}$	2140	J/kg.K	r_{ev}	4	cm
$c_{v,w}$	1290	J/kg.K	r_{inn}	6.5	cm
C_{cap}	1.08	kJ/K	r_{su}	6.35	cm
C_{em}	3.01	kJ/K	r_w	5.7	cm
c_f	4182	J/kg.K	T_∞	22	°C
C_{hx}	14.8	kJ/K	T_c	69	°C
$C_{LQ,E}$	3.2	kJ/K	T_{set}	70	°C
C_r	24.5	kJ/K	α_0	0	-
C_{su}	0.8	kJ/K	α_1	-1.7e-3	-
$C_{TS,E}$	0.05	kJ/K	α_2	7e-3	-
C_w	0.7	kJ/K	α_3	-7e-4	-
h_{hx}	15	$W/m^2.K$	β_0	0	-
I	-0.01	-	β_1	1.3e-3	-
k_{AL}	237	W/m.K	β_2	1.62e-2	-
k_{cu}	400	W/m.K	β_3	-1.7e-3	-
k_s	400	W/m.K	ρ_a	1.2	kg/m^3
k_w	200	W/m.K	ρ_{LQ}	1000	kg/m^3
L_{AL}	5	cm	τ	1	s
L_{cap}	35.8	cm	-	-	-

Table 7.1: Summary of model parameters with values

In previous studies [78], the emulated electric motor was successfully cooled using a thermosyphon. Approximately 1kW of heat was continuously rejected to ambient surroundings so as to maintain the operating temperature below 70°C . One gap that merits investigation is integrated heat rejection pathways for higher thermal loads. The remainder of this study focuses on the performance of the control algorithms on the active cooling and their impacts on the cooling system power consumption and the target temperature tracking. A series of experimental tests to evaluate the controllers' performance for the driving profile shown in Fig. 7.7 will be conducted. This operating cycle features accelerations, steady state speeds, and deaccelerations. The overall efficiency of the electric motor is assumed to be 95% which produces the heat load.

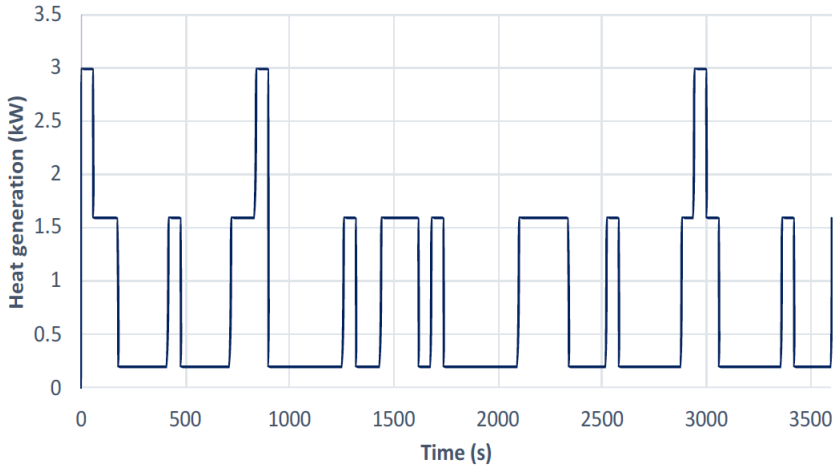

Figure 7.7: Electric motor heat generation as function time.

The target electric motor operating temperature, T_{set}, is set at 70°C. The four controllers are tested one at the time, and the time dependent heating power is applied; Test 1 - NMPC, Test 2 - SMC, Test 3 - SF, and Test 4 - PI. The controllers regulate the liquid cooling system two actuators' speed and operating time to maintain

the electric motor's temperature below the maximum prescribed temperature.

Test No.	Control Strategy	Maximum Temperature (°C)	Maximum Instantaneous Power Consumption		Energy Consumption (kJ)		Power Consumption	
			Pump (W)	Fan (VA)	Pump	Fan	Pump (W-hr)	Fan (VA-hr)
1	NMPC	70.1	68	55	15.2	3.1	4.22	0.87
2	SMC	70.6	68.9	55	21.5	16.3	5.96	4.55
3	SF	70.1	69.8	55	28.8	24.4	7.99	6.78
4	PI	70.2	70.7	55	14.5	11.8	4.02	3.29

Table 7.2: Experimental test matrix exploring the power consumption of the cooling system subject to a time-dependent driving cycle.

The experimental results, presented in Fig. 7.8, include the electric motor, endcap, and ambient temperatures, as well as the coolant and acetone temperatures at the radiator and heat sink inlets. Once the heat load (input) is applied, the e-motor and cradle metal temperatures gradually increased from ambient room temperature of 23°C to operating limits. The cooling system initially relies on the acetone filled passive system which collects the heat via the endcap. This endcap heats and vaporizes the working fluid at 58°C. The vapor travels to the heat sink where it releases the latent and sensible heat to the surrounding. In general, the vapor reaches the heat sink at 900s and immediately raises the measured temperature from 23°C to 53°C due to the cradle to heat sink thermosyphon effect.

The parallel liquid cooling system offers on-demand heat removal based on the electric motor operating temperature requirements. The real time controllers maintain the e-motor's temperature such that $|T_{em} - T_{set}|$ =0.6°C. During the passive mode of operation, the coolant temperature at the radiator's inlet essentially remains constant due to no fluid circulation. Once the electric motor's temperature becomes high, the controller actively commands the pump and the fan combination until the temperature resides below the minimum threshold. Upon initial operation, the radiator coolant temperature quickly reaches the motor temperature before dropping

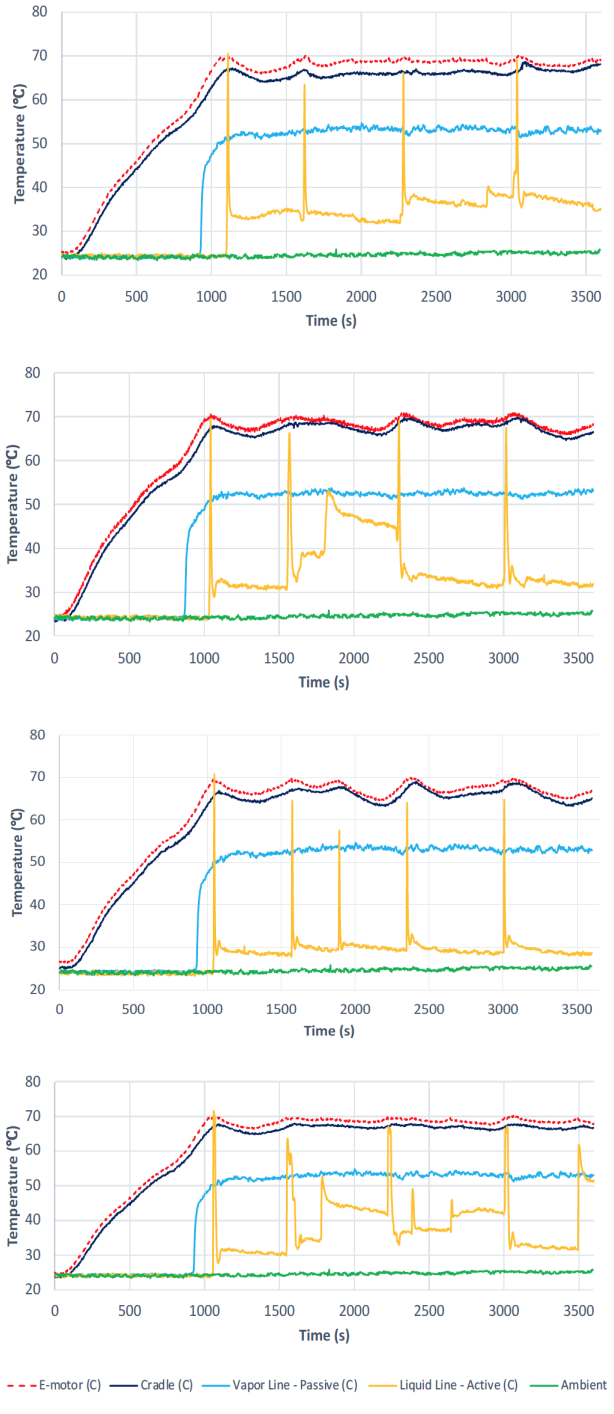

(a)

(b)

(c)

(d)

Figure 7.8: Thermal responses of the electric motor, cradle, working fluid at the heat sink's inlet, coolant fluid at the radiator's inlet, and ambient for the presented driving cycle with implementation of (a) Test 1 – NMPC; (b) Test 2 – SMC; (c) Test 3 – SF; and (d) Test 4 – PI.

due to the initial fluid in the coil. This pattern repeats as the coolant pump and fan are cycled on and off which introduces the fluctuations in the motor and cradle temperature profiles.

Four controllers are introduced in the cooling system, and the motor temperature plus pump and fan power consumption investigated as shown in Table 7.2 and Fig. 7.9 and Fig. 7.10. As expected, the NMPC requires less power to keep the electric motor's temperature below its maximum prescribed operating limit. The experimental data demonstrate that the NMPC regulates the fan and pump operations independently unlike the other controllers. This technique reduces the fan operation significantly which impacts the total power required to reject the excess heat. The results also show that the state flow controller could offer smooth operating cycles for pump and fan operations, refer to Figs. 7.9(c) and 7.10(c). This control strategy switches the actuators between on and off modes as opposed to the other methods that vary the actuators' speed between zero to maximum. This speed variations, discrete VS continues, may influence the system's durability and reduce the actuators' efficiency in some instances.

In summary, this experimental study demonstrates that the proposed hybrid cooling system featuring the NMPC controller is an efficient strategy to maintain the motor below the maximum prescribed operating temperature. Compared to the classical PI method, the NMPC could reduce the fan power consumption by 73% (2.42 VA-hr) for only a 5% (0.2 W-hr) increase in pump power usage over the entire cycle.

7.6 Conclusion

Autonomous vehicles with electric propulsion systems require an advanced thermal management system to accommodate low to high heat rejection demands with zero to minimum external power requirements. This study proposed a hybrid cooling system that incorporates a passive heat transfer pathway with a computer-controlled liquid cooling system. The 'cooling system relies on passive mode while the liquid system offers on-demand cooling based on the electric motor's heat generation rate for reduced cooling system power consumption. Four different controllers are developed using Nonlinear Model Predictive Control, Classical Control, Sliding Mode Control, and Stateflow algorithms. The performance of the cooling system is investigated for a specific time-dependent driving cycle over a 60-minute run time. Compared to the classical PI method, the NMPC strategy could regulate the electric motor temperature with 73% reduction in fan power consumption for only a 5% increase in pump power usage.

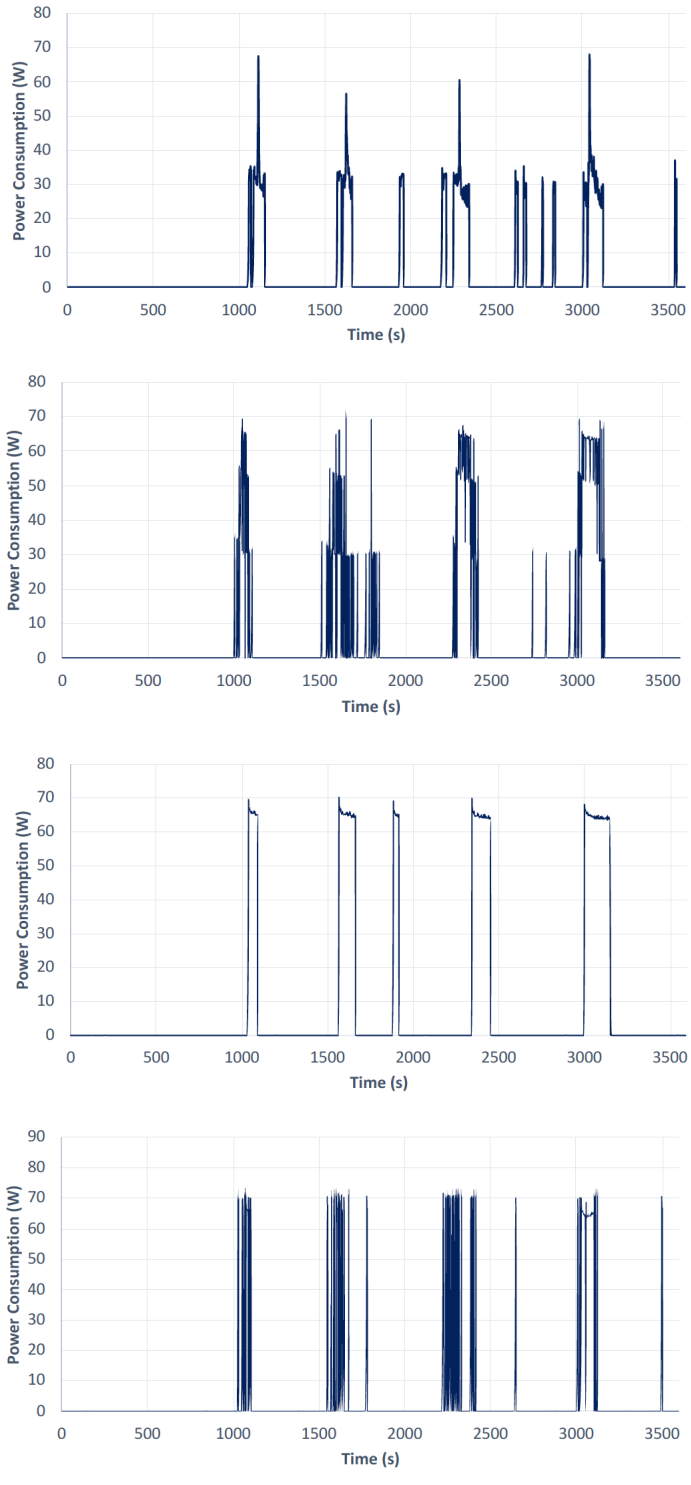

Figure 7.9: Pump power consumption due to the operation of active cooling system featuring (a) Test 1 – NMPC; (b) Test 2 – SMC; (c) Test 3 – SF; and (d) Test 4 – PI

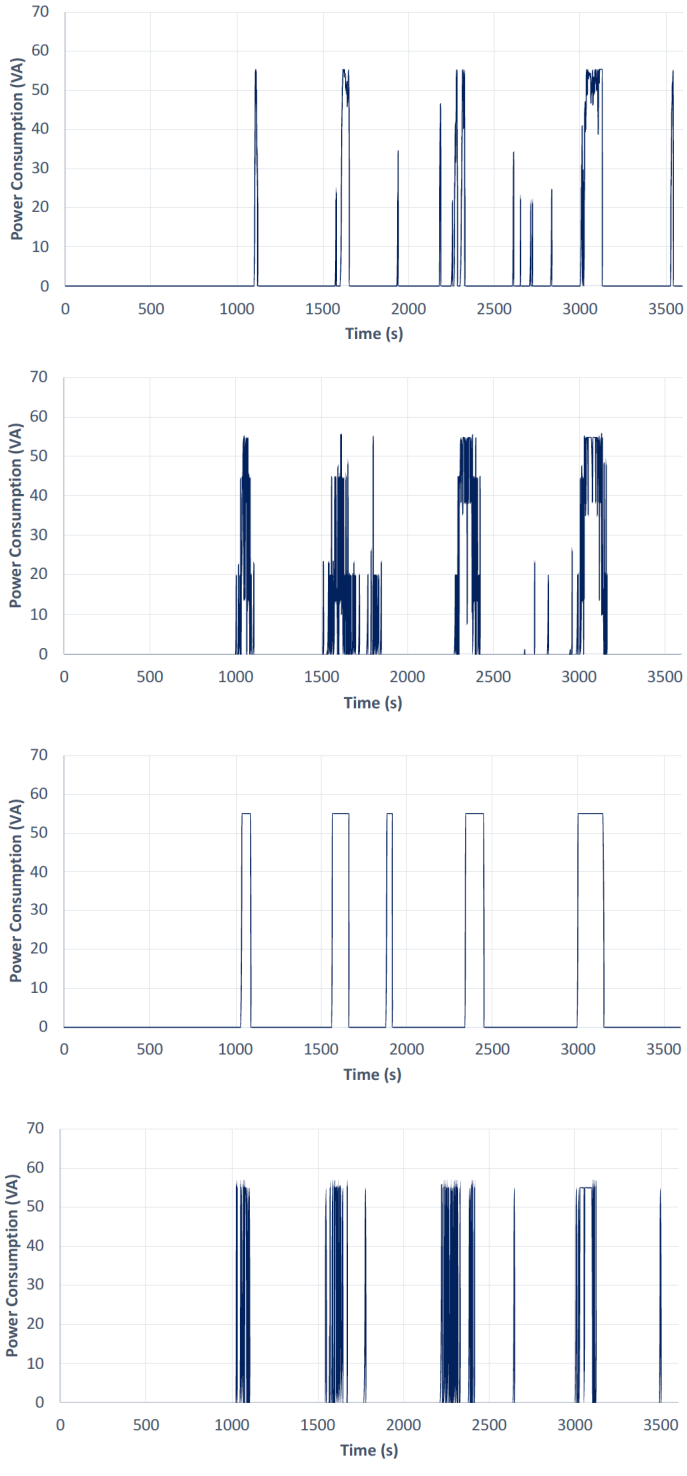

Figure 7.10: Fan power consumption due to the operation of active cooling system featuring (a) Test 1 – NMPC; (b) Test 2 – SMC; (c) Test 3 – SF; and (d) Test 4 – PI

Chapter 8

Conclusions

Vehicle electrification continues to grow fast in the automotive and aerospace industries to make electrical energy the primary energy source for transportations. However, the integration of electric motors with battery packs in a compact structure has required a complex design with advanced onboard electronics. While an electric powertrain offers several advantages over traditional systems, the configuration creates complex thermal challenges due to the unique operating conditions, design configuration, size, and heat rejection needs. These challenges have made thermal management a crucial design aspect for enhanced powertrain electrification.

The integration of an electric motor instead of giant internal combustion engines significantly reduces the powertrain's heat generation during the operating time. This paradigm shift in mobility created an exciting opportunity to design and develop an advanced vehicle thermal management system that can handle low, medium, and high heat dissipation with minimal external power requirements. The presented dissertation proposed a hybrid cooling strategy that contains at least one passive heat rejection pathway in parallel with an advanced computer-controlled liquid cooling system in a thermal bus configuration. The goal is to minimize the cooling system

power consumption by relying on passive cooling solutions over the low and moderate heat generation modes, while a compact computer-controlled variable speed active system offers on-demand cooling for excessive heat-dissipating scenarios. The hybrid approach significantly reduces the active cooling system operating time which immediately impacts the total cooling system power consumption. Besides, should the active cooling system stops operating, the passive cooling system allows continued operation at reduced loads.

The dissertation offers several hybrid cooling system architectures for eclectic vehicle thermal management. Each design is followed by a comprehensive computational model which simulates the dynamic behavior of the cooling system subject to several steady state and transient input loads. The developed mathematical models are then validated through experimental testing designed and developed in the laboratory. The outcomes demonstrate that there is a good agreement between the numerical and experimental results. The validated mathematical models are then used to create real-time supervisory controllers and optimize the hybrid cooling system design configuration for different driving conditions.

First, a heat pipe-based thermal bus is proposed. The mechanism passively transfers the heat between an electric motor and a remote heat changer. A U-shaped pulsating heat pipe is numerically modeled to describe the thermal behavior of heat pipe-based thermal bus subject to a specific time-dependent heat input. The numerical simulations demonstrate that low to moderate thermal load can be transferred to the ambient with no external power requirements.

Second, a novel hybrid thermal management with multiple passive heat rejection pathways in a parallel configuration with a conventional active cooling system is introduced. A mathematical model for each individual heat rejection pathway is developed to investigate the proposed hybrid ground vehicle cooling system's thermal

behavior. The numerical results indicate that parallel passive heat rejection pathways offer adequate cooling for moderate heat dissipation needs over a single ambient temperature.

Third, an experimentally study is conducted to explore the thermal response of an electric motor hybrid cooling system featuring a thermal bus with multiple passive cooling pathways coupled with a computer-controlled liquid cooling system. The experimental results showed that the designed hybrid cooling system could maintain the heat load's temperature with the target temperature limit with 93% energy saving for a light-duty application.

Fourth, a heat pipe-based hybrid cooling system is designed for electric motor cooling applications. The passive system consists of multiple capillary-forced heat pipes with an attached finned structure heat sink. A computer-controlled conventional liquid cooling system is then supplied to the heat load for excessive heat dissipation demands. The complete system is mathematically modeled using a lumped parameter approach. The created mathematical model is validated through benchtop experimental testing for several heat inputs and configurations. The results indicate the proposed hybrid cooling system could save up to 33% of the energy consumption while 250VA thermal load is applied.

Fifth, an optimization problem is set up to minimize a hybrid cooling system design configuration for electric motor cooling. The cooling system consists of multiple passive and active heat rejection pathways. The electric motor cradle size, coolant reservoir, and heat exchanger dimensions are the design variables, while the cost function includes the system weight. The constraints correspond to a medium-size vehicle for a low, medium, and heat rejection requirements. This numerical study demonstrates that reducing the overall cooling system weight is feasible for light-duty to medium-duty vehicles.

Sixth, four different real-time supervisory controllers are developed based on Nonlinear Model Predictive Control, Classical Control, Sliding Mode Control, and Stateflow algorithms. The hybrid cooling system's performance and the controllers are investigated for a specific time-dependent driving cycle over a 60-minute run time. Compared to the classical PI method, the NMPC strategy could regulate the electric motor temperature with 73% reduction in fan power consumption for only a 5% increase in pump power usage.

Overall, the presented research conducted on hybrid cooling strategy demonstrates that hybrid strategy is an efficient cooling solution for electric and hybrid vehicles. The computational and experimental results show that the electric vehicle's heat loss is manageable with a properly designed passive cooling system with a little liquid cooling system operation over multiple driving cycles. The reduced reliance on active cooling enhances the cooling system efficiency with minimal temperature tracking error. Future work includes implementing a hybrid cooling system on a read electric vehicle and learning about the thermal challenges on the road over real driving conditions.

8.1 Recommendations for Further Study

The dissertation established a fundamental basis to address the cooling challenges for the next generation of electric vehicles. The numerical and experimental results demonstrated that the proposed hybrid cooling strategy is an efficient solution to maintain the onboard heat load(s) within their proscribed operating range with minimal power requirements and negligible temperature tracking error. Further work is summarized as follows.

- The presented study incorporated a gravity-aided thermosyphon as a passive

heat transfer pathway between the heat load and the heat exchanger. However, the configuration of thermosyphon may bring some thermal challenges for vehicular applications as the vehicle's orientations continuously vary with the road profile. A loop heat pipe could be a suitable alternative passive solution due to its limited sensitivity to gravity and extra ordinary heat transfer capabilities.

- In previous experimental studies, an emulated electric motor simulated the input heat to the hybrid cooling system. Further experimental testing may be conducted on an actual electric vehicle with in-hub electric motors. Under the real operating conditions, the testing will introduce thermal and control challenges that an electric vehicle may experience over a real driving scenario.

- The study considered a single heat load interfaced with the developed hybrid cooling systems. A complete vehicle thermal management system may be designed, modeled, and tested for an electric vehicle containing several heat loads with different operating temperature limits.

Appendices

References

[1] H. Lu, X. Ma, and M. Azimi, "Us natural gas consumption prediction using an improved kernel-based nonlinear extension of the arps decline model," *Energy*, vol. 194, p. 116905, 2020.

[2] Z. Li, A. Khajepour, and J. Song, "A comprehensive review of the key technologies for pure electric vehicles," *Energy*, vol. 182, pp. 824–839, 2019.

[3] P. Kopelias, E. Demiridi, K. Vogiatzis, A. Skabardonis, and V. Zafiropoulou, "Connected & autonomous vehicles–environmental impacts–a review," *Science of the total environment*, vol. 712, p. 135237, 2020.

[4] J. Kim, J. Oh, and H. Lee, "Review on battery thermal management system for electric vehicles," *Applied thermal engineering*, vol. 149, pp. 192–212, 2019.

[5] H. Min, Z. Zhang, W. Sun, Z. Min, Y. Yu, and B. Wang, "A thermal management system control strategy for electric vehicles under low-temperature driving conditions considering battery lifetime," *Applied Thermal Engineering*, vol. 181, p. 115944, 2020.

[6] D. Moyle, M. Lasecki, and B. Cornish, "Thermal Kits for Truck Fleets," *Proceedings of SAE World Congress*, no. 2006-01-3542, Detroit, MI, 2006.

[7] T. T. Wang and J. R. Wagner, "A Smart Engine Cooling System - Experimental Study of Integrated Actuator Transient Behavior," *Proceedings of SAE World Congress*, no. 2015-01-1604, Detroit, MI, 2015.

[8] X. Tao, K. Zhou, J. R. Wagner, and H. Hofmann, "An Electric Motor Thermal Management System for Hybrid Vehicles: Modelling and Control," *International Journal of Vehicle Performance*, vol. 2, no. 3, pp. 207–227, 2016.

[9] P. Luskin and R. Berlin, "Systems Engineering Methodology for Fuel Efficiency and Its Application to the TARDEC Fuel Efficient Demonstrator (fed) Program," *Proceedings of the Ground Vehicle Systems Engineering and Technology Symposium (GVSETS)*, no. TARDEC-20983RC, Warren, MI, 2010.

[10] H.-i. Kim, J. Shon, and K. Lee, "A Study of Fuel Economy and Exhaust Emission According to Engine Coolant and Oil Temperature," *Journal of Thermal Science and Technology*, vol. 8, no. 1, pp. 255–268, 2013.

[11] S. Park and D. Jung, "Design of Vehicle Cooling System Architecture for a Heavy Duty Series-hybrid Electric Vehicle Using Numerical System Simulations," *Journal of Engineering for Gas Turbines and Power*, vol. 132, no. 9, p. 092802, 2010.

[12] I. Bayraktar, "Computational Simulation Methods for Vehicle Thermal Management," *Applied Thermal Engineering*, vol. 36, pp. 325–329, 2012.

[13] X. Tao and J. R. Wagner, "An Engine Thermal Management System Design for Military Ground Vehicle-simultaneous Fan, Pump and Valve Control," *SAE International Journal of Passenger Cars-Electronic and Electrical Systems*, vol. 9, no. 2016-01-0310, pp. 243–254, 2016.

[14] X. Tao, K. Zhou, A. Ivanco, J. R. Wagner, H. Hofmann, and Z. Filipi, "A Hybrid Electric Vehicle Thermal Management System - Nonlinear Controller Design," *Proceedings of SAE World Congress*, Detroit, MI, 2015.

[15] T. T. Wang, A. Jagarwal, J. R. Wagner, and G. Fadel, "Optimization of an Automotive Radiator Fan Array Operation to Reduce Power Consumption," *IEEE/ASME Transactions on Mechatronics*, vol. 20, no. 5, pp. 2359–2369, 2015.

[16] Y. F. Maydanik, "Loop Heat Pipes," *Applied thermal engineering*, vol. 25, no. 5-6, pp. 635–657, 2005.

[17] Z. Rao, S. Wang, M. Wu, Z. Lin, and F. Li, "Experimental Investigation on Thermal Management of Electric Vehicle Battery with Heat Pipe," *Energy Conversion and Management*, vol. 65, pp. 92–97, 2013.

[18] A. E. El-Sharkawy, "Potential Automotive Applications of Heat Pipes," *Proceedings of SAE World Congress*, no. 980060, Detroit, MI, 1998, doi: 10.4271/980060.

[19] T. J. Hendricks, "Heat Pipe/two-phase Flow Systems for Vehicle Passenger Cabin Cooling," *Proceedings of SAE World Congress*, no. 2002-01-1970, Detroit, MI, 2002, doi:10.4271/2002-01-1970.

[20] G. Burban, V. Ayel, A. Alexandre, P. Lagonotte, Y. Bertin, and C. Romestant, "Experimental Investigation of a Pulsating Heat Pipe for Hybrid Vehicle Applications," *Applied Thermal Engineering*, vol. 50, no. 1, pp. 94–103, 2013.

[21] Y. Zhang, A. Faghri, and M. Shafii, "Analysis of Liquid–vapor Pulsating Flow in a U-shaped Miniature Tube," *International Journal of Heat and Mass Transfer*, vol. 45, no. 12, pp. 2501–2508, 2002.

[22] A. Faghri and Y. Zhang, "Thermal Modeling of Unlooped and Looped Pulsating Heat Pipes," *J. Heat Transfer*, vol. 123, no. 6, p. 1159, 2001.

[23] H. Ma, C. Wilson, B. Borgmeyer, K. Park, Q. Yu, S. Choi, and M. Tirumala, "Effect of Nanofluid on the Heat Transport Capability in an Oscillating Heat Pipe," *Applied Physics Letters*, vol. 88, no. 14, p. 143116, 2006.

[24] X. Yang, Y. Yan, and D. Mullen, "Recent Developments of Lightweight, High Performance Heat Pipes," *Applied Thermal Engineering*, vol. 33, pp. 1–14, 2012.

[25] R. K. Shah, "Advances in Automotive Heat Exchanger Technology," *SAE transactions*, pp. 631–641, 2003, doi:10.4271/2003-01-0533.

[26] Y.-M. Chen and J.-M. Ting, "Ultra High Thermal Conductivity Polymer Composites," *Carbon*, vol. 40, no. 3, pp. 359–362, 2002.

[27] J. Chen and I. Huang, "Thermal Properties of Aluminum–graphite Composites By Powder Metallurgy," *Composites Part B: Engineering*, vol. 44, no. 1, pp. 698–703, 2013.

[28] L. Yolshina, R. Muradymov, I. Korsun, G. Yakovlev, and S. Smirnov, "Novel Aluminum-graphene and Aluminum-graphite Metallic Composite Materials: Synthesis and Properties," *Journal of Alloys and Compounds*, vol. 663, pp. 449–459, 2016.

[29] Y. Huang, Q. Ouyang, D. Zhang, J. Zhu, R. Li, and H. Yu, "Carbon Materials Reinforced Aluminum Composites: a Review," *Acta Metallurgica Sinica (English Letters)*, vol. 27, no. 5, pp. 775–786, 2014.

[30] I. Golecki, L. Xue, R. Leung, T. Walker, A. Anderson, D. Dewar, C. Duncan, and J. Van Horik, "Properties of High Thermal Conductivity Carbon-carbon Composites for Thermal Management Applications," in *1998 High-Temperature Electronic Materials, Devices and Sensors Conference (Cat. No. 98EX132)*, pp. 190–195, IEEE, 1998.

[31] A. Babapoor, M. Azizi, and G. Karimi, "Thermal Management of a Li-ion Battery Using Carbon Fiber-PCM Composites," *Applied Thermal Engineering*, vol. 82, pp. 281–290, 2015.

[32] C. Zweben, "Advances in Composite Materials for Thermal Management in Electronic Packaging," *Jom*, vol. 50, no. 6, pp. 47–51, 1998.

[33] P. Goli, S. Legedza, A. Dhar, R. Salgado, J. Renteria, and A. A. Balandin, "Graphene-enhanced Hybrid Phase Change Materials for Thermal Management of Li-ion Batteries," *Journal of Power Sources*, vol. 248, pp. 37–43, 2014.

[34] A. Greco, X. Jiang, and D. Cao, "An Investigation of Lithium-ion Battery Thermal Management Using Paraffin/porous-graphite-matrix Composite," *Journal of Power Sources*, vol. 278, pp. 50–68, 2015.

[35] S. Mallik, N. Ekere, C. Best, and R. Bhatti, "Investigation of Thermal Management Materials for Automotive Electronic Control Units," *Applied Thermal Engineering*, vol. 31, no. 2-3, pp. 355–362, 2011.

[36] A. Faghri, "Heat Pipes: Review, Opportunities and Challenges," *Frontiers in Heat Pipes (FHP)*, vol. 5, no. 1, 2014.

[37] K. K. Parsons and T. J. Mackin, "Design and Simulation of Passive Thermal Management System for Lithium-ion Battery Packs on an Unmanned Ground Vehicle," *Journal of Thermal Science and Engineering Applications*, vol. 9, no. 1, p. 011012, 2017.

[38] M. Chernysheva, S. Yushakova, and Y. F. Maydanik, "Copper-water Loop Heat Pipes for Energy-efficient Cooling Systems of Supercomputers," *Energy*, vol. 69, pp. 534–542, 2014.

[39] C. Park, J. Zuo, P. Rogers, and J. Perez, "Hybrid Loop Thermal Bus Technology for Vehicle Thermal Management," *Proceedings 24th Army Science Conference*, Orlando, FL, 2004.

[40] C. Park, A. Vallury, and J. Perez, "Advanced Hybrid Cooling Loop Technology for High Performance Thermal Management," *4th International Energy Conversion Engineering Conference and Exhibit (IECEC)*, no. AA2006-4059, p. 4059, San Diego, CA, 2006.

[41] X. Tang, J. Zuo, and M. Goryca, "Development of Heat Pipe Loop Technology for Military Vehicle Electronics Cooling," *NDIA Ground Vehicle Systems Engineering and Technology Symposium*, Dearborn, MI, 2010.

[42] Z. Ling, F. Wang, X. Fang, X. Gao, and Z. Zhang, "A Hybrid Thermal Management System for Lithium Ion Batteries Combining Phase Change Materials with Forced-air Cooling," *Applied energy*, vol. 148, pp. 403–409, 2015.

[43] H. Fathabadi, "High Thermal Performance Lithium-ion Battery Pack Including Hybrid Active–passive Thermal Management System for Using in Hybrid/electric Vehicles," *Energy*, vol. 70, pp. 529–538, 2014.

[44] S. Shoai Naini, J. A. Huang, R. Miller, J. R. Wagner, D. Rizzo, S. Shurin, and K. Sebeck, "A Thermal Bus for Vehicle Cooling Applications-Design and Analysis," *SAE International Journal of Commercial Vehicles*, vol. 10, no. 2017-01-0266, pp. 122–131, 2017.

[45] S. Berber, Y.-K. Kwon, and D. Tománek, "Unusually High Thermal Conductivity of Carbon Nanotubes," *Physical Review Letters*, vol. 84, no. 20, p. 4613, 2000.

[46] P. Kim, L. Shi, A. Majumdar, and P. L. McEuen, "Thermal Transport Measurements of Individual Multiwalled Nanotubes," *Physical Review Letters*, vol. 87, no. 21, p. 215502, 2001.

[47] S. Launay, V. Sartre, and J. Bonjour, "Analytical Model for Characterization of Loop Heat Pipes," *Journal of Thermophysics and Heat Transfer*, vol. 22, no. 4, pp. 623–631, 2008.

[48] S. Mo, P. Hu, J. Cao, Z. Chen, H. Fan, and F. Yu, "Effective Thermal Conductivity of Moist Porous Sintered Nickel Material," *International Journal of Thermophysics*, vol. 27, no. 1, pp. 304–313, 2006.

[49] P.-Y. A. Chuang, "An Improved Steady-state Model of Loop Heat Pipes Based on Experimental and Theoretical Analyses," Ph.D. Dissertation, Department of Mechanical Engineering, Pennsylvania State University, State College, PA, 2003.

[50] T. T. Wang and J. Wagner, "Advanced Engine Cooling System Subjected to Ram Air Effect—Nonlinear Adaptive Multiple Input and Multiple Output (NAMIMO) Control," *IEEE Transactions on Vehicular Technology*, vol. 66, no. 9, pp. 7730–7740, 2017.

[51] H. S. Lee, *Thermal Design: Heat Sinks, Thermoelectrics, Heat Pipes, Compact Heat Exchangers, and Solar Cells*. John Wiley & Sons, 2010.

[52] "Uqm pm 145 e-motor specifications datasheet, https://www.uqm.com/products/propulsion," accessed October 2017.

[53] M. H. Salah, T. H. Mitchell, J. R. Wagner, and D. M. Dawson, "Nonlinear-control strategy for advanced vehicle thermal-management systems," *IEEE Transactions on Vehicular Technology*, vol. 57, no. 1, pp. 127–137, 2008.

[54] M. A. Masrur, "Toward ground vehicle electrification in the us army: an overview of recent activities," *IEEE Electrification Magazine*, vol. 4, no. 1, pp. 33–45, 2016.

[55] Z. Qian, Y. Li, and Z. Rao, "Thermal performance of lithium-ion battery thermal management system by using mini-channel cooling," *Energy Conversion and Management*, vol. 126, pp. 622–631, 2016.

[56] M. Malik, I. Dincer, and M. A. Rosen, "Review on use of phase change materials in battery thermal management for electric and hybrid electric vehicles," *International Journal of Energy Research*, vol. 40, no. 8, pp. 1011–1031, 2016.

[57] J. Huang, S. S. Naini, R. Miller, D. Rizzo, K. Sebeck, S. Shurin, and J. Wagner, "A hybrid electric vehicle motor cooling system—design, model, and control," *IEEE Transactions on Vehicular Technology*, vol. 68, no. 5, pp. 4467–4478, 2019.

[58] X.-h. Qu, L. Zhang, W. Mao, and S.-b. Ren, "Review of metal matrix composites with high thermal conductivity for thermal management applications," *Progress in Natural Science: Materials International*, vol. 21, no. 3, pp. 189–197, 2011.

[59] S. S. Naini, J. A. Huang, R. Miller, J. R. Wagner, D. Rizzo, K. Sebeck, and S. Shurin, "An innovative electric motor cooling system for hybrid vehicles-model and test," tech. rep., SAE Technical Paper, 2019.

[60] S. S. Naini, J. A. Huang, R. Miller, J. R. Wagner, D. Rizzo, K. Sebeck, and S. Shurin, "A Hybrid Thermal Bus for Ground Vehicles Featuring Parallel Heat Transfer Pathways," *SAE International Journal of Commercial Vehicles*, vol. 11, no. 2018-01-1111, 2018.

[61] S. Noie, "Heat transfer characteristics of a two-phase closed thermosyphon," *Applied Thermal Engineering*, vol. 25, no. 4, pp. 495–506, 2005.

[62] "Six wheeled military ground vehicle, https://www.army.mil/article/139889," accessed October 2018.

[63] R. J. McGlen, R. Jachuck, and S. Lin, "Integrated Thermal Management Techniques for High Power Electronic Devices," *Applied Thermal Engineering*, vol. 24, no. 8-9, pp. 1143–1156, 2004.

[64] N. Putra and B. Ariantara, "Electric Motor Thermal Management System Using L-shaped Flat Heat Pipes," *Applied Thermal Engineering*, vol. 126, pp. 1156–1163, 2017.

[65] J. Zhao, P. Lv, and Z. Rao, "Experimental Study on the Thermal Management Performance of Phase Change Material Coupled with Heat Pipe for Cylindrical Power Battery Pack," *Experimental Thermal and Fluid Science*, vol. 82, pp. 182–188, 2017.

[66] J. A. Huang, S. S. Naini, J. R. Wagner, D. Rizzo, K. Sebeck, S. Shurin, *et al.*, "An Integrated Cooling System for Hybrid Electric Vehicle Motors: Design and Simulation," *SAE International Journal of Commercial Vehicles*, vol. 11, no. 2018-01-1108, pp. 255–266, 2018.

[67] W. Elenbaas, "Heat Dissipation of Parallel Plates By Free Convection," *Physica*, vol. 9, no. 1, pp. 1–28, 1942.

[68] P. Teertstra, M. Yovanovich, and J. Culham, "Analytical Forced Convection Modeling of Plate Fin Heat Sinks," *Journal of Electronics Manufacturing*, vol. 10, no. 04, pp. 253–261, 2000.

[69] S. Kakaç, R. K. Shah, and W. Aung, "Handbook of Single-phase Convective Heat Transfer," New York: Wiley, 1987.

[70] F. Gao, S. S. Naini, J. Wagner, and R. Miller, "An Experimental and Numerical Study of Refrigerator Heat Leakage at the Gasket Region," *International Journal of Refrigeration*, vol. 73, pp. 99–110, 2017.

[71] W. Su, H. Eichi, W. Zeng, and M.-Y. Chow, "A survey on the electrification of transportation in a smart grid environment," *IEEE Transactions on Industrial Informatics*, vol. 8, no. 1, pp. 1–10, 2011.

[72] A. A. Pesaran, "Battery thermal management in ev and hevs: issues and solutions," *Battery Man*, vol. 43, no. 5, pp. 34–49, 2001.

[73] J. Smith, R. Singh, M. Hinterberger, and M. Mochizuki, "Battery thermal management system for electric vehicle using heat pipes," *International Journal of Thermal Sciences*, vol. 134, pp. 517–529, 2018.

[74] J. Qu, C. Wang, X. Li, and H. Wang, "Heat transfer performance of flexible oscillating heat pipes for electric/hybrid-electric vehicle battery thermal management," *Applied Thermal Engineering*, vol. 135, pp. 1–9, 2018.

[75] J. Huang, S. Shoai Naini, R. Miller, D. Rizzo, K. Sebeck, S. Shurin, and J. Wagner, "Development of a heat pipe–based battery thermal management system for hybrid electric vehicles," *Proceedings of the Institution of Mechanical Engineers, Part D: Journal of Automobile Engineering*, vol. 234, no. 6, pp. 1532–1543, 2020.

[76] Q. Su, S. Chang, Y. Zhao, H. Zheng, and C. Dang, "A review of loop heat pipes for aircraft anti-icing applications," *Applied Thermal Engineering*, vol. 130, pp. 528–540, 2018.

[77] M. Nishikawara and H. Nagano, "Optimization of wick shape in a loop heat pipe for high heat transfer," *International Journal of Heat and Mass Transfer*, vol. 104, pp. 1083–1089, 2017.

[78] S. S. Naini, R. Miller, J. Wagner, D. Rizzo, and K. Sebeck, "An electric motor thermal bus cooling system for vehicle propulsion-design and test," *SAE International Journal of Advances and Current Practices in Mobility*, vol. 2, no. 2020-01-0745, pp. 2011–2018, 2020.

[79] J. Huang, S. S. Naini, R. Miller, D. Rizzo, K. Sebeck, and J. Wagner, "Unmanned autonomous ground hybrid vehicle thermal management system: design and control," *International Journal of Vehicle Performance*, vol. 6, no. 3, pp. 356–379, 2020.

[80] Y. Ye, Y. Shi, L. H. Saw, and A. A. Tay, "Performance assessment and optimization of a heat pipe thermal management system for fast charging lithium ion battery packs," *International Journal of Heat and Mass Transfer*, vol. 92, pp. 893–903, 2016.

[81] W. Li, X. Peng, M. Xiao, A. Garg, and L. Gao, "Multi-objective design optimization for mini-channel cooling battery thermal management system in an electric vehicle," *International Journal of Energy Research*, vol. 43, no. 8, pp. 3668–3680, 2019.

[82] D. Reay, R. McGlen, and P. Kew, *Heat pipes: theory, design and applications*. Butterworth-Heinemann, 2013.

[83] "Specification sheet accessed october 2020 at https://www.uqm.com/english/products/propulsion/commercial-vehicles/medium-duty/default.aspx," accessed October 2020.

[84] K. Ito and K. Kunisch, *Lagrange multiplier approach to variational problems and applications*. SIAM, 2008.

[85] F. Hasankhani and A. Khademi, "Efficient and fair heart allocation policies for transplantation," *MDM policy & practice*, vol. 2, no. 1, p. 2381468317709475, 2017.

[86] F. Hasankhani and A. Khademi, "Is it time to include post-transplant survival in heart transplantation allocation rules?," *Available at SSRN 3416214*, 2019.

[87] F. Un-Noor, S. Padmanaban, L. Mihet-Popa, M. N. Mollah, and E. Hossain, "A comprehensive study of key electric vehicle (ev) components, technologies, challenges, impacts, and future direction of development," *Energies*, vol. 10, no. 8, p. 1217, 2017.

[88] R. Yuan, T. Fletcher, A. Ahmedov, N. Kalantzis, A. Pezouvanis, N. Dutta, A. Watson, and K. Ebrahimi, "Modelling and co-simulation of hybrid vehicles: A thermal management perspective," *Applied Thermal Engineering*, p. 115883, 2020.

[89] B. Orr, A. Akbarzadeh, M. Mochizuki, and R. Singh, "A review of car waste heat recovery systems utilising thermoelectric generators and heat pipes," *Applied Thermal Engineering*, vol. 101, pp. 490–495, 2016.

[90] G. Fang, W. Yuan, Z. Yan, Y. Sun, and Y. Tang, "Thermal management integrated with three-dimensional heat pipes for air-cooled permanent magnet synchronous motor," *Applied Thermal Engineering*, vol. 152, pp. 594–604, 2019.

[91] Y. Deng, C. Feng, E. Jiaqiang, H. Zhu, J. Chen, M. Wen, and H. Yin, "Effects of different coolants and cooling strategies on the cooling performance of the power lithium ion battery system: A review," *Applied Thermal Engineering*, vol. 142, pp. 10–29, 2018.

[92] G. Xia, L. Cao, and G. Bi, "A review on battery thermal management in electric vehicle application," *Journal of power sources*, vol. 367, pp. 90–105, 2017.

[93] M. H. Salah, T. H. Mitchell, J. R. Wagner, and D. M. Dawson, "A smart multiple-loop automotive cooling system—model, control, and experimental study," *IEEE/ASME Transactions On Mechatronics*, vol. 15, no. 1, pp. 117–124, 2009.

[94] X. Tao and J. Wagner, "A thermal management system for the battery pack of a hybrid electric vehicle: modeling and control," *Proceedings of the Institution of Mechanical Engineers, Part D: Journal of Automobile Engineering*, vol. 230, no. 2, pp. 190–201, 2016.

[95] H. Nazir, M. Batool, F. J. B. Osorio, M. Isaza-Ruiz, X. Xu, K. Vignarooban, P. Phelan, A. M. Kannan, *et al.*, "Recent developments in phase change materials for energy storage applications: A review," *International Journal of Heat and Mass Transfer*, vol. 129, pp. 491–523, 2019.

[96] L. Fan and J. M. Khodadadi, "Thermal conductivity enhancement of phase change materials for thermal energy storage: a review," *Renewable and sustainable energy reviews*, vol. 15, no. 1, pp. 24–46, 2011.

[97] S. Li, Q. Zheng, Y. Lv, X. Liu, X. Wang, P. Y. Huang, D. G. Cahill, and B. Lv, "High thermal conductivity in cubic boron arsenide crystals," *Science*, vol. 361, no. 6402, pp. 579–581, 2018.

[98] Q. Huang, X. Li, G. Zhang, J. Deng, and C. Wang, "Thermal management of lithium-ion battery pack through the application of flexible form-stable composite phase change materials," *Applied Thermal Engineering*, vol. 183, p. 116151, 2021.

[99] N. Lamaison, C. L. Ong, J. B. Marcinichen, and J. R. Thome, "Two-phase mini-thermosyphon electronics cooling: Dynamic modeling, experimental validation and application to 2u servers," *Applied Thermal Engineering*, vol. 110, pp. 481–494, 2017.

[100] P. K. Vijayan, A. K. Nayak, and N. Kumar, *Single-phase, Two-phase and Supercritical Natural Circulation Systems*. Woodhead Publishing, 2019.

[101] M. Shtein, R. Nadiv, M. Buzaglo, and O. Regev, "Graphene-based hybrid composites for efficient thermal management of electronic devices," *ACS applied materials & interfaces*, vol. 7, no. 42, pp. 23725–23730, 2015.

[102] J. R. Patel and M. K. Rathod, "Recent developments in the passive and hybrid thermal management techniques of lithium-ion batteries," *Journal of Power Sources*, vol. 480, p. 228820, 2020.

[103] D. Reay, P. Kew, and R. McGlen, "Heat pipe: Theory, design and applications (6th edn.) buterworth," 2014.

[104] H. Durand, M. Ellis, and P. D. Christofides, "Economic model predictive control designs for input rate-of-change constraint handling and guaranteed economic performance," *Computers & Chemical Engineering*, vol. 92, pp. 18–36, 2016.

[105] T. He, D. D.-C. Lu, L. Li, J. Zhang, L. Zheng, and J. Zhu, "Model-predictive sliding-mode control for three-phase ac/dc converters," *IEEE Transactions on Power Electronics*, vol. 33, no. 10, pp. 8982–8993, 2017.